Characterizing Novel Molecular Regulators of Antiviral Gene Expression

by

Michael J. McFadden

Department of Molecular Genetics and Microbiology
Duke University

Date:_____

Approved:

_____
Stacy Horner, Supervisor

_____
Micah Luftig

_____
Mari Shinohara

_____
Debra Silver

_____
Kathryn Meyer

Dissertation submitted in partial fulfillment of
the requirements for the degree of Doctor of Philosophy in the Department of
Molecular Genetics and Microbiology in the Graduate School
of Duke University

2020

ABSTRACT

Characterizing Novel Molecular Regulators of Antiviral Gene Expression

by

Michael J. McFadden

Department of Molecular Genetics and Microbiology
Duke University

Date:_____

Approved:

_____
Dr. Stacy Horner, Supervisor

_____
Dr. Micah Luftig

_____
Dr. Mari Shinohara

_____
Dr. Debra Silver

_____
Dr. Kathryn Meyer

An abstract of a dissertation submitted in partial
fulfillment of the requirements for the degree
of Doctor of Philosophy in the Department of
Molecular Genetics and Microbiology in the Graduate School of
Duke University

2020

Abstract

The intracellular innate immune response to viral infection is among the first lines of defense against these pathogens. For the early establishment of an antiviral cellular state and initiation of inflammatory responses, type I interferons (IFNs) are particularly important, as they potently induce the production of hundreds of IFN-stimulated genes (ISGs), many of which have antiviral functions. The type I IFN response requires tight molecular coordination to achieve both efficient production of antiviral proteins and controlled shutoff of inflammatory responses to avoid tissue damage and autoimmunity. Despite the importance of regulation of this antiviral response, current knowledge of the molecular controls governing its activation and suppression remains incomplete. Further, although ISGs have diverse functions and are induced to differing potencies, our understanding of regulatory controls governing the expression of individual or subclasses of ISGs is limited.

Current knowledge of type I IFN response regulation is predominantly centered on transcriptional and post-translational regulatory controls. However, post-transcriptional regulation of antiviral responses has begun to emerge as an important layer of control. An example of these post-transcriptional regulatory controls is the RNA base modification N6-methyladenosine (m^6A), which regulates many aspects of mRNA metabolism through transcript-specific effects. m^6A deposition is mediated by a cellular complex of proteins including METTL3 and METTL14 (METTL3/14) and other cofactors, and m^6A can also be removed from RNA by the demethylase proteins FTO and ALKBH5. The presence of m^6A on viral and host RNAs has been shown to influence the outcome of infection by diverse viruses. However, the role of m^6A in the response to type

I IFNs has not been explored. To investigate the role of m^{6}A in the type I IFN response, we began by manipulating m^{6}A levels in the transcriptome through perturbation of the expression of the cellular m^{6}A machinery and measuring the induction of ISGs after IFN treatment. We found that depletion of the m^{6}A methyltransferase proteins METTL3 and METTL14 (METTL3/14) resulted in less protein production of a subset of ISGs, including the antiviral genes IFITM1 and MX1, after IFN treatment. However, the expression of other ISGs and the overall activation of the IFN responses were unchanged. Using methyl RNA immunoprecipitation and sequencing (meRIP-seq), we found that the transcripts of many ISGs are modified by m^{6}A, and these included the METTL3/14-regulated ISGs IFITM1 and MX1 that we had identified. Using polysome profiling and ribosome profiling, we determined that METTL3/14-regulated ISGs are translationally enhanced by METTL3/14. Additionally, ablation of putative m^{6}A sites within the 3'UTR of IFITM1 decreased the translation of a reporter molecule. Overexpression of the m^{6}A reader protein YTHDF1, which has known roles in promoting translation, enhanced the expression of IFITM1 in an m^{6}A binding-dependent fashion. These experiments characterized METTL3/14 and m^{6}A as novel enhancers of the type I IFN response. To determine whether m^{6}A contributes to type I IFN-mediated viral restriction, we depleted or overexpressed METTL3/14 and pretreated cells with a low dose of IFN-β prior to infection with vesicular stomatitis virus (VSV). Interestingly, METTL3/14 depletion decreased the expression of ISGs and allowed increased VSV infection, while METTL3/14 overexpression had the opposite effect. Together, these studies demonstrate that METTL3/14 and m^{6}A enhance the antiviral effect of type I IFN by

promoting the translation of ISGs to support the establishment of an antiviral cellular state.

Having discovered a role for m^6A in the type I IFN response, we also investigated the role of an m^6A demethylase protein, FTO. FTO polymorphisms can have profound effects on human health. Certain polymorphisms are associated with fat mass and obesity, cardiovascular disease, while others can cause growth retardation or embryonic lethality. However, the molecular functions of FTO and the cellular pathways that it affects are still not well characterized. We depleted FTO and measured the production of ISGs following IFN-β treatment and found that the production of m^6A-regulated ISGs was increased, as expected. However, unexpectedly, we found that FTO depletion increased the mRNA levels of a subset of ISGs. Pulse labeling of nascent transcripts revealed that FTO suppresses the transcription of these ISGs and that FTO-depleted cells are primed for the production of certain ISGs in response to IFN. We then used cells lacking PCIF1, the writer of 2'-O-N6-dimethyladenosine (m^6Am), an RNA modification that FTO can also remove, and found that FTO-mediated regulation of ISGs occurs independently of the m^6Am modification. These results identify FTO as a transcriptional regulator of a subset of ISGs, which will add an important dimension to our understanding of the molecular functions of FTO and its contributions to inflammatory disease. Future research revealing the mechanisms by which FTO suppresses ISG transcription will be of great interest. Together, these data identify novel functions of m^6A and its related cellular machinery in both positive and negative regulation of the type I IFN response and antiviral gene expression.

Dedication

To my parents, Michael, and Lisa McFadden, who have always nourished my interest in science and discovery, instilled a relentless work ethic in me, taught me the value of self-belief, and provided me the opportunities to achieve my goals.

Contents

List of Tables

List of Figures

Acknowledgements

My development as an effective scientist began during my undergraduate research experience in Dr. Zhiyong Xi's laboratory at Michigan State University. My mentor, Dr. Deepak Joshi, and the rest of my lab mates taught me the importance of meticulousness, and I learned how ask and answer important scientific questions. I would like to thank all of my former lab mates for their mentorship and training that led me to graduate school.

Thank you to my graduate advisor, Dr. Stacy Horner, for her dedication to mentorship and my development as a scientist. I have received tremendous training as a writer, communicator, teacher, and researcher during my time in the Horner lab. I have also felt that Stacy has encouraged my creativity and scientific exploration in multiple projects, while also keeping me focused and making progress on the right directions at the right time. It is difficult to imagine I would've had the same breadth of training in nearly any other environment, and for these reasons I feel the Horner lab will continue to produce successful scientists for many years.

My graduate school experience and training were enriched in immeasurable ways by other Horner lab members, past and present. Thank you to Allison, Christine, and Nandan for being phenomenal mentors, colleagues, and friends. Your accomplishments encouraged me to set the bar high and the examples you set in research, grantsmanship, and professional development have been a tremendous help. I'd also like to thank Kevin for being an outstanding contributor to my projects and the lab, and for being a great friend. Thank you to Matt and Daltry for all of your help and suggestions and friendship, as well, and I look forward to your continued success in the

lab. Thanks to Moonhee, as well, for keeping the lab running and your willingness to lend experimental support and advice.

The graduate students in my cohort have been great friends and colleagues who have inspired me to work hard toward my achievements and given me an outlet to escape from the pitfalls of graduate school. Thanks to entire cohort and especially Al and Hannah for your friendship. Additionally, the MGM department more broadly has been full of students and professors who I've been lucky to spend time with because of their intelligence, work ethic, and enthusiasm. I have also formed many memories with other graduate students in sports and over drinks. I am grateful for having formed these connections with so many friends.

My parents have always nurtured my scientific curiosity and encouraged me to work hard to achieve my academic potential. I am forever grateful to them and to my brother for all that they've done for me throughout my life. I owe all of my success to them. Finally, thank you to my partner, Alex, for being my supporter and my rock throughout graduate school and all the ups and downs that have come with it.

1. Introduction

Parts of this chapter were adapted with permission from a published manuscript: “Protect this house: Cytosolic sensing of viruses” published in Current Opinion in Virology (2017) by authors Michael J. McFadden (first author), Nandan S. Gokhale, and Stacy M. Horner [1].

1.1 Intracellular detection of viruses & antiviral signaling pathways

Human pathogenic viruses are a major global health concern, often leading to serious illness or death. Viral infection represents a significant challenge to host cells, as the ability to detect infection and inhibit viral replication is one of the key factors determining host susceptibility to infection. Many human pathogenic viruses have evolved strategies to avoid detection by the host cell, or to inhibit other antiviral factors, demonstrating the importance of antiviral innate immunity to protect against viral infection [2,3]. In order to activate antiviral responses and limit viral replication, cells must detect molecular signatures of viral components, mount signaling responses to induce the production of signaling molecules known as cytokines, respond to these cytokines to activate antiviral gene expression programs, and regulate these responses to recruit immune cells, activate adaptive immune responses, and ultimately repress these events to return to a normal cellular state after viral clearance. While epithelia generally provide a first barrier of defense against viral infection, the innate immune response to viruses is among the first cellular defense mechanisms following infection. The ability to recognize invading viral pathogens and to distinguish their components from those of the host cell is critical to initiate the innate immune response. The

efficiency of this detection is an important factor in determining the susceptibility of the cell to viral infection. Innate sensing of viruses is, therefore, an indispensable step in the line of defense for cells and organisms. Recent discoveries have uncovered novel sensors of viral components and hallmarks of infection, as well as mechanisms by which cells discriminate between self and non-self. This section highlights the mechanisms used by cells to detect viral pathogens in the cytosol, and recent advances in the field of cytosolic sensing of viruses.

Pattern recognition receptors (PRRs) act as sensors for the products of viral infection, which are known as pathogen-associated molecular patterns (PAMPs). Viral PAMPs can include viral proteins or nucleic acids that are sensed by PRRs as non-self to elicit antiviral innate immune responses, primarily driven by type I and III interferons (IFN). This section focuses on the PRRs that sense viral nucleic acid PAMPs within the cytosol of the cell generated during RNA and DNA virus infection. Here, I describe how the cytosolic nucleic acid sensing PRRs, the RIG-I-like Receptors (RLRs) and DNA sensors, discriminate between self and non-self to activate antiviral immune responses.

1.1.1 RLRs sense cytosolic viral RNA and activate antiviral responses

The RLRs, members of the DExD/H box family of helicases, include retinoic acid-inducible gene I (RIG-I), melanoma differentiation factor 5 (MDA5), and laboratory of genetics and physiology 2 (LGP2). This family of cytosolic viral sensors is crucial for recognition of a large number of RNA viruses [4]. These sensors distinguish virus-associated RNAs from cellular RNAs to activate downstream signaling of antiviral innate immunity driven by mitochondrial antiviral signaling protein (MAVS), which aggregates into filaments following activation by PRRs [5]. Filamentous MAVS serves as a platform for interaction with other proteins involved in the signaling cascade, such as tumor

necrosis factor receptor-associated factor (TRAF) proteins, which are important for MAVS signaling through TANK-binding kinase 1 (TBK1) and IκB-kinase-ε (IKKε), and the IκB kinase complex (IKK) [6]. TBK1/IKKε and IKK phosphorylate IRF3/IRF7 and the inhibitory subunit of NF-κB (IκBα), respectively. The transcription factors IRF3, IRF7, and NF-κB then translocate to the nucleus to induce transcription of type I IFNs (IFN-α and IFN-β). Type I IFN production drives autocrine and paracrine responses through the IFN-α/β receptor, which activates the JAK/STAT signaling pathway to ultimately induce the transcription of hundreds of IFN-stimulated genes (ISGs). These include many antiviral factors, which can inhibit viral replication in various ways [7-9].

1.1.1.1 RIG-I

RIG-I senses a number of RNA viruses ranging from flaviviruses, alphaviruses, coronaviruses, reoviruses, paramyxoviruses, orthomyxoviruses, rhabdoviruses, arenaviruses, and bunyaviruses [10,11]. RIG-I recognizes PAMPs, including short double-stranded RNA (dsRNA) containing either a 5’ triphosphate or 5’ diphosphate moiety that are generally unique to viral RNA [12-14]. Interestingly, a recent report identified RIG-I as a PRR for Crimean-Congo hemorrhagic fever virus (CCHFV), whose RNA genome is 5’-monophosphorylated, implicating an additional ability of RIG-I to sense 5’-monophosphate-containing viral RNAs [15]. Therefore, while canonical ligands of RIG-I have been identified, future research may uncover additional features of ligands, such as post-transcriptional RNA modifications, that allow RIG-I to distinguish self from non-self. Indeed, self RNAs are distinguished from foreign RNAs by post-transcriptional modifications of their 5’ triphosphate ends, which contain the RNA cap structures. These include cap0: 7-methylguanosine addition to the gamma phosphate on the 5’ end of mRNAs; cap1: identical to cap0, with 2’-O-methylation of the first nucleotide

following the 5’ triphosphate; and cap2: identical to cap1, with an additional 2’-O-methyl group on the second nucleotide. The 2’-O-methylation present in cap1 is crucial for avoiding recognition by RIG-I [16,17]. In addition, 2’-O-methylation protects host mRNAs from sequestration by IFN-induced proteins with tetratricopeptide repeats (IFITs), which would otherwise inhibit the translation of these proteins [18]. In fact, certain viruses including flaviviruses, coronaviruses, and alphaviruses have co-opted cellular RNA capping strategies, likely to evade detection by RLRs [19,20]. RIG-I contains several functional domains that regulate sensing of PAMPs and its subsequent activation. It is comprised of two N-terminal caspase activation and recruitment domains (CARDs), followed by two tandem helicase domains (Hel1, Hel2) separated by an insertion domain (Hel2i), as well as a C-terminal repressor domain (RD) [12,21,22]. In resting cells, Hel2i interacts with the second CARD, keeping RIG-I in an auto-inhibited state [23,24]. The RD inhibits self-association of RIG-I, preventing its interaction with MAVS [21]. Upon sensing viral RNA, RIG-I undergoes a conformational change, in which the RD interacts with viral RNA and the helicase domains, breaking the interaction of Hel2i with the CARD2 to release the CARDs for interaction with MAVS, which also contains a CARD motif [22,23]. Following this conformational change, both the RD and CARDs are subject to post-translational modifications (PTMs). First, the RD of RIG-I is subject to Lysine (K) 63-linked poly-ubiquitination by the E3 ubiquitin ligase RIPLET [25,26]. This promotes tripartite motif-containing protein 25 (TRIM25) K63-linked ubiquitination of the RIG-I CARDs [27]. Mex-3 RNA Binding Family Member C (MEX3C) was recently identified as an additional essential E3 ubiquitin ligase that mediates K63-linked ubiquitination on RIG-I CARDs [28], and TRIM4 was found to enhance RIG-I signaling via K63-linked ubiquitination that is redundant with TRIM25 and RIPLET [29]. Recent structural work

has demonstrated that K63-linked ubiquitination of RIG-I stabilizes assembly of its CARDs into a helical tetramer. This tetramer of RIG-I CARDs facilitates interaction with MAVS, and nucleates MAVS filament formation [30]. Removal of specific PTMs, including lysine acetylation by histone deactylase 6 (HDAC6) and dephosphorylation of RIG-I CARDs by protein phosphatase 1 (PP1), is required for full RIG-I activation [31-33]. In addition to regulation by its structure and by PTMs, RIG-I is regulated at the cell biological level. In resting cells, RIG-I is localized to the cytoplasm where it can detect PAMPs of invading viruses. However, upon activation, RIG-I interacts with various proteins, including TRIM25 and 14-3-3ε, to form a translocon that facilitates RIG-I re-localization into intracellular membranes for interaction with MAVS [34,35]. Taken together, these complex regulatory mechanisms prevent aberrant activation of RIG-I.

1.1.1.2 MDA5

While some overlap exists between the viruses sensed by RIG-I and MDA5 – such as flaviviruses, alphaviruses, coronaviruses, reoviruses, and paramyxoviruses – MDA5 plays an indispensable role in detection of picornaviruses and caliciviruses [36]. MDA5 has similar structural domains to RIG-I (CARDs-helicases-RD) and also signals downstream through MAVS. However, MDA5 senses long dsRNA, which are viral replication intermediates [37,38]. Similar to RIG-I, 2'-O-methylation at the 5' end of RNAs prevents MDA5 sensing [39]. While RIG-I recognizes the terminal end of dsRNA, MDA5 recognizes the internal duplex structure of dsRNA in a length-dependent fashion [38]. The crystal structure of MDA5 bound to dsRNA reveals that MDA5 stacks along dsRNA, forming filamentous structures, in a head-to-tail arrangement for signaling [40]. The ATP hydrolysis activity of the helicase domains is required for MDA5 filament formation [40,41]. These filaments expose the CARDs of MDA5 for interaction with the CARD motif

of MAVS [40]. PTMs also regulate MDA5 function. Like RIG-I, PP1 dephosphorylates MDA5 CARDs, leading to MDA5 activation [33]. However, unlike RIG-I, little is known about other PTMs that may regulate MDA5 activation, such as K63-linked ubiquitination [4]. In addition, little is known about the cell biology that regulates MDA5 activation. Future studies to address these aspects of the regulation of MDA5 will be of interest.

1.1.1.3 LGP2

LGP2 is less well characterized than RIG-I and MDA5, but increasing evidence suggests that LGP2 may act as a negative regulator of RIG-I-directed signaling and as an enhancer of MDA5-directed signaling [42-45]. LGP2 has similar domains to RIG-I and MDA5 (Helicase-RD), however it lacks the N-terminal CARDs required for interaction with MAVS. While it has been shown that LGP2 recognizes both dsRNA and single-stranded RNA (ssRNA), with a preference for RNA with a 5'triphosphate, LGP2 is not able to independently activate downstream signaling to MAVS because it lacks N-terminal CARDs required for this interaction. In addition, multiple conflicting functions have been attributed to LGP2, including negative regulation of RIG-I [42,43], as well as negative regulation of MDA5 [46], and positive regulation of MDA5 [44,46]. Recently, LGP2 was found to regulate the binding of MDA5 to RNA and regulate MDA5 filament assembly for enhanced signaling activity [44]. Therefore, it seems LGP2 may serve multiple, diverse functions in response to different viruses. Further research will be required to appreciate the role and function of LGP2 in regulation of RNA virus sensing and downstream signaling.

1.1.2 Cytosolic DNA sensors activate antiviral responses

The presence of DNA in the cytosol is an indicator of pathogen infection or of cellular damage. Considering the multitude of intracellular pathogens capable of replicating in the cytosol, the detection of their nucleic acids is imperative for cellular defense against not only viruses, but also bacterial and eukaryotic pathogens. While sensors and pathways related to detection of RNA viruses are well defined, many sensors of viral DNA have only recently been identified. The roles of many of these proteins in initiating innate immune responses to DNA are not fully understood [47]. In addition, the signaling pathways leading to the production of IFN following detection of viral DNA PAMPs are less well defined than pathways activated by detection of RNA PAMPs. Nonetheless, the past decade has produced numerous discoveries uncovering key factors in DNA-sensing pathways, referred to as the IFN-stimulatory DNA (ISD) pathway [48,49]. A number of cytosolic DNA sensors activate this pathway to signal through stimulator of interferon genes (STING). STING binds to and is activated by cyclic dinucleotides, such as cyclic GMP-AMP (cGAMP) [50]. Activated STING then translocates from the endoplasmic reticulum (ER) to perinuclear compartments, such as the Golgi, endosomes, and autophagy-related compartments [51,52], which leads to its palmitoylation for signaling [53]. It then recruits kinases that phosphorylate IRF3 and activate signaling in a fashion similar to MAVS [54]. Interestingly, STING can also activate STAT6 for transcriptional induction of ISGs [55]. Ultimately, activation of STING signaling elicits type I IFN induction and similar antiviral response strategies as those seen in MAVS signaling. Thus, while cells use different sensors to detect RNA and DNA viruses, the signaling pathways ultimately converge in similar antiviral response strategies.

1.1.2.1 cGAS

Cyclic GMP-AMP synthase (cGAS) is the primary protein required for type I IFN induction in response to cytosolic DNA. cGAS detects DNA in the cytosol as a result of DNA virus infection or DNA transfection and synthesizes the second messenger cGAMP [56]. cGAMP subsequently binds to STING, leading to its activation [57]. While cGAS was only recently identified, it is already recognized as the primary cytosolic DNA sensor. Indeed, recent reports suggest that cGAS may mediate the ability of other DNA sensors to activate STING and the ISD pathway [58]. cGAS senses DNA viruses such as herpesviruses, human papillomavirus, adenovirus, and hepatitis B virus, as well as retroviruses such as human immunodeficiency virus-1 (HIV-1), simian immunodeficiency virus, and murine leukemia virus [59,60]. Additionally, cGAS plays a role in the innate immune response to a number of positive-sense RNA viruses, although cGAS is likely activated by mitochondrial DNA released into the cytosol due to mitochondrial damage during infection, rather than sensing of viral RNA [61-63].

Structural studies on cGAS have provided important insights into how it recognizes DNA and synthesizes the second messenger cGAMP. cGAS is composed of an N-terminal unstructured region, followed by a nucleotidyl transferase domain, and a C-terminal male abnormal 21 domain [56]. Resting cGAS exists in a bilobal conformation, with a zinc thumb located between the lobes. cGAS binds to dsDNA via this zinc thumb, which induces a conformational change in cGAS. The catalytic pocket of cGAS is then accessible for synthesis of cGAMP [60,64,65]. This synthesis generates 2’3’-cGAMP, an endogenous cGAMP, which contains two unique phosphodiester bonds [60,66-68]. Interestingly, 2’3’-cGAMP binds STING with much higher affinity than cGAMP molecules with different phosphodiester linkages, demonstrating the importance

of the specific product of cGAS to activate innate immunity [68]. This production of cGAMP is essential for STING activation, as catalytically inactive cGAS does not induce type I IFN, despite its ability to bind DNA [56]. cGAMP activates STING by inducing a conformational change after which STING dimerizes and is subject to K63-linked ubiquitination by TRIM56 and TRIM32 [69,70]. Further mechanisms governing cGAS activity, such as regulation by other PTMs, remain uncharacterized. Given its widespread or ubiquitous expression and the requirement of cGAS in the ISD pathway, future studies to uncover these regulatory mechanisms will be of great interest.

1.1.2.2 DAI

DNA-dependent activator of IFN-regulatory factors (DAI) was the first cytosolic DNA sensor of antiviral innate immunity to be discovered [71]. DAI binds to cytosolic DNA derived from both viruses and host cells [71,72]. Viruses sensed by DAI include herpes simplex virus-1 (HSV-1), human cytomegalovirus (HCMV), and mouse cytomegalovirus (MCMV) [71-73]. Interestingly, the ability of DAI to sense self DNA in the cytosol may play a role in the development of autoimmune disease. For example, DAI expression is upregulated in people with systemic lupus erythematosus (SLE), and in SLE mouse models [74]. The role of DAI in initiating the IFN response to cytosolic DNA appears to be either cell type-specific, or redundant, as DAI-deficient mice and cells derived from these mice elicited normal IFN responses to both DNA virus infection and synthetic DNA [75,76].

The mechanism by which DAI senses cytosolic DNA is not well understood. A recent study used *in vitro* pull-down assays to show that DAI binds to DNA in a sequence-independent, but length-dependent manner [76]. Interestingly, this study also shows that DNA may serve as a scaffold upon which DAI can aggregate and that

artificial dimerization of DAI induced type I IFN expression in the absence of DNA, suggesting that dimerization or oligomerization of DAI drives downstream signaling [76]. Further research will be required to gain a better understanding of the mechanisms by which DAI senses DNA. While STING is known as the major adaptor protein in DNA sensing pathways, it has not been clearly demonstrated that DAI signals through STING [77]. Interestingly, DAI has recently been shown to play a role in detection of influenza A viral RNA species and activation of MLKL-dependent necroptotic cell death, establishing a role for DAI as a sensor of foreign RNAs, in addition to its DNA sensing properties [78]. Therefore, while DAI may be dispensable for the innate immune response to viral DNA, future efforts should focus on dissecting the DAI pathway, given its possible roles in cell type-specific antiviral responses, and its contribution to autoimmune diseases.

1.1.2.3 AIM2-like receptors (ALRs)

The ALRs are a family of proteins that have also been suggested to acts as sensors of the ISD pathway [79,80]. They are also known to be required for inflammasome activation in response to multiple pathogens [81-83]. The inflammasome is an inflammatory response induced following transcriptional activation of caspase-1, which then cleaves IL-1 cytokines into IL-1β and IL-18 to promote inflammation [84]. The ALR family consists of five members in humans: absent in melanoma 2 (AIM2), gamma-interferon-inducible protein 16 (IFI16), Pyrin and HIN domain family member 1 (PYHIN1), myeloid cell nuclear differentiation antigen (MNDA), and Pyrin domain-only protein 3 (POP3). AIM2 and IFI16 are the two most prominent members of the ALR family and are members of the pyrin and HIN domain (PYHIN) family. Both AIM2 and IFI16 have been shown to be required for inflammasome activation after DNA virus sensing. AIM2 activates inflammasomes in response to herpes simplex virus-1 (HSV-1),

vaccinia virus, and mouse cytomegalovirus [83], whereas IFI16 activates inflammasomes in response to HSV-1 [85].

In addition to its role in inflammasome activation, IFI16 activates the ISD pathway by sensing non-self DNA in both the nucleus and cytosol [79,80]. Depletion of IFI16 has been shown to dampen the IFN response to viruses such as the retrovirus HIV-1, HSV-1, and human cytomegalovirus (HCMV) [86-88]. While these studies have implicated IFI16 as an important sensor of both cytosolic and nuclear foreign DNA, a recent study demonstrated that in mice, ALRs are not required for the ISD response **[89]. Further, by using genetic knockouts, human IFI16 was shown to be non-essential for the IFN response to HCMV infection. Alternatively, cGAS was essential for the ISD response in both mice and human cells. [89]. Thus, similar to DAI, ALRs such as IFI16 either serve a cell type-specific role in initiating the ISD pathway or have a redundant role with other factors. These recent findings highlight the uncertainty surrounding many putative DNA sensors, and the clear requirement of the recently discovered cGAS as the PRR of the ISD pathway.

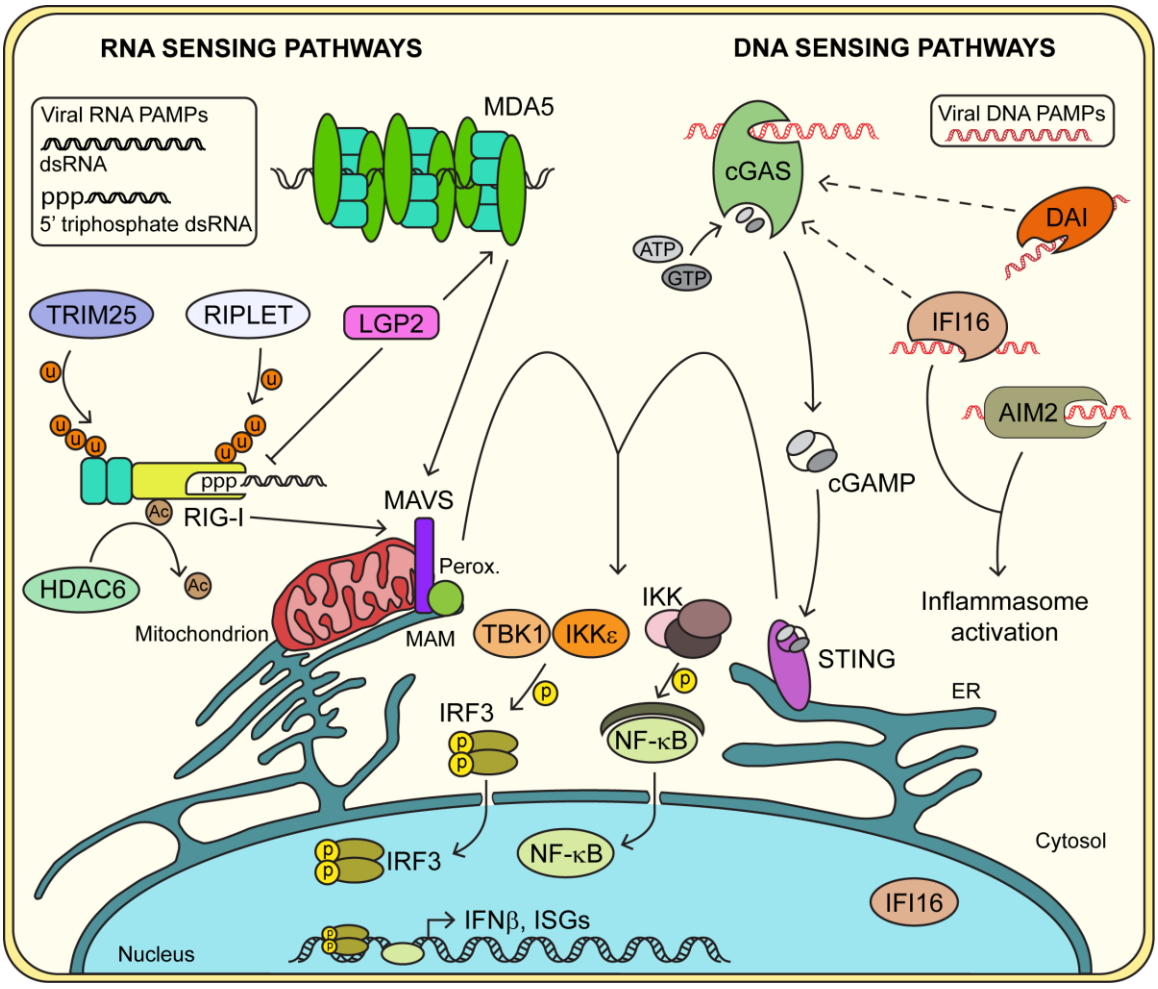

Figure 1: Cytosolic sensing of viral nucleic acids.
Following RIG-I sensing of short dsRNA, this sensor is further activated through K63-linked ubiquitination by TRIM25 and RIPLET, as well as through lysine deacetylation by HDAC6. Following sensing of long dsRNA, MDA5 oligomerizes along the dsRNA. Both RIG-I and MDA5 activate signaling through the adaptor MAVS located on mitochondria, mitochondrial-associated ER membranes (MAM), and peroxisomes (perox.), leading to the activation and nuclear translocation of IRF3 and NF-κB and the production of type I IFN and ISGs. Viral DNA PAMPs are sensed by cGAS which catalyzes the production of cGAMP after binding to DNA. cGAMP then signals through the adaptor STING, located on ER membranes to activate IRF3 and NF-κB. Other viral DNA sensors in the cytosol such as DAI and IFI16 are also postulated to function through this pathway. Activation of IFI16 or AIM2 following viral DNA detection leads to inflammasome activation. Figure from [1].

1.1.3 Convergence of signaling pathways on IFN-stimulating transcription factors

While different cytosolic PRRs recognize distinct PAMPs and activate different signaling pathways, they ultimately converge on the activation of the transcription factors IRF3, IRF7, and NF-κB. This suggests that, despite needing unique surveillance proteins to recognize unique viral pathogens, cells ultimately respond to these diverse cytosolic PAMPs in very similar ways. A shared function of IRF3, IRF7, and NF-κB is the production of cytokines, especially type I IFNs. The fact that cytosolic sensing pathways converge on type I IFN production demonstrates the importance of this cytokine for antiviral responses.

1.2 Type I IFN response

1.2.1 Antiviral roles of type I IFNs

Interferons were first discovered in 1957 when researchers realized that influenza virus-infected chick embryo cells produced and released a substance into the surrounding fluid that would induce viral interference in uninfected cells. This substance did not appear to be derived from the virus, but rather produced by cells and was hypothesized to be a small protein called interferon [90,91]. Subsequent findings led to the discovery of multiple families of interferons and the importance of type I IFNs for viral restriction, as well as the pathway and responses activated by type I IFNs (Table 1) [92]. Type I IFNs elicit autocrine and paracrine cellular responses that induce the transcriptional upregulation of hundreds of ISGs, and many of these genes encode antiviral effector proteins [93], which are essential for viral restriction [94,95]. The type I IFN response is very efficient; indeed, transcriptional induction of many ISGs is observable within 15 minutes of IFN stimulation [96,97]. This activation occurs as type I

IFNs bind to their dimeric receptor (IFNAR), composed of IFNAR1 and IFNAR2 [98-100]. Then, IFNAR engagement activates the Janus family kinases JAK1 and TYK2 [101,102], which phosphorylate the transcription factors STAT1 and STAT2 [103,104]. This allows the heterodimerization of STAT1 and STAT2, which act as both signal transducers and transcription factors, and their interaction with an additional transcription factor, IRF9, to form the ISGF3 transcription factor complex [105,106], although more recent evidence suggests that ISGF3 formation may occur when activated STAT1 associates with pre-formed STAT2-IRF9 dimers in the nucleus [107]. Nuclear ISGF3 then binds to interferon-stimulated response elements within the promoters of ISGs to elicit their transcriptional activation (Figure 2). The production of ISGs creates a complex antiviral cellular state, in which cells can restrict multiple stages of viral replication [108].

Table 1: Discoveries that have revealed the JAK-STAT pathway (figure from [92])

Year	Milestone
1957	Isaacs and Lindenmann describe interferon
1975–1977	Oligonucleotide [2′-5′ oligoadenylates(s)] inhibitors of protein synthesis induced by IFN found
1979	Actinomycin-sensitive IFN-β-dependent new protein induction shown
1984	IFN-α-induced transcriptional stimulation of specific genes (ISGs) demonstrated; no new protein synthesis required
1986–1988	IFN-dependent promoters identified (ISREs, interferon-stimulated response elements)
1988–1989	IFN-α-induced ISRE binding protein complexes (ISGF3; E complex) in cytoplasm in 1–2 min; in nucleus in 5 min
1989	Genetic selection system for defective IFN-induced transcription described and first cell mutant selected
1989	IFN-γ-dependent promoters (GAS, gamma IFN-activated sequences, and GAF, gamma IFN-activated factor) identified
1989–1991	JAKs 1 and 2 and TYK2 identified
1990	ISGF-3 partially purified; identified subunits 113, 91, 84, 48

1991	Noncomplementing mutant cells unresponsive to both IFN-α and IFN-γ described
1992	cDNA clones sequenced later called STAT1 (a and b) and STAT2; RNA for IRF9 completing make up of ISGF3, establishing STAT family of proteins
1992	First IFN response mutant identified as Tyk2 by molecular complementation
1992	Upon IFN activation by IFN-α STAT1 and STAT2 are tyrosine phosphorylated; STAT1 also tyrosine phosphorylated after IFN-γ treatment
1993–1994	Major signaling events driven by IFN and IL-6 pinpointed by molecular complementation of mutant cells
1994	JAK3 described and sequenced
1994–1995	STAT3, 4, 5A, 5B, and 6 all described and sequenced
1995–1998	Functional and structural domains of STATs described
1996	*Drosophila* STAT (dSTAT92E) first described; later studied extensively genetically
1996	Mouse genetics identifies physiological functions for all STATs in various specific cells
1997	Negative regulation of pathways initially characterized
1998	First crystal structures of STATs
2000	Initial information that human mutations in JAKs and STATs and persistent activation of STATs cause disease
2000	First posttranslational modifications of STATs in addition to phosphorylations noted (methylation, acetylation, etc.)
2001	Comprehensive gene target sets identified

In addition to its role in initiating antiviral cellular programs in infected cells and neighboring bystander cells, the type I IFN response also results in the production of other cytokines, such as CCL2, CXCL10, TNF, IL-1, IL-6, IL-8, IL-12, IL-18, and others [109]. Many of these cytokines have specific proinflammatory functions and recruit immune cells such as monocytes, T cells, natural killer cells, and dendritic cells [110]. Additionally, the type I IFN response promotes antigen presentation to initiate the adaptive immune response and further enhances the adaptive immune response by regulating the effector functions of T cells and antibody production [110]. Thus, the essential role of type I IFNs in antiviral responses begins with the upregulation of viral restriction factors at the intracellular level, but also expands to regulation of systemic adaptive immune responses for viral clearance.

Evidence of the importance of type I IFNs and the type I IFN response is abundant. A recent report revealed that a patient with IFNAR1 deficiency succumbed to herpes simplex virus-1 induced encephalitis, which is a rare clinical manifestation of a fairly ubiquitous virus [111], thus demonstrating the importance of the type I IFN response for controlling the replication of common pathogenic viruses. An additional report revealed that neutralizing auto-antibodies against type I IFNs may account for life-threatening COVID-19 pneumonia in at least 2.6 percent of these cases in women and at least 12.5 percent in men [95]. This study demonstrates the importance of type I IFNs for immune responses to emerging pathogenic viruses in the human population. In order to overcome the type I IFN response as a barrier to infection, many viruses encode factors to interfere with IFN production or IFN signaling, and may also target certain antiviral proteins for degradation or cleavage [112]. Indeed, in order to recapitulate the pathogenesis of human viruses in murine models, type I IFN response deficient animals are often required, as certain families of viruses have not evolved to counteract the murine type I IFN response [113]. All of these examples demonstrate the crucial role of type I IFNs and the ability to induce the type I IFN response for viral restriction.

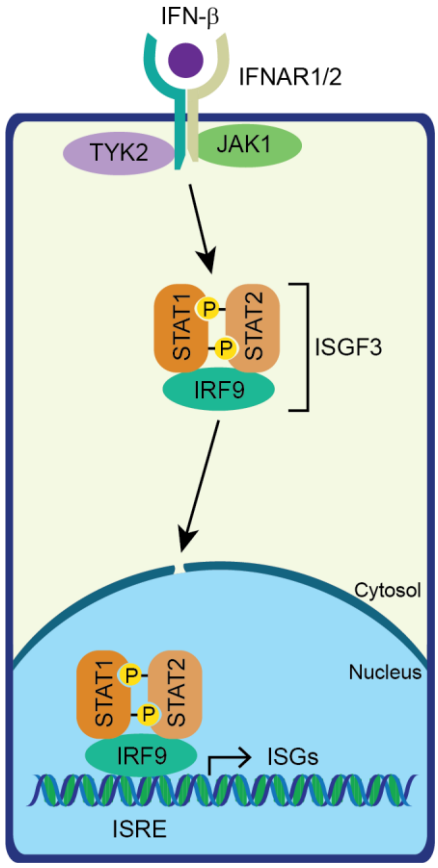

Figure 2: The type I IFN response pathway.

1.2.2 Regulatory factors governing ISG expression

The low basal expression of ISGs and their inducibility through the JAK-STAT pathway suggests that these genes can also have detrimental effects on host cells and tissues if their expression is prolonged or constant. Indeed, certain ISGs are linked to cancer and must be properly regulated for other biological processes such as the cell cycle and embryonic development [114-117]. Additionally, type I IFN overproduction can lead to type I interferonopathies, including Aicardi Goutieres Syndrome, systemic lupus erythematosus, and vasculopathies [118]. For these reasons, type I IFNs also induce genes whose functions are to suppress the JAK-STAT signaling pathway, such as the

suppressor of cytokine signaling family proteins SOCS1 and SOCS3, which bind to JAK1 and TYK2 and inhibit their catalytic activity [119,120]. Additionally, USP18 is an IFN inducible repressor of the JAK-STAT pathway, which competes with JAK1 for binding to IFNAR2, repressing the activation of JAK1 [121]. Thus, the type I IFN response includes a negative feedback loop in order to restore cells to their basal state after IFN activation.

The signaling proteins involved in the activation of the type I IFN response and these negative regulatory proteins are the primary basis for regulation of this response. However, it is notable that ISGs are induced to differing potencies, and even have distinct activation kinetics [97], revealing that additional regulatory controls govern the activation of ISGs on an individual basis. Additionally, a number of reports have revealed differential activation of subsets of ISGs, demonstrating that additional molecular controls function in regulating the expression of certain ISGs [122-125] Several additional regulatory controls for the activation and suppression of ISGs are understood, and these controls govern multiple layers of gene expression. For example, epigenetic modifiers have been shown to regulate the transcription of ISGs. The chromatin-remodeling BAF complex is recruited to ISG promoters by ISGF3 to maintain open chromatin and allow transcription [126,127]. Alternatively, the lysine methyltransferase EHMT2 suppresses ISG transcription through specific di-methylation of histone H3 [128]. At the post-translational level, protein modifications such as tyrosine and serine phosphorylation of STAT1 and STAT2 regulate their activation [129]. Thus, reversible modifications are important regulators of the type I IFN response. Post-transcriptional regulation of this response is poorly understood and mostly limited to a few examples of microRNAs that regulate signaling molecules [130-132], or RNA binding proteins that

regulate the stability of ISG transcripts [133]. How RNA base modifications govern the type I IFN response pathway and the expression of individual or subclasses of ISGs has not yet been explored, although the cap1 modification appears to regulate the translation of certain ISGs [134].

RNA base modifications are emerging as important regulators of cellular responses to external stimuli, such as stress responses [135-140] or stem cell development and fate decisions [141,142]. As the type I IFN response is an example of a cellular stress response whose activation must be finely tuned, the role of RNA base modifications in regulation of this response is an exciting avenue to explore, and is the basis for the work presented in this dissertation.

1.3 RNA base modifications and N6-methyladenosine (m^6A)

RNA base modifications are specific chemical moieties that are added to nucleosides within mRNA transcripts or other RNA species and are essential regulators of RNA metabolism [143-145]. Prior to the maturation of an mRNA, a number of processes occur, such as 5' 7-methylguanosine capping, which protects mRNAs from degradation and aids in their translation [146], splicing to remove intronic regions and generate further diversity of the expressed proteome [147], and 3' polyadenosine tailing, which influences mRNA stability, localization, and translation [148]. mRNA processes are highly coordinated by RNA binding proteins and ribonucleoprotein complexes, also known as RNA regulons [149]. In addition to the relatively well-understood functions of 5' 7-methylguanosine cap, splicing, and 3' polyadenosine tailing, the functions of a number of internal RNA base modifications are beginning to be elucidated, and recent years have yielded many important discoveries for these modifications, many of which have

emerging roles in regulation of transcript stability (Figure 3) [144,150]. The most common internal base modification of eukaryotic mRNA is N6-methyladenosine (m^6A), and our understanding of the functions of this modification has rapidly expanded in the last decade [151]. While the presence of internal m^6A modification of mRNA was first described in the 1970s [152-155], it was not until recent years that its functions have begun to be elucidated. This renaissance in m^6A research was enabled by a number of crucial technical advances and discoveries that have enabled research describing the mechanistic functions of m^6A, as well as the role of m^6A in many biological processes [156]. These sections will highlight pivotal advances that have enabled systematic studies of m^6A function, and the effects of m^6A on modified mRNA and biological processes.

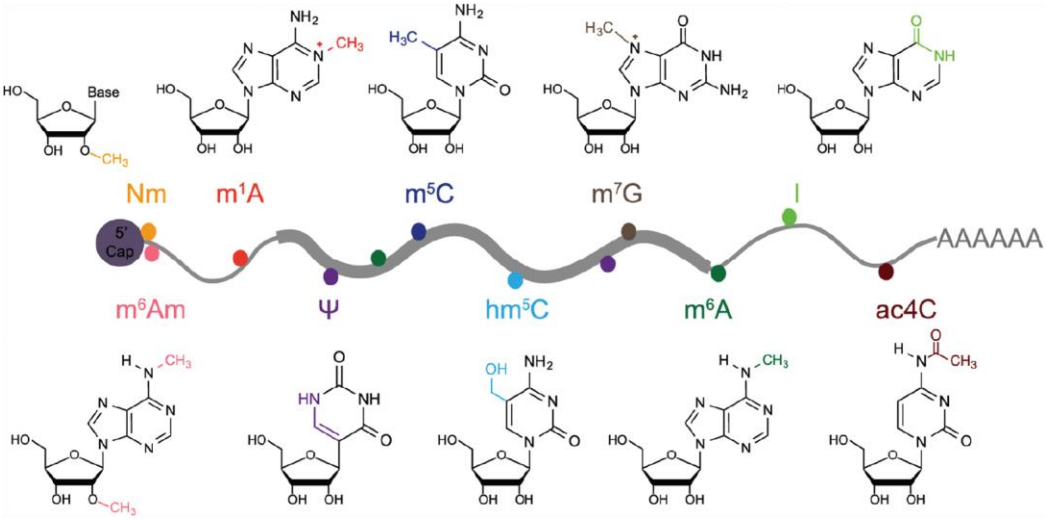

Figure 3: RNA base modifications in eukaryotic mRNA.
In addition to the 5' cap (7-methylguanosine, m^7G), a number of additional modifications can occur on eukaryotic mRNA: the first transcribed nucleotides contain 2'O methylation (Nm) or 2'O,N6-dimethylation (m^6Am); additional internal modifications include N1-methyladenosine (m^1A); pseudouridine (Ψ); 5-methylcytosine (m^5C); 5'hydroxymethylcytosine (hm^5C); N6-methyladenosine (m^6A), inosine (I), and N4-acetylcytosine (ac^4C). Figure from [150].

1.3.1 Mapping m^{6}A in the transcriptome

A major advance for the detection of m^{6}A and mapping of sites of m^{6}A modification globally within the transcriptome was the development of antibodies that specifically recognized m^{6}A within an RNA molecule and their application in m^{6}A mapping techniques, the first of which is known as m^{6}A-seq or methyl RNA immunoprecipitation and sequencing (meRIP-seq) (Figure 4) [157,158]. This technique utilizes immunoprecipitation of fragmented cellular RNA (~150 base pairs) with an anti-m^{6}A antibody, allowing specific purification of m^{6}A-modified RNA regions. A portion of the total RNA is also kept separately, such that both the immunoprecipitated fraction and the total RNA fractions can be subjected to downstream next-generation sequencing. Regions of RNA that are enriched in the immunoprecipitated fraction can then be identified across the transcriptome using software for bioinformatics analysis. The first studies to employ meRIP-seq revealed that, across the transcriptome, m^{6}A is enriched within the 3'UTR and the last exon of mRNAs [157,158]. The 3'UTR is a common binding site for RNA binding proteins and microRNAs, which exert regulatory functions on mRNA [159]. Therefore, these studies suggested m^{6}A could regulate mRNA expression by modulating mRNA interactions with regulatory factors. Additionally, this m^{6}A distribution and methylation of many individual transcripts was conserved in human cells and murine cells, suggesting evolutionarily conserved functions for the modification [157,158].

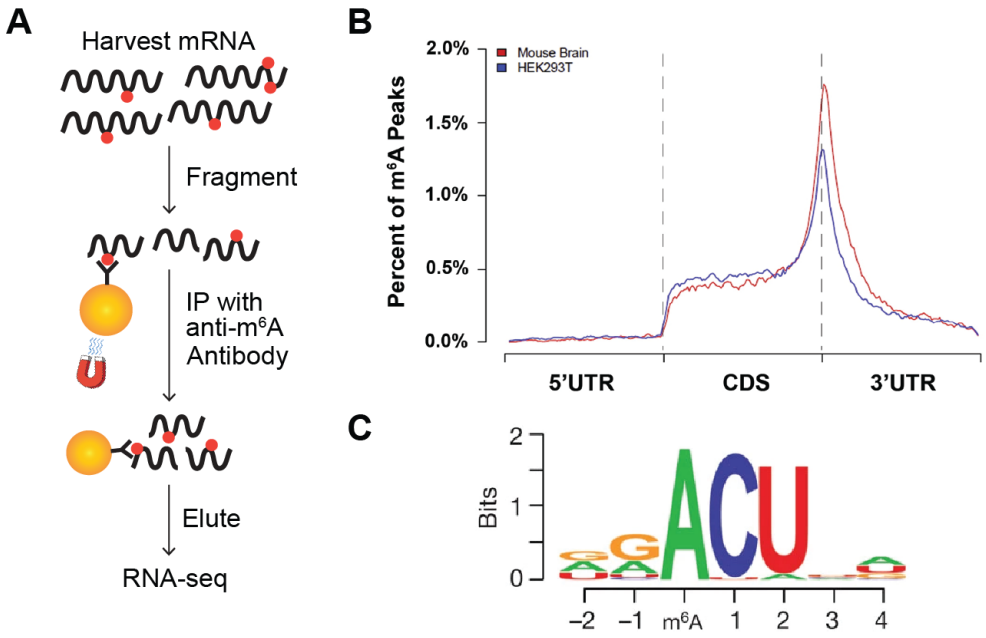

Figure 4: The distribution of m^{6}A within cellular mRNA.
(A) Schematic of meRIP-seq workflow. **(B)** Metagene plot showing the distribution of m^{6}A within cellular mRNA from the mouse brain or human HEK293T cells. Adapted from [157]. **(C)** m^{6}A is enriched within a degenerate consensus motif. Adapted from [158].

These studies also revealed that m^{6}A exists within a degenerate consensus sequence motif, most often occurring within a GGA^{m}CU sequence, and with [G/A]AC seeming to be a minimal sequence requirement for m^{6}A modification [157,158]. However, these sites are not always modified, revealing that there are likely additional sequence or structural factors that guide m^{6}A deposition, as well as trans-regulatory factors that have yet to be fully understood. Indeed, understanding the factors that guide the specificity and selectivity of m^{6}A modification remains one of the most pressing challenges for the field. Additionally, meRIP-seq relies on RNA fragmentation, which results in regions of enrichment of modified RNAs, but does not give exact information as to which nucleotide is modified. As multiple candidate m^{6}A motifs can exist within a fragment enriched by meRIP-seq, knowing which specific adenosine residue is modified, or whether multiple modifications may be present within fragments is challenging.

meRIP-seq also does not reveal stoichiometry, or what percentage of a specific transcript is modified by m^{6}A. Some biochemical techniques exist for identification and quantification of m^{6}A at a single nucleotide level [160,161], but these are labor intensive and difficult and thus are less frequently employed. The development of m^{6}A mapping techniques utilizing cross-linking at or near individual m^{6}A sites and enabling the detection of m^{6}A at single nucleotide resolution is a major advance for m^{6}A mapping technology, but also faces additional challenges relative to meRIP-seq, such as the need for more biological input material and more labor intensive protocols [162,163]. The reliance of these mapping techniques on commercially available antibodies may also lead to biases in m^{6}A mapping such as false positives or false negatives where the antibodies do not recognize specific m^{6}A sites [164]. Therefore, additional advances in m^{6}A mapping technologies will enable more precise m^{6}A mapping within the transcriptome and future discoveries for the field at large.

1.3.2 The cellular m^{6}A machinery

The discovery of the cellular enzymes that control m^{6}A deposition on RNA was another crucial advance for the discovery of m^{6}A function, as these findings led to the ability to easily perturb m^{6}A levels within the transcription through manipulation of the expression of these enzymes. m^{6}A deposition is controlled by a complex of proteins minimally composed of the methyltransferase like proteins METTL3 and METTL14, of which METTL3 is the catalytic subunit [165,166] (Figure 5). Additional proteins associate with this m^{6}A methyltransferase complex and help to guide its specificity, including WTAP, VIRMA, HAKAI, ZC3H13, and RBM15 [167-170]. m^{6}A deposition is thought to occur co-transcriptionally, and the methyltransferase complex has been shown to associate with RNA polymerase II [171]. Interestingly, m^{6}A is also a reversible

modification and its removal can be mediated by proteins within the AlkB homology family, namely FTO and ALKBH5 [172,173]. The discovery that m^{6}A is a reversible modification was particularly exciting, as it suggested that this modification could be removed dynamically in response to external stimuli to regulate mRNA functions, analogous to epigenetic modifications of DNA or post-translational modifications of proteins. However, it is unclear whether m^{6}A removal occurs in the cytosol [174], thus the addition and removal of m^{6}A likely mainly occur in the nucleus, but it is clear that cellular responses to stimuli can alter the occurrence of m^{6}A on specific transcripts. This may occur through changes to transcription dynamics, alterations to the methyltransferase complex such as post-translational modifications or differential interactions with RNA-binding proteins, or alterations to the m^{6}A demethylase proteins, such as post-translational modifications or competition for m^{6}A binding [135,175-177].

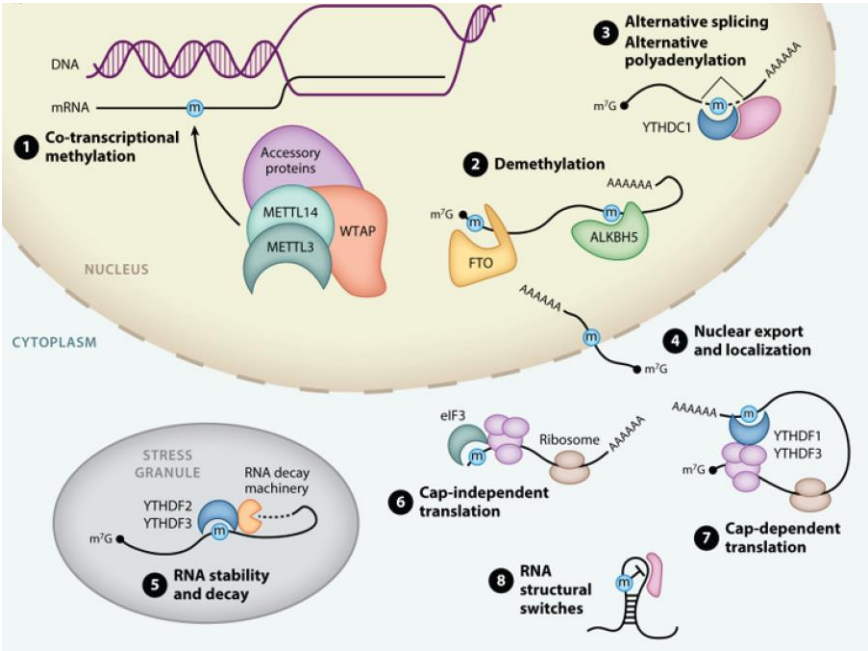

Figure 5: The cellular m^{6}A machinery and its functions.
Figure from [178].

m^{6}A modification can induce structural changes to mRNAs, which can facilitate or inhibit their interactions with RNA binding proteins [164,179-181]. In particular, certain proteins have been well characterized for their ability to recognize m^{6}A and elicit various functions on modified transcripts. The most well-studied of these m^{6}A binding 'reader' proteins are within the YTH domain family of proteins, including YTHDF1, YTHDF2, YTHDF3, YTHDC1, and YTHDC2 [182]. The YTHDF proteins are primarily cytoplasmic and thus they regulate cytoplasmic RNA processes of m^{6}A-modified transcripts. YTHDF1 is primarily known for its role in enhancing the translation of m^{6}A-modified transcripts [183], while YTHDF2 facilitates the interaction of m^{6}A-modified transcripts with the cellular mRNA decay machinery, thus enhancing turnover of modified RNAs [184], and YTHDF3 is thought to be involved in both of these processes through interactions with YTHDF1 and YTHDF2 [185]. While initial discoveries of the roles of the YTHDF proteins appeared to assign distinct roles to YTHDF1 and YTHDF2, more recent findings suggest that these proteins may have overlapping functions and be involved in the same processes [185-187], although the functions of these proteins are probably not entirely generalizable as they appear to elicit transcript-specific effects. The nuclear m^{6}A reader protein YTHDC1 is involved in regulation of polyadenylation and splicing [188], and YTHDC2 enhances both mRNA degradation and translation through interactions with the 5'-3' exoribonuclease XRN1 and the small ribosomal subunit, respectively [189]. In addition to the YTH domain proteins, a number of additional proteins that preferentially bind to m^{6}A have been identified, as well as several that are repelled by m^{6}A [180,181]. Many of these discoveries have only been made in recent years, and the roles of m^{6}A binding proteins and the transcript-specific effects of m^{6}A are still emerging. However, m^{6}A appears capable of exerting regulatory effects on all aspects of mRNA

metabolism (Figure 5), and through these effects, m^{6}A can modulate many biological processes.

1.3.3 m^{6}A regulation of biological processes

Through its many effects on modified mRNAs, m^{6}A controls many cellular pathways and biological processes, and our understanding of these effects of m^{6}A is rapidly expanding. Among the first biological roles discovered for m^{6}A are its regulation of heat shock stress, during which m^{6}A enhances the translation of heat shock-induced genes [135,136], and the ability of stem cells to differentiate and maintain pluripotency [141,190,191]. These studies revealed that m^{6}A is important for cellular responses to external stimuli as well as cell development and identity. m^{6}A was also found to be critical for mammalian development, as METTL3 deletion resulted in embryonic lethality [141]. The biological roles of m^{6}A are vast, including organismal differentiation, cell differentiation, stress responses, hematopoiesis, immune cell function, oncogenesis, circadian rhythm, and neural function [140,141,190-203].

Another interesting role of m^{6}A is regulation of viral infection (reviewed in [178]). Recent studies have shown that m^{6}A can regulate the expression of viral genes for DNA viruses, RNA viruses, and retroviruses. Additionally, m^{6}A has diverse roles in regulating viral RNA processes. We were among the first groups to reveal a role for m^{6}A during viral infection, when we discovered that the m^{6}A machinery regulates hepatitis C virus (HCV) infection [187]. We identified a region of m^{6}A modification on the RNA genome of HCV that regulates its packaging into virions. However, the contributions of m^{6}A regulation of host processes during viral infection were not clear, and I was interested in exploring the role of m^{6}A during viral infection. Some of these roles are now emerging

and our understanding of m^{6}A modulation of host processes that can influence viral infection has grown significantly.

1.4 m^{6}A regulates viral processes and host responses to viral infection

During viral infection, the molecular processes of host cells are altered as viruses co-opt, usurp, or inhibit cellular machinery to facilitate their replication. Recent studies have revealed that chemical modification of RNA is an example of a host processes that viruses can exploit. In particular, the role of the RNA modification m^{6}A during viral infection has generated a great deal of interest. m^{6}A can regulate many aspects of RNA biology [204], including RNA structure, splicing, stability, localization, and translation [173,179,183,184,205], thus its effects on viral RNAs are diverse (reviewed in [178]). In addition to these effects, m^{6}A has been shown to regulate cellular responses to viral infection, which is the focus of this section. m^{6}A is deposited on RNA by a cellular complex of 'writer' enzymes, composed of METTL3 and METTL14 (METTL3/14) [166] and other proteins [168,206] and is the most abundant chemical modification to eukaryotic mRNA. Its effects on RNA metabolism are mediated by m^{6}A 'reader' proteins, such as the YTH domain family proteins (YTHDF1, YTHDF2, YTHDF3, YTHDC1), and others [207]. Additionally, m^{6}A can be removed from RNA by demethylase 'eraser' proteins including FTO and ALKBH5 [172,173]. Because m^{6}A can affect both viral and host processes, its regulatory effects on viral infection are complex. A more complete understanding of the effects of m^{6}A at the virus-host interface will require additional understanding of its effects on the cellular response to infection.

Viruses are equipped with strategies to manipulate host gene expression and cellular processes in ways that promote their replication. Meanwhile, host cells modulate

their own processes in response to infection to limit viral replication. First, host cells PRRs to detect PAMPs and initiate innate immune responses [208]. Signaling molecules called cytokines can then be produced to transmit innate immune signals for the expression of antiviral genes that directly limit viral infection and to orchestrate functional adaptive immune responses [209]. Many viruses have also developed mechanisms to inhibit host innate immune responses [112]. Therefore, the interplay between viruses and their host cells is intricate and complex, resulting in cells undergoing many dynamic changes during infection. m^6A regulates many biological processes, including stress responses such as the integrated stress response, heat shock, and UV damage [135,137,139], and therefore likely regulates these or other stress responses important for viral infection. Recent research has shed light on the regulatory roles of m^6A on host responses to viral infection, including detection of viral RNA, innate immune pathways, stress response pathways, and metabolism; however, many intriguing questions in this field have yet to be explored. This section highlights recent discoveries describing the mechanisms by which m^6A regulates host processes during viral infection and some of the most pressing questions for future research.

1.4.1 Sensing of m^6A-modified RNAs

PRRs that detect foreign RNA depend on specific molecular signatures and structures to distinguish these RNAs from host RNAs. Recognition of viral nucleic acids is an important cellular surveillance strategy, and the ability to protect ‘self’ nucleic acids from detection by PRRs is essential to avoid autoimmune disease [210] (see also Chapter 1.1.1). Interestingly, RNA modifications such as the 7-methylguanosine cap (cap0) and 2’O methylation of the first and second transcribed nucleotides (cap1 and cap2) play essential roles in distinguishing self from non-self RNAs within the cytosol of

cells. Mimicry or co-option of capping and 2'-O-methylation processes by viruses to avoid detection by PRRs also demonstrates the importance of these modifications as key determinants of self [19,211].

The role of m^6A in modulating recognition of RNA substrates by PRRs is also beginning to be uncovered (Figure 6). For example, certain Toll-like receptors (TLRs) have been found to respond differently to RNAs derived from different organisms [212]. Human total RNA only weakly stimulates the TNF-α response downstream of TLRs, while bacterial total RNA is a potent stimulator. Interestingly, tRNA from humans or bacteria does not strongly activate TNF-α. Given that tRNA species and human mRNAs are highly post-transcriptionally modified, these data suggested that these modifications may suppress TLR recognition of RNA. Indeed, early studies revealed that in vitro-transcribed RNAs containing modified nucleosides are less potent activators of TLRs than their unmodified counterparts, and m^6A is particularly effective at inhibiting TLR activation [212]. Similarly, in vitro-transcribed polyU/UC RNA from HCV, which is a strong RIG-I ligand, binds poorly to RIG-I when modified by m^6A [213]. These studies suggest a role for m^6A in shielding RNA species from detection by PRRs. An additional study found that m^6A modification of human circular RNAs is necessary to inhibit their recognition by RIG-I, and this study proposes a model in which the m^6A reader protein YTHDF2 sequesters circular RNAs away from RIG-I [214]. While YTHDF2 is generally known for its role in facilitating the degradation of its m^6A-modified target RNAs, it has also been linked to mRNA localization and phase separation [184,215], which could explain its role in circular RNA sequestration. These studies suggest multiple roles for m^6A in prevention of aberrant innate immune activation in response to endogenous RNAs. Additionally, the m^6A writer Mettl3 was found to be essential for suppression of

endogenous long double stranded RNA levels in murine hematopoietic stem cells. These RNA species activate cellular sensors such as MDA5, which specifically detects long double stranded RNAs and, like RIG-I, also signals through MAVS, as well as the OAS-RNase L and PKR-eIF2α pathways. Thus, Mettl3 deletion resulted in aberrant upregulation of ISGs and failure of hematopoietic stem cells to differentiate [216]. The mechanisms by which METTL3 and m^6A suppress endogenous double stranded RNA levels are not yet clear, although m^6A could enable recognition by a reader protein such as YTHDF2 and subsequent degradation of these RNAs, or m^6A could directly modulate the RNA structures to prevent recognition by the described cellular sensors. m^6A-mediated effects on RNA structures have been previously described [164,179], and these effects may be sufficient to interrupt long dsRNA structures and inhibit MDA5 recognition. Together these studies implicate m^6A as an important molecular signature that can contribute to protecting self RNAs from innate immune sensing through sequestration by m^6A reader proteins, preventing RNA binding protein interactions, direct structural changes, or other mechanisms that have not yet been identified.

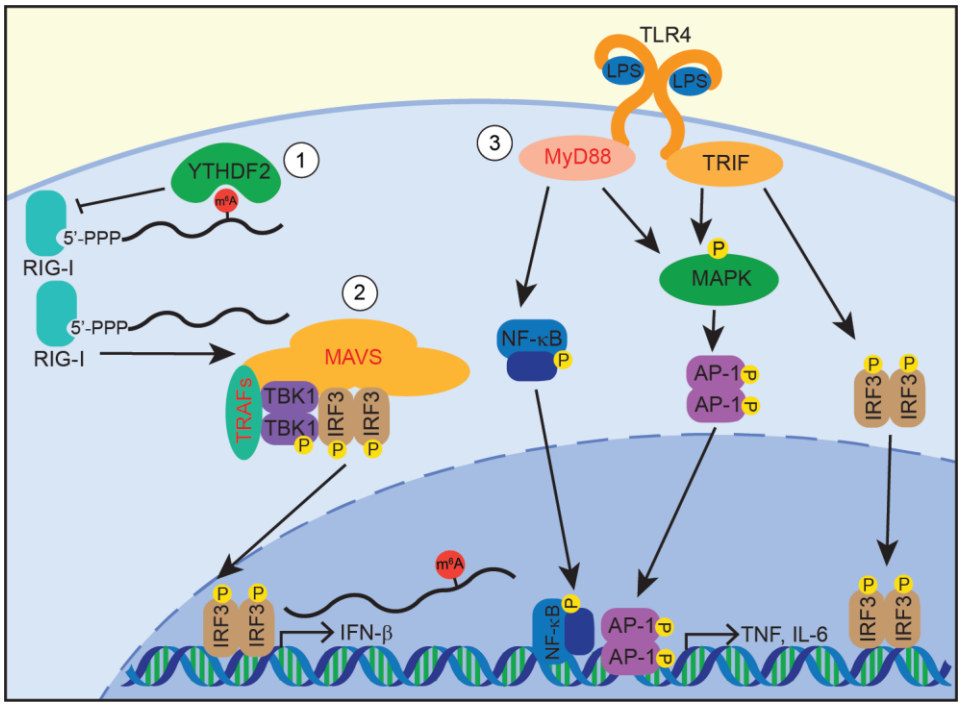

Figure 6: m^{6}A regulates innate immune signaling pathways.
m^{6}A regulates the induction of cytokine responses through multiple mechanisms. 1) m^{6}A, perhaps via interactions with the YTHDF2 protein, inhibits detection of RNAs by RIG-I, whose role is to sense foreign RNAs and activate the MAVS signaling pathway [212-214,216-218]. 2) m^{6}A promotes the expression of MAVS and TRAFs by promoting the nuclear export of their mRNAs [176]. This induces signaling of the MAVS pathway, which activates the transcription factor IRF3 through the interaction of MAVS, TRAFs, and the kinase TBK1. Activated IRF3, along with NF-κB, induces transcription at the IFN-β promoter [1]. 3) METTL3 regulates MyD88 isoform usage in response to LPS stimulation of the TLR4 pathway [219]. TLR4 signals through proteins such as MyD88, MAPKs, and TRIF to activate the transcription factors NF-κB, AP-1, and IRF3. These transcription factors induce the production of proinflammatory cytokines like TNF, IL-6, and IFN-β [220]. YTHDF2 also regulates the TLR4 pathway [221] (not shown). Proteins whose expression are known to be regulated by m^{6}A or m^{6}A-related enzymes are shown in red text.

Supporting the role of m^{6}A in preventing sensing of RNAs by PRRs, recent studies have found evidence that viruses use m^{6}A to protect their RNA from recognition by PRRs. One study found that both the genome, antigenome, and mRNAs of the negative-sense, single-stranded RNA virus human metapneumovirus (HMPV) are m^{6}A-modified [217]. By depleting m^{6}A-related proteins, this study showed that m^{6}A has a

proviral effect for HMPV, likely through its effects on both host and viral RNAs. Abrogation of m^{6}A sites in the HMPV genome resulted in viral mutants that induced more type I IFN and whose replication was attenuated. Interestingly, IFN induction by these mutants was dependent on RIG-I and appeared to be mediated by RIG-I specifically recognizing the m^{6}A-deficient genome and anti-genome, rather than the viral mRNAs. While it is not yet clear how m^{6}A inhibits RIG-I binding to HMPV RNA, it is possible that m^{6}A also inhibits RIG-I oligomerization along the RNA, thus preventing downstream signaling [217]. This study provides evidence of a virus co-opting m^{6}A modification to mask its RNA from cellular PRRs. An additional report suggests that both hepatitis B virus (HBV) and HCV, which have been shown to contain m^{6}A, may utilize similar strategies to avoid innate immune detection [218]. m^{6}A on HBV RNA was previously found to enhance reverse transcription and destabilize HBV transcripts [222], while we showed m^{6}A on HCV inhibits packaging of its RNA genome [187]. A recent study tested the ability of m^{6}A on the RNA of these viruses using in vitro-transcribed viral RNA containing mutations at putative m^{6}A sites and found that these m^{6}A sites potentially inhibited RIG-I recognition of HBV and HCV RNA [218]. However, further work is required to ensure that the putative m^{6}A sites mutated in these studies are indeed modified following transfection of the in vitro-transcribed RNAs will be of importance and to reconcile other differences with the other published work that shows that during infection m^{6}A actually negatively regulates infection [187,222].

The ability of m^{6}A to serve as an additional feature beyond the m^{7}G cap and 2'-O-methylation to mark cellular RNAs as self is an exciting function that the field is just beginning to understand. Future work detailing the mechanisms by which m^{6}A inhibits

activation of RIG-I and other RNA sensors will contribute to our understanding of the functions of m^{6}A during viral infection, and also provide valuable information for designing attenuated vaccines, or for delivery of RNA therapeutics [223-225]. Additionally, whether m^{6}A modification in certain structural or sequence contexts on viral RNA could actually serve as a molecular signature to recruit innate immune surveillance proteins will be interesting to explore further. Indeed, m^{6}A-induced structural alterations in RNA have been shown to regulate RNA binding proteins interactions [179-181]. Additionally, a recent report suggested that, in IFN-stimulated cells, the antiviral protein ISG20 can specifically recognize an m^{6}A-modified site in HBV RNA, perhaps through interaction with YTHDF2, and facilitate degradation of this RNA [226]. Other innate immune effector proteins are also known to recognize specific features of RNAs, such as IFIT1 which inhibits cap0 RNA translation [18,227], or ZAP, which recognizes CG dinucleotides within viral RNA [228]. Therefore, there are many interesting possibilities to explore regarding the roles of m^{6}A for RNA recognition by innate immune surveillance proteins.

1.4.2 Cytokine production and responses

After detection of foreign nucleic acids or other components of viruses, signaling pathways are activated by PRRs that detect specific PAMPs and drive the production of cytokines, such as IFNs, which initiate antiviral responses and orchestrate the adaptive immune response [208]. For example, as mentioned in the previous section, detection of viral RNA by RIG-I or MDA5 activates the MAVS pathway and a signaling cascade that activates proteins such as TBK1, TRAF proteins (TRAF2, TRAF3, and TRAF6), and the transcription factors IRF3 and IRF7 [229]. Interestingly, m^{6}A appears to play a role in the MAVS pathway by regulating the production of several of the signaling molecules in the

pathway (Figure 6). In murine models, it was found that *Mavs*, *Traf3*, and *Traf6* transcripts are m^{6}A-modified, and that DDX46 can bind these mRNAs after viral infection to recruit the m^{6}A eraser ALKBH5, which demethylates these transcripts. Following demethylation, *Mavs*, *Traf3*, and *Traf6* mRNAs are increasingly retained in the nucleus, dampening signaling and production of IFNs [176]. These studies suggest that m^{6}A can promote antiviral signaling pathways by regulating the expression of signaling molecules.

m^{6}A may also be involved in regulation of other PAMP signaling pathways, such as the response to lipopolysaccharide (LPS) (Figure 6). A recent study found that the m^{6}A reader protein YTHDF2 inhibits the inflammatory response to LPS, which signals through TLR4 to activate NF-κB and MAPK signaling [220,221]. However, it is unclear whether this YTHDF2-mediated regulation is dependent on m^{6}A. Additional evidence of a role for m^{6}A in LPS signaling was found in dental pulp cells, in which METTL3 depletion led to increased expression of a particular isoform of MyD88, a signaling molecule in the TLR4 pathway (Figure 6) [219]. This short isoform of MyD88 acts as a dominant-negative regulator of TLR4/MyD88 signaling, and therefore led to decreased activation of NF-κB and MAPK signaling [219]. Therefore, it appears METTL3 may modulate MyD88 splicing to promote the LPS-induced inflammatory response. While m^{6}A can regulate the splicing of certain transcripts [230], it is not yet clear whether *MyD88* mRNA is m^{6}A-modified or whether METTL3 has other trans-regulatory effects on the transcript. Taken together, these studies do seem to suggest roles for m^{6}A in the LPS response. In addition to its recently discovered roles in viral RNA and LPS-driven innate immune signaling pathways, m^{6}A likely has additional roles in other signaling responses that stimulate induction of cytokines and inflammatory responses. Therefore,

future explorations in these areas will be invaluable for understanding the role of m^{6}A in inflammatory conditions and autoimmune disease.

In addition to regulating innate immune signaling pathways, m^{6}A has recently been found to directly regulate the production of the important antiviral cytokine IFN-β [231,232] (Figure 7). Following infection by human cytomegalovirus, the expression of m^{6}A writers, erasers, and reader proteins was found to increase substantially. Interestingly, m^{6}A profiling revealed that after innate immune activation, the *IFNB1* transcript was m^{6}A-modified and that this methylation decreased its half-life [231]. These results suggest that m^{6}A suppresses IFN-β production, which could be exploited by viruses by inducing m^{6}A modification of *IFNB1* mRNA. In further support of this hypothesis, an additional study found that human cytomegalovirus replication was decreased in METTL3 depleted cells due to enhanced expression of IFN-β [232]. This study found that YTHDF2 binds to m^{6}A-modified *IFNB1* mRNA to facilitate its degradation [232]. Thus, these two studies converged on the idea that m^{6}A dampens IFN-β production and contributes to turnover of this proinflammatory cytokine. This regulatory feature of m^{6}A may be important for controlling inflammatory conditions and autoimmunity, which have been linked to excessive IFN production [118]. Additionally, the apparent ability of human cytomegalovirus to exploit this control of IFN-β expression to facilitate its replication by increasing m^{6}A modification of the *IFNB1* transcript and thus decreasing its production is an exciting discovery. Whether other viruses also influence the production of IFN-β or other cytokines by manipulating m^{6}A modification on the transcripts of cytokines or molecules that regulate their production will be an interesting avenue for future research.

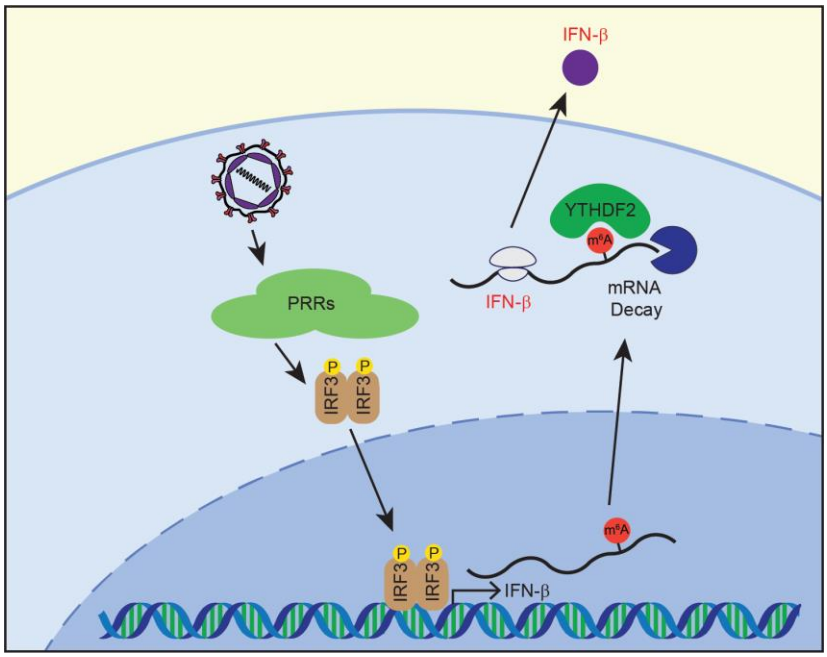

Figure 7: m^{6}A regulates IFN-β expression.
Following viral detection by PRRs and the activation of signaling pathways such as those described above, type I IFNs are produced [1]. The *IFNB1* transcript is m^{6}A modified, and m^{6}A recruits the reader protein YTHDF2 to facilitate *IFNB1* degradation, dampening the production of IFN-β [231,232].

As m^{6}A has been found to regulate the pathways that lead to cytokine production and the transcripts of cytokines themselves, a role for m^{6}A in cellular response pathways induced by cytokines is an interesting area to explore. A recent study in murine models found that the m^{6}A reader protein Ythdf3 indirectly regulates the transcription of ISGs by promoting the translation of *Foxo3*, which represses transcription of a subset of ISGs [233]. Surprisingly, Ythdf3 regulation of Foxo3 occurred independently of METTL3-mediated m^{6}A modification. This study elucidated an interesting role for Ythdf3 in regulating the type I IFN response, although these studies have yet to be replicated in human cells. Aside from this finding, it is unknown how m^{6}A regulates the type I IFN response. As m^{6}A has emerged as an important regulator of viral infection with functions in cytokine induction pathways, its role in regulating the type I IFN response and antiviral

gene expression are an important avenue for research. Does m^{6}A regulate the induction or suppression of the JAK-STAT pathway? Are the transcripts of ISGs regulated by m^{6}A? Could m^{6}A mediated regulation of the type I IFN response influence viral infection? These are among the questions underlying the research presented in this dissertation. In addition to these directions, future research describing how m^{6}A regulates responses to other cytokines will also be of interest, especially as these results would help to inform how m^{6}A regulates the cross-talk between the innate and adaptive immune responses.

1.4.3 Immune cell activation and function

Cytokines produced during viral infection recruit immune cells and influence their maturation and activation. As m^{6}A can control cytokine production, as seen for IFN-β, it likely also regulates the communication between virus-infected cells and immune cells, although this specific type of regulation has yet to be described. However, roles have recently been described for m^{6}A in regulating immune cell function (Figure 8). Dendritic cells (DCs) are a class of antigen presenting cells with important roles in linking innate and adaptive immune responses. m^{6}A has now been shown to regulate DC maturation [196]. Using murine DCs, it was found that Mettl3 promoted DC maturation in a manner dependent on its m^{6}A catalytic activity, likely through its promotion of the translation of the m^{6}A-modified transcripts *CD40*, *CD80*, and *Tirap*. Tirap is a signaling protein in the TLR4/MyD88 pathway, and thus its expression is important for TLR4 signaling and downstream DC activation, whereas CD40 and CD80 are co-stimulatory molecules important for T cell activation. Importantly, DCs lacking Mettl3 are deficient in their ability to promote T cell proliferation, demonstrating the importance of m^{6}A in the maturation and function of DCs [196]. While the relevance of these findings have not been explored

in the context of viral infection, many viruses also stimulate the MyD88 pathway through Tirap [234]. Additionally, it is known that DCs are potent producers of cytokines like type I IFNs in response to viral infection and are crucial for initiation of adaptive immune responses, as they activate naïve T cells [235]. Therefore, these findings provide some insight into potential roles of m^6A in linking the innate and adaptive immune responses to control viral infection.

Interestingly, m^6A also controls the homeostasis and differentiation of naïve T cells [197] (Figure 8). Recent work found that naïve T cells from conditional Mettl3 knockout mice are deficient in their ability to proliferate and differentiate into effector T cells. The model of T cell differentiation used in this study activates JAK1/STAT5 signaling [236], and in Mettl3 knockout T cells, this signaling was impaired, likely due to increased abundance of the transcripts and proteins of key suppressors of this pathway, Socs1, Soc3, and Cish. These transcripts were all m^6A-modified and lost m^6A in Mettl3 knockout naïve T cells, which led to their stabilization [197]. Additionally, m^6A was found to regulate CD4+ regulatory T cells, which are important for controlling inflammation, likely through similar mechanisms [198]. Together, these results elucidate a role for m^6A in the JAK1/STAT5 signaling pathway and in T cell homeostasis.

While the functions of m^6A in immune cells have not been directly studied during viral infection, these studies clearly demonstrate its importance in the normal function and activation of immune cells, which are crucial for viral clearance. Additionally, these results demonstrate how understanding the transcript-specific roles of m^6A in immune pathway regulation and control of immune cell functions will be useful for the development of future immunoregulatory therapies. As m^6A is known to play important roles in stem cell fate decisions [142], cell development and maturation appears to be an

important general biological function of m^{6}A. Therefore, the discovery of additional roles of m^{6}A in DCs and T cells, as well as other immune cell subsets, such as macrophages, natural killer cells, and B cells will be of great importance for our overall understanding of the roles of m^{6}A in immunity.

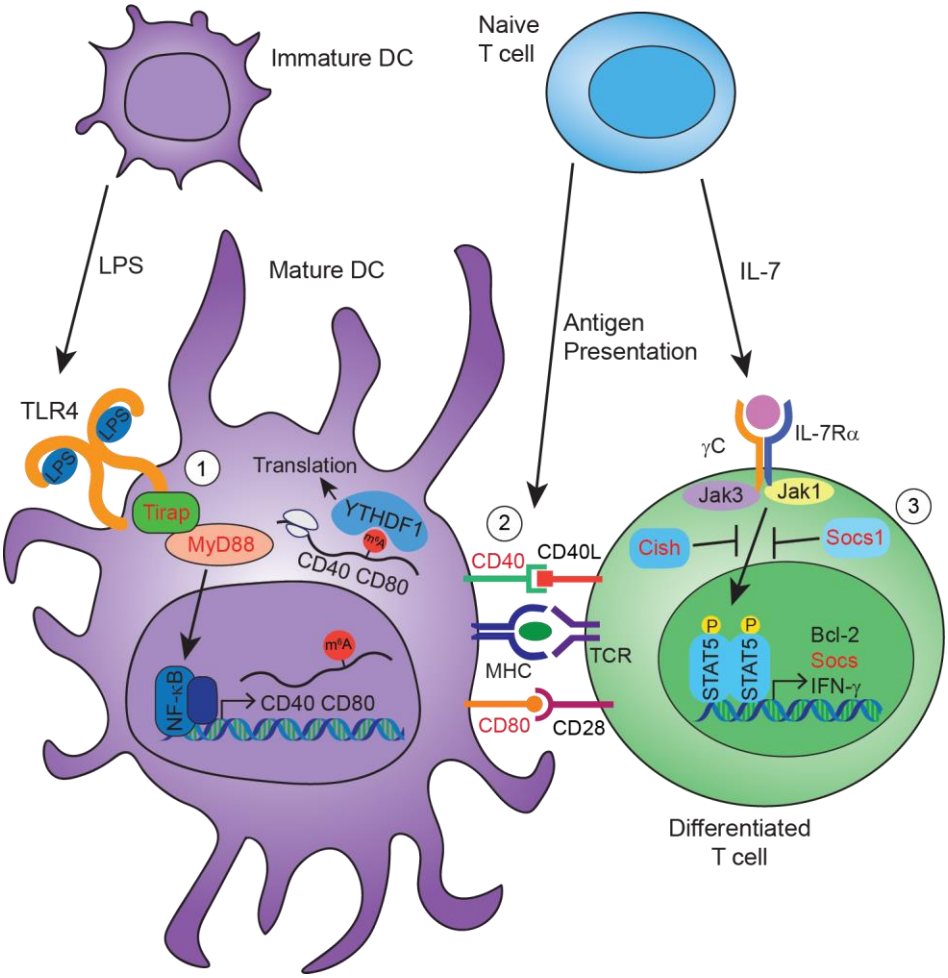

Figure 8: m^{6}A regulates immune cell function.
1) LPS treatment of murine DCs induces signaling through the TLR4/MyD88 pathway to activate the transcription factor NF-κB, which drives transcription of its target genes and DC maturation [220,235]. m^{6}A regulates DC maturation by promoting the translation of *Tirap*, which encodes an important adaptor protein for TLR4/MyD88 interaction [196]. m^{6}A may also regulate MyD88 splicing [219]. 2) After activation, mature DCs can present antigens to T cells to influence their differentiation. This process involves MHC

presentation of antigen peptides and interaction with T cell receptors (TCR), as well the interaction of co-stimulatory molecules such as CD40 and CD80 [235]. m^{6}A contributes to this process by promoting the translation of *CD40* and *CD80* mRNAs [196]. 3) T cells can also be activated by cytokines like IL-7. IL-7 signals through its receptor composed of IL-7Rα and the common gamma chain (γC), activating JAK1 and JAK3, which induce the activation and homodimerization of STAT5, inducing cytokines like IFN-γ and genes involved in T cell survival and differentiation [236]. Additionally, this pathway induces suppressor of cytokine signaling (SOCS) proteins, such as SOCS1 and SOCS3, as well as Cish, all of which repress activation of the IL-7 pathway. The mRNA of Socs1, Socs3, and Cish are m^{6}A-modified, and m^{6}A destabilizes their transcripts, thus promoting the IL-7 pathway and T cell survival and differentiation [197]. Molecules whose expression are known to be regulated by m^{6}A or m^{6}A-related enzymes are shown in red text.

1.4.4 Stress responses and metabolism

In addition to induced immune responses, viral infection can induce cellular stress responses and can influence cellular metabolism [237]. As m^{6}A can regulate many cellular pathways, including stress responses, its roles in infection-induced pathways will be important to understand. Indeed, many studies have found that diverse viral infections shape the m^{6}A distribution within the host transcriptome [175,186,238-240]. However, in-depth functional validation of these m^{6}A changes has been rare, and recent research suggests that some of these findings may be worth revisiting, as gene expression changes can influence m^{6}A peak calling [241]. We recently profiled changes induced to the m^{6}A epitranscriptome during *Flaviviridae* infection using rigorous analyses and investigated functional roles for some of these changes [175]. Of the viruses studied (dengue virus, Zika virus, West Nile virus, and HCV), each induced alterations to m^{6}A modifications on certain transcripts, and some of these alterations were common across all viruses. Among the genes whose m^{6}A status changed during infection by all of these viruses was *RIOK3*, a transcript that gained m^{6}A during infection, which encodes a serine/threonine kinase that may regulate antiviral signaling. Interestingly, innate immune signaling driven by the transcription factor IRF3 was found to be important for the gain of m^{6}A following infection, and m^{6}A modification increased *RIOK3* translation.

The m^{6}A status of *CIRBP*, a stress-induced RNA binding protein, also changed in response to infection, although this transcript lost m^{6}A and consequently was increasingly alternatively spliced to its short isoform. Importantly, ER stress-inducing treatment was sufficient to induce the loss of m^{6}A on *CIRBP*, and *Flaviviridae* infection is known to induce ER stress responses [242]. While the precise mechanisms by which m^{6}A status changes during infection are not clear, these data suggest that activation of host cell pathways during infection can influence the m^{6}A status of individual transcripts. Additionally, many genes with m^{6}A alterations were found to be capable of regulating *Flaviviridae* infection, including RIOK3 and CIRBP. These results point to functional roles for changes to the m^{6}A landscape during viral infection, and set the stage for further investigation of the mechanisms responsible for m^{6}A alterations [175].

Some possible mechanisms by which viral infection could induce changes to the m^{6}A landscape include differential transcription rates of m^{6}A-modified genes, changes in the expression, localization, or function of METTL3/14 or other RNA binding proteins involved in m^{6}A targeting, or similar changes to m^{6}A demethylase proteins like FTO or ALKBH5. Indeed, multiple viruses have been found to perturb the expression of the m^{6}A machinery. These include human cytomegalovirus, which increases the abundance of the m^{6}A machinery [231,232], or enterovirus 71, which increases the expression of METTL3 and METTL14 and changes the subcellular localization of reader, writer, and eraser proteins [243]. These alterations to the m^{6}A machinery may benefit viruses by allowing modification of their RNAs or by influencing the m^{6}A profile of the infected host cell. Interestingly, a recent study found that during VSV infection in mice, demethylation at a specific arginine residue in Alkbh5 impairs its m^{6}A demethylase activity [177]. Alkbh5 deficiency in macrophages resulted in perturbations to cellular metabolism. In

particular, Ogdh, an enzyme involved in the TCA cycle, was found to be strongly downregulated in these cells, as Alkbh5 normally demethylates the Ogdh transcript, which increases its stability and expression. Ogdh deficiency, in turn, was found to decrease the abundance of the metabolite itaconate, which was capable of promoting VSV replication [177]. Therefore, these results point to demethylation of Alkbh5 as a means of controlling Ogdh expression, which in turn regulates the production of itaconate. Importantly, this study identified a mechanism by which the m^{6}A-modification of a cellular RNA can change in response to viral infection. Determining whether this interesting cellular response is specific to VSV infection, or relevant for other viruses, will be an important future step. Additionally, these results should set the stage for additional discoveries of mechanisms by which viral infection influences the cellular m^{6}A landscape. Such discoveries will be of utmost importance for our understanding of how viruses manipulate m^{6}A distribution for their benefit and how host cells utilize alteration of m^{6}A to restrict viral replication.

Our understanding of the functional roles of m^{6}A in modulating host processes during viral infection is rapidly expanding, and these discoveries will also broaden our understanding of m^{6}A biology. Because of the diverse, transcript-specific effects of m^{6}A that can affect both viral and host RNAs, m^{6}A regulates viral infection in complex ways. In order to achieve a more synergistic understanding of the mechanisms by which m^{6}A and its related cellular machinery regulate viral infection, future research must continue to address the transcript-specific and position-specific roles of m^{6}A in regulation of cellular pathways in response to individual, as well as pan-viral infection. Additional mechanistic understanding of how m^{6}A regulates RNA sensing by PRRs, diverse cytokine production and responses, stress responses, immune cell biology, and cross-

talk between the innate and adaptive immune system will be of great interest. Tissue- and cell type-specific m^{6}A machinery knockout animal models will likely be very useful in gaining a better of understanding of the roles of m^{6}A in immune responses during viral infection. Finally, understanding whether and how viruses manipulate the m^{6}A machinery and abundance or position of m^{6}A in the host transcriptome will inform our understanding of the role of m^{6}A at the virus-host interface and also elucidate potential m^{6}A-based therapies for viral infection or immunopathies.

1.5 Summary of the work presented in this dissertation

Despite recent advances in our understanding of the regulatory effects of m^{6}A on host processes during viral infection, the role of m^{6}A during the type I IFN response has not been elucidated. I have discovered a role for METTL3/14 and m^{6}A in supporting the translation of a subset ISGs during the type I IFN response. This enhancement of antiviral gene expression by m^{6}A augments the antiviral effects of the type I IFN response, contributing to viral restriction. Further, I have found a role for FTO in suppressing the transcription of a subset of ISGs that are distinct from METTL3/14-regulated ISGs. In Chapter 2, I will discuss our work revealing the mechanisms by which m^{6}A regulates the expression of a subset of ISGs and how m^{6}A contributes to viral restriction during the type I IFN response. In Chapter 3, I will discuss our discovery of the role of FTO in suppressing the transcription of ISGs and the priming of FTO-depleted cells to respond to type I IFN treatment. Taken together, this work reveals novel molecular regulators of antiviral gene expression, which act on multiple levels of gene expression. These findings build on our understanding of how m^{6}A regulates viral

infection and how the m^6A machinery are involved in antiviral responses and inflammatory gene expression.

2. Post-transcriptional regulation of antiviral gene expression by m^6A

This chapter was adapted from a manuscript entitled "Post-transcriptional regulation of antiviral gene expression of antiviral gene expression by N6-methyladenosine" available as a preprint [244]. The authors are Michael J. McFadden, Haralambos Mourelatos, Alexa B.R. McIntyre, Nathan S. Abell, Nandan S. Gokhale, Helene Ipas, Blerta Xhemalce, Christopher E. Mason, and Stacy M. Horner.

2.1 Introduction

The IFN family cytokines are potent inhibitors of viral infection that induce hundreds of ISGs, many of which have antiviral activity [245,246]. Type I IFNs (IFN-α and IFN-β) are produced in response to viral infection, and they activate autocrine and paracrine signaling responses through the JAK-STAT pathway [92]. Specifically, type I IFNs bind to a dimeric receptor (IFNAR), composed of two subunits, IFNAR1 and IFNAR2. IFNAR engagement then activates the Janus kinases JAK1 and TYK2, which phosphorylate the transcription factors STAT1 and STAT2, inducing their hetero-dimerization and interaction with IRF9, to form the ISGF3 transcription factor complex. ISGF3 then translocates into the nucleus, where it binds to IFN-stimulated response elements within the promoters of ISGs to elicit their transcriptional activation [92]. Many of these ISGs encode antiviral effector proteins that inhibit multiple stages of viral replication and thus establish an early defense against viral replication [93]. Dysregulation of type I IFNs can lead to viral susceptibility or autoimmune disease

[247,248], demonstrating the importance of tight regulatory control of both IFN activation and the IFN response. Indeed, both activation and suppression of the type I IFN response are coordinated at multiple levels, such as by epigenetic modifiers [127,128,249] or by post-transcriptional mechanisms including microRNA regulation and alternative splicing [250,251]. However, our overall understanding of post-transcriptional regulation of ISG expression is still emerging. Additionally, while a number of studies have identified subsets of ISGs that have unique transcriptional regulators, other mechanisms that govern the regulation of subclasses of ISGs have not been well characterized [252-254].

The RNA base modification m^6A is deposited on RNA by a methyltransferase complex of METTL3 and METTL14 (METTL3/14), among other proteins [166]. m^6A coordinates biological processes through various effects on modified mRNAs [151,182], including increased mRNA turnover and translation, as well as other processes. These effects are mediated by m^6A reader proteins, such as YTHDF proteins [183,184,255]. Specifically, YTHDF1 increases translation [183], YTHDF2 mediates mRNA degradation [184], and YTHDF3 cooperatively enhances both of these processes [185], although in some cases these proteins may have overlapping functions [256]. Through the actions of m^6A reader proteins, m^6A can regulate infection by many viruses through modulation of both viral and host transcripts [178]. We recently profiled changes to the m^6A landscape of host mRNAs during *Flaviviridae* infection and identified both proviral and antiviral transcripts regulated by m^6A during infection [257]. Others have found that m^6A prevents RNA sensing or regulates the expression of signaling molecules involved in the production of cytokines such as type I IFNs [176,213,214,217,219,258] and that m^6A can destabilize the *IFNB1* transcript, thereby directly regulating the production of IFN-β

[231,232]. Therefore, m^{6}A plays important roles in viral infection and the antiviral response [259]; however, a role for m^{6}A in the response to type I IFN and the production of ISGs has not been described.

Here, we mapped m^{6}A in the IFN-β-induced transcriptome and identified many ISGs that are m^{6}A-modified. We found that METTL3/14 and m^{6}A promote the translation of certain m^{6}A-modified ISGs, in part through interactions between the transcripts of m^{6}A-modified ISGs and the m^{6}A reader protein YTHDF1. Importantly, we found that METTL3/14 and m^{6}A-mediated enhancement of ISG expression promotes the antiviral effects of the IFN response, as METTL3/14 perturbation affected the replication of vesicular stomatitis virus (VSV) in IFN-β-primed cells. Together, these results establish m^{6}A as a post-transcriptional regulator of ISGs for an effective cellular antiviral response.

2.2 Results

2.2.1 METTL3/14 regulates the translation of certain ISGs.

IFN-β induces the transcription of ISGs to shape the innate response to viral infection [245]. To investigate whether m^{6}A regulates the type I IFN response, we measured the IFN-β-induced expression of several ISGs with known antiviral functions [9] following depletion of the m^{6}A methyltransferase complex METTL3/14 in Huh7 cells. The IFN-β-induced protein expression of the ISGs IFITM1 and MX1, but not ISG15 and EIF2AK2 (also called PKR), was reduced following depletion of METTL3/14 (Figure 9A; see Methods for information on IFITM1 antibody specificity). Similar results were also seen following METTL3/14 depletion in A549 cells, primary neonatal human dermal fibroblasts (NHDF), and also at multiple time points (8 h, 16 h, and 24 h) after IFN-β in Huh7 cells (Figure 10A-10C); however we note MX1 protein levels were not as strongly

affected in A549 and NHDF cells as in Huh7 cells. Conversely, overexpression of METTL3/14 increased the abundance of IFITM1 and MX1, but not ISG15 and EIF2AK2, in response to IFN-β in Huh7 cells (Figure 9B). Importantly, the METTL3/14-regulated ISGs, IFITM1 and MX1, were not expressed without stimulation of cells by IFN-β (Figure 9A-9B). Therefore, any confounding effects of METTL3/14 perturbation on endogenous IFN-β production are negligible for these experiments.

The METTL3/14 m^6A methyltransferase complex regulates many aspects of mRNA metabolism [255]. To determine how METTL3/14 regulates the protein abundance of certain ISGs, we first tested whether METTL3/14 depletion led to a decrease in induction of ISG mRNA in response to IFN-β. We measured the induction of ISG mRNA in response to IFN-β over a timecourse using RT-qPCR (Figure 10D). Neither the mRNA abundance nor the kinetics of IFN-β-mediated induction of the METTL3/14-regulated ISGs *IFITM1* and *MX1* were affected by METTL3/14 depletion. The mRNA levels of the non-METTL3/14-regulated ISG *EIF2AK2* was unaffected, while *ISG15* mRNA was increased (Figure 10D). These data indicate that the mRNA abundance of *IFITM1* and *MX1* does not underlie the observed differences in protein levels, suggesting that neither the transcription nor the mRNA stability of these ISGs are regulated by METTL3/14 (Figure 10D). Further, using RNA-seq following IFN-β treatment, we noted little effect of METTL3/14 depletion on the mRNA abundance of a defined set of core ISGs [260] (Figure 10E) or expressed ISGs more broadly (Table 2). These data are in agreement with a previous report that found that collective ISG RNA stability is unaffected by METTL3 depletion [232].

As METTL3/14 depletion resulted in less protein expression of IFITM1 and MX1 without affecting their transcript levels, we tested whether METTL3/14 regulates the

protein stability of these genes. However, despite the expected decrease in IFITM1 and MX1 protein expression after METTL3/14 depletion and IFN induction, the rate of their protein decay was not affected following treatment with cycloheximide, which blocks protein synthesis (Figure 11A-11B).

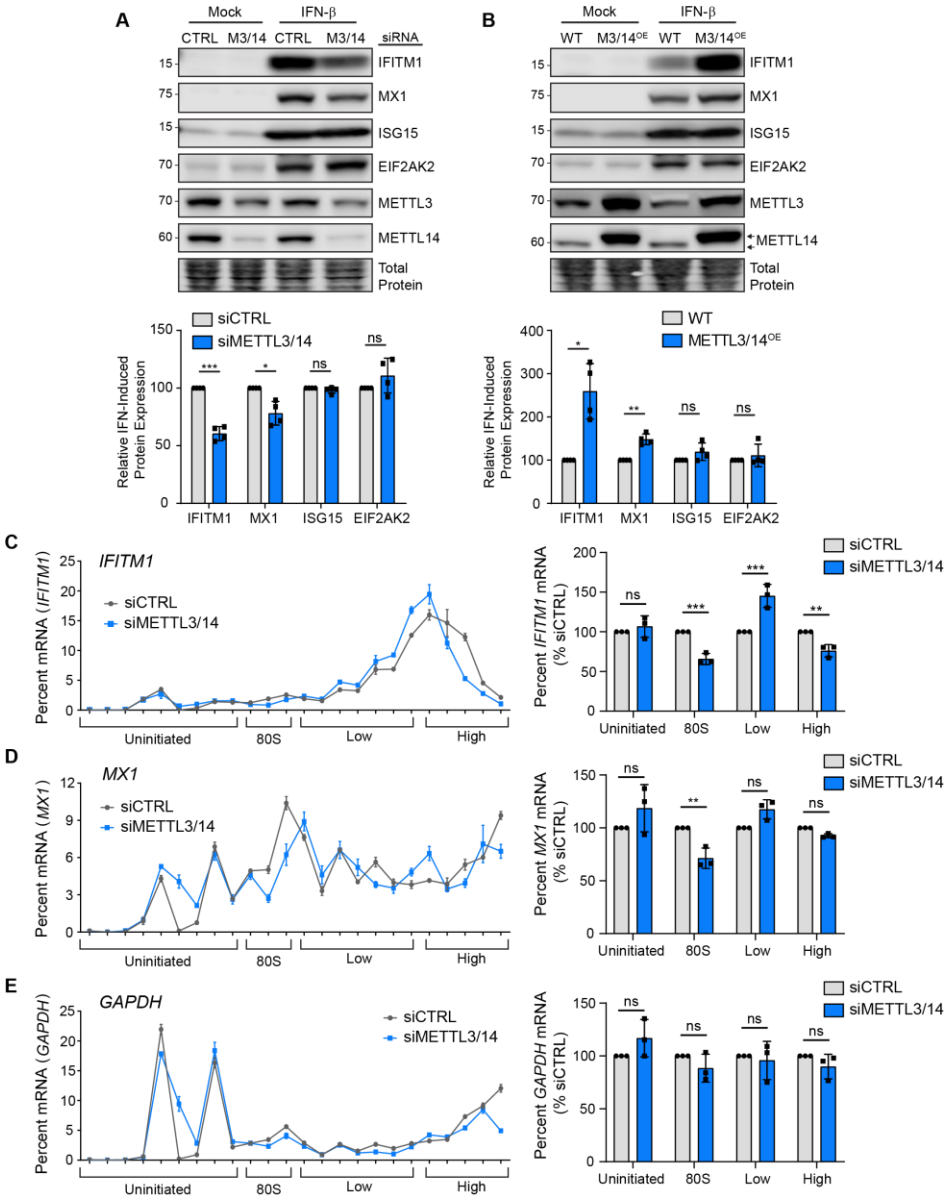

Figure 9: METTL3/14 regulates the translation of certain ISGs.
(A, B) Immunoblot analysis of extracts from Huh7 cells transfected with siRNAs to METTL3/14 (M3/14) or control (CTRL) (A) or stably overexpressing FLAG-METTL14

(M3/14OE; top arrow denotes FLAG-METTL14; bottom arrow denotes endogenous METTL14) (B) prior to mock or IFN-β (24 h) treatment. Relative ISG expression from 4 replicates of (A) and (B) is quantified below relative to siCTRL +IFN-β (A) or WT +IFN-β (B). **(C-E)** RT-qPCR analysis of the relative percentage of IFITM1 (C), MX1 (D), and GAPDH (E) mRNA across 24 sucrose gradient fractions isolated from extracts of IFN-β-treated (6 h) Huh7 cells treated with CTRL or METTL3/14 siRNA. The uninitiated (free, 40S, and 60S subunits), initiated (80S), low or high molecular weight polysomes, are noted. Graphs on the right show the percentages of mRNAs in combined fractions for IFITM1, MX1, or GAPDH. Percentages from fractions were added to yield the total percentage in each category. Values are the mean ± SEM of 4 biological replicates (A-B), the mean ± SD of 3 technical replicates, representative of 3 experiments (C-E, left graphs), and the mean ± SEM of 3 biological replicates (C-E, right graphs). * $p < 0.05$, ** $p < 0.01$, *** $p < 0.005$ by unpaired Student's t test (A-B), and 2-way ANOVA with Sidak's multiple comparisons test (C-E). ns = not significant. See also Figures 10-11.

Additionally, as both METTL3/14 and m^6A have been shown to promote the nuclear export of certain mRNAs [261], we also tested whether the nuclear export of select ISGs was altered by METTL3/14 depletion. However, after IFN stimulation, METTL3/14 depletion did not alter the nuclear-cytoplasmic ratio of the METTL3/14-regulated ISGs *IFITM1* and *MX1*, the non-regulated ISGs *ISG15* and *EIF2AK2*, a non-methylated control *HPRT1* [184], or the nuclear-localized control *MALAT1* (Figure 11C). Therefore, METTL3/14 does not regulate these ISGs through changes to their protein stability or nuclear export.

To test whether METTL3/14 regulates the translation of *IFITM1*, we measured the polysome occupancy of *IFITM1* induced by IFN-β in control cells or in those depleted of METTL3/14. METTL3/14 depletion did not change overall polysome density, as observed by the similar relative absorption across fractions (Figure 11D). However, METTL3/14 depletion did result in lower levels of *IFITM1* mRNA in the 80S fractions and a shift from the heavy to the light polysome fractions (Figure 9C), indicating impaired translation of *IFITM1* following METTL3/14 depletion. A similar, yet less pronounced shift was observed for *MX1* (Figure 9D), while the polysome occupancy of the housekeeping

control gene *GAPDH* was unaffected (Figure 9E). These results indicate that METTL3/14 regulates the translation of certain ISGs, such as IFITM1 and MX1.

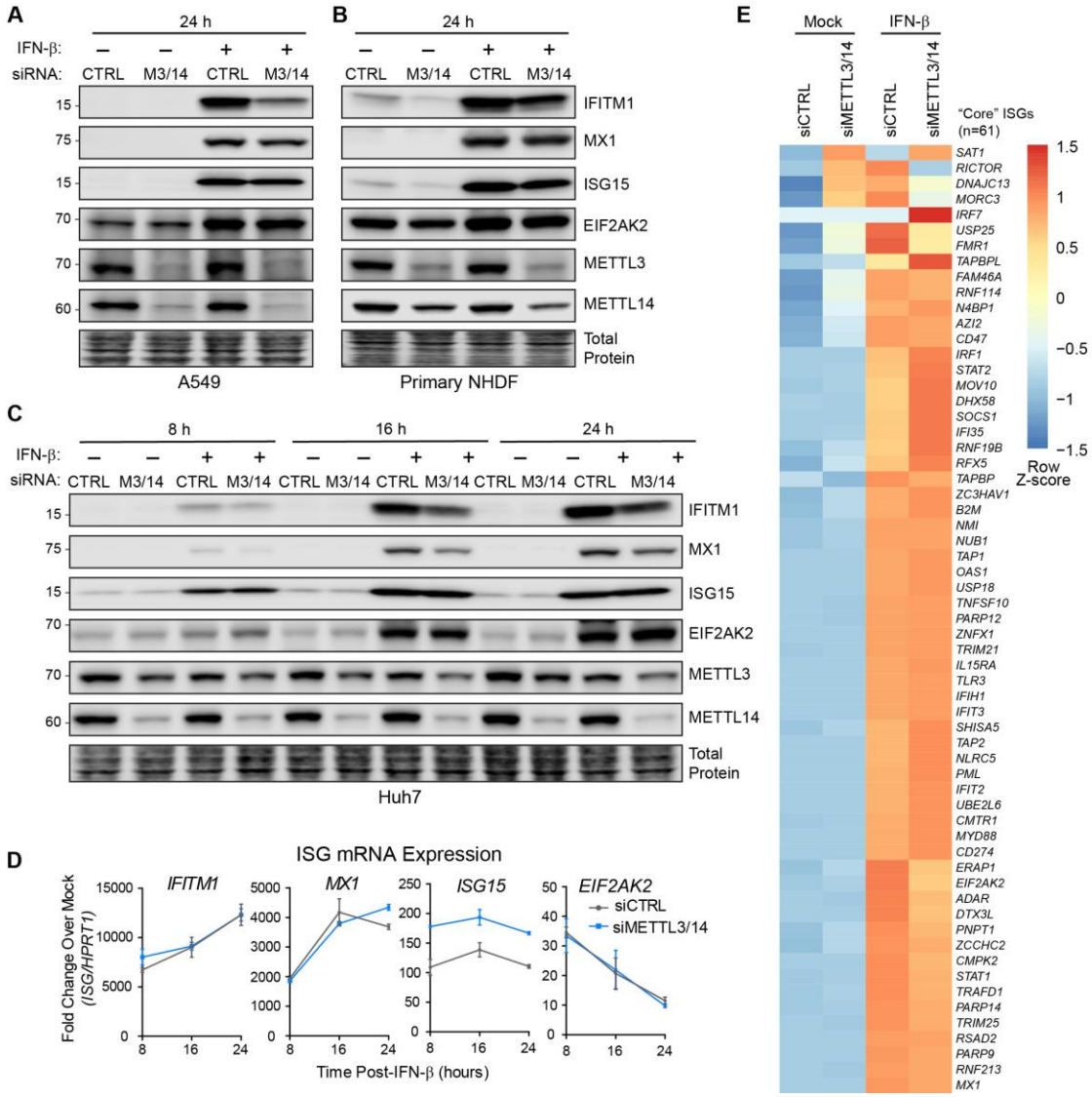

Figure 10: Related to Figure 9.

(A-C) Immunoblot analysis of extracts from A549 cells (A), primary neonatal human dermal fibroblast cells (B), or Huh7 cells (C) transfected with siRNAs to METTL3/14 (M3/14) or control (CTRL) (36 h) prior to treatment with mock or IFN-β for 24 h (A, B) or a timecourse of 8 hours, 16 hours, and 24 hours (C). All immunoblots are representative of 4 biological experiments. **(D)** RT-qPCR analysis of ISG induction normalized to *HPRT1* following IFN-β treatment of Huh7 cells treated with non-targeting control (CTRL) or METTL3/14 siRNA plotted as fold change over mock treatment for each ISG. Values are the mean ± SD of 3 technical replicates, representative of 4 experiments. **(E)** RNA-

seq analysis following siRNA transfection and IFN-β treatment (3 biological replicates). Heat map shows the Row Z-score for each ISG (n=61) with Euclidean row clustering.

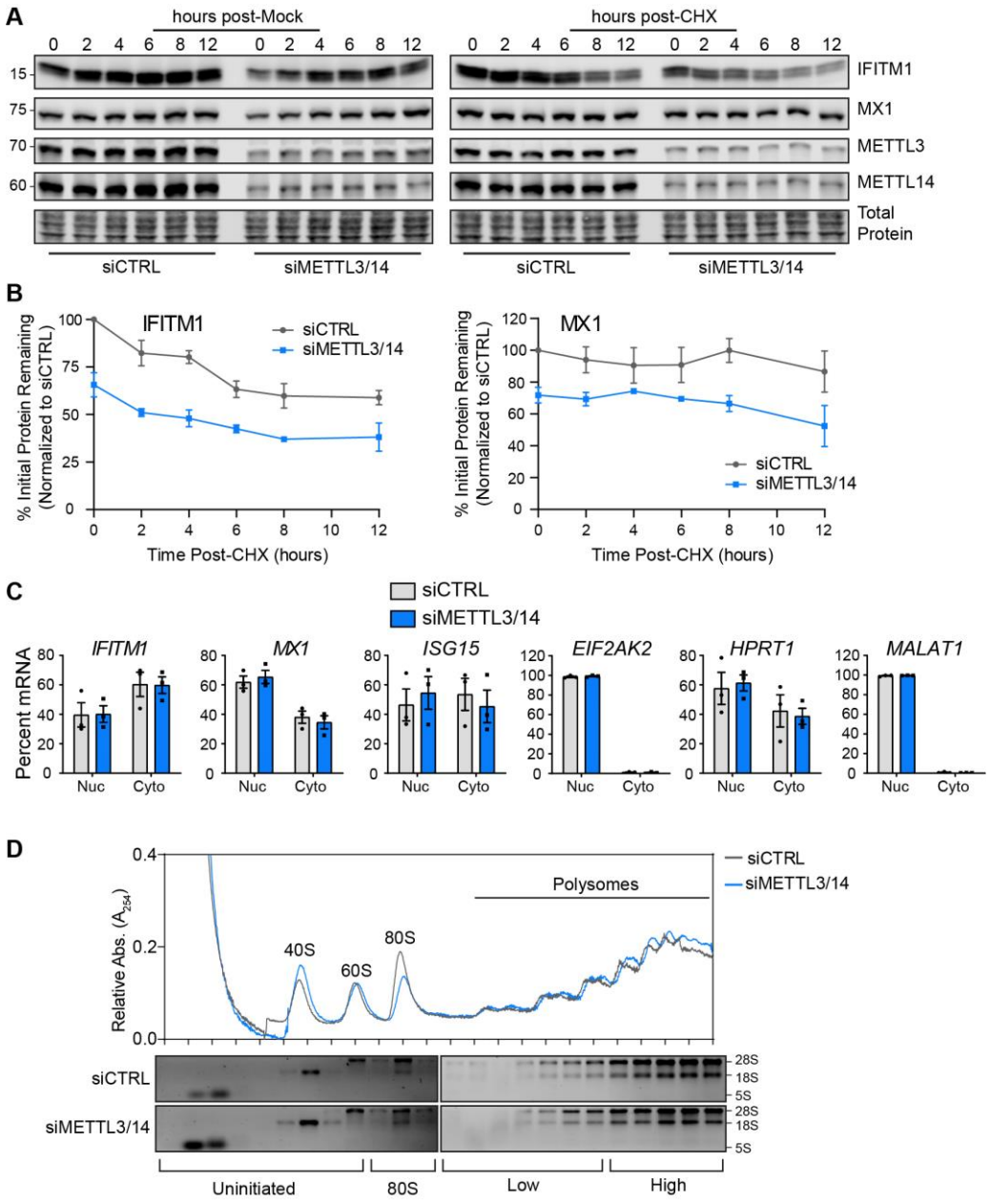

Figure 11: Related to Figure 9.

(A) Immunoblot analysis of ISG protein levels following cycloheximide (CHX) treatment. Following siRNA transfection, cells were treated with IFN-β (16 h) to induce ISGs, then mock or CHX treated along with a second dose of IFN-β, and lysates were harvested at

indicated timepoints. **(B)** Quantification of ISG expression in (A), normalized to total protein, and plotted as percent of initial protein remaining at each timepoint, relative to siCTRL timepoint 0. **(C)** RT-qPCR analysis of the percent mRNA in nuclear (Nuc) and cytoplasmic (Cyto) fractions in siRNA-treated Huh7 cells following IFN-β (12 h). **(D)** Relative absorbance values of sucrose gradient fractions isolated from extracts of IFN-β-treated (6 h) Huh7 cells treated with indicated siRNA. The 40S, 60S, and 80S subunit peaks, as well as polysome peaks, are noted. RNA from each fraction was separated by agarose gel electrophoresis and visualized with ethidium bromide to see the ribosomal RNA bands. Values are the mean ± SEM of 3-4 biological replicates (B), and the mean ± SEM of 3 biological replicates (C). Data in (D) are representative of 3 biological experiments.

Table 2: RNA-seq analysis of gene expression changes following IFN-β treatment and METTL3/14 depletion.

Table 2.1: siCTRL IFN / siCTRL Mock
Table 2.2: siMETTL3/14 Mock / siCTRL Mock
Table 2.3: siMETTL3/14 IFN / siCTRL IFN
Due to size, this table has not been included in this document. It can be downloaded from this link: Table 2

2.2.2 METTL3/14-regulated ISGs are modified by m^{6}A.

To determine whether the METTL3/14-regulated ISGs *IFITM1* and *MX1*, as well as other ISGs, are m^{6}A-modified, we mapped m^{6}A in the IFN-induced transcriptome in Huh7 cells using methylated RNA immunoprecipitation and sequencing (MeRIP-seq) [157,158]. After defining the ISGs in this experiment (Figure 13A; Table 3), we then called peaks in read coverage post-m^{6}A immunoprecipitation compared to input using the MeTDiff m^{6}A peak caller [262] (Table 3). We observed that peaks across mRNAs were enriched around the end of the coding sequence and the beginning of the 3' UTR, as expected [157,158] (Figure 12A). The most highly enriched RNA sequence motif within peaks was [U/A]GGAC, which matches the known m^{6}A motif of DRA^{m}C [157,158] (Figure 12A). We found that approximately 85% percent of ISGs, classified as those

upregulated more than 4-fold following IFN treatment, were m^{6}A-modified, as compared to 74% percent of the expressed transcriptome of Huh7 cells (mean coverage ≥ 10) (Figure 12B). This was consistent with a previous study that found that ISGs were m^{6}A-modified at a similar percentage to the transcriptome [232]. The percent of ISGs that are m^{6}A-modified was similar among other classes of ISGs, including a 'core' class of ISGs that are evolutionarily conserved among vertebrate species and a subset of 14 of these core ISGs with known antiviral functions [260] (Figure 12B). Plotting the MeRIP-seq reads relative to the input reads of individual genes can be informative of m^{6}A status, as m^{6}A peak calling methods have known limitations [241]. Thus, we generated plots for *IFITM1*, *MX1*, *ISG15*, and *EIF2AK2* and used the m^{6}A peak callers MeTDiff [262] and meRIPPer (https://sourceforge.net/projects/meripper/) (Table 3) to reveal that the METTL3/14-regulated genes *IFITM1* and *MX1* had m^{6}A peaks (Figure 12C-D), while *ISG15* and *EIF2AK2* lacked called m^{6}A peaks (Figure 12E-F). These plots suggested that the 3' UTR of *ISG15* may also contain an m^{6}A site (Figure 12E).

We then compared the m^{6}A status of ISGs from our MeRIP-seq experiment to data from previously published studies that profiled m^{6}A after IFN-inducing treatments, such as dsDNA [231] or human cytomegalovirus (HCMV) infection [232] (Figure 13B). This comparison showed consistent prediction of m^{6}A methylation status for core antiviral ISGs among all three studies (Figure 13B). Indeed, dsDNA treatment potently activates IFN production and elicited m^{6}A modification of the same core antiviral ISGs found in our experiment. Infection with HCMV also elicited m^{6}A modification of certain ISGs, although fewer peaks were called in these ISGs after HCMV infection than after IFN-β treatment or dsDNA treatment (Figure 13B). We note this virus encodes factors to dampen IFN signaling [263], therefore ISGs are likely not as strongly induced as

compared to dsDNA or IFN-β treatment. The presence of m^{6}A on many ISGs suggests that m^{6}A may regulate the antiviral type I IFN response.

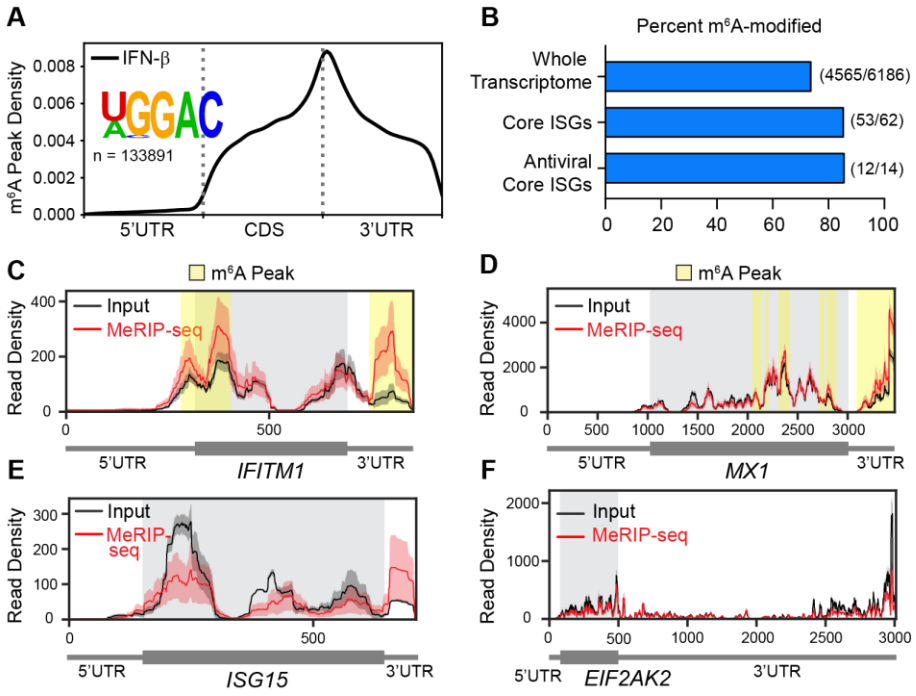

Figure 12: METTL3/14-regulated ISGs are modified by m^{6}A.
(A) Metagene plot of predicted m^{6}A distribution across the transcriptome following IFN-β treatment (8 h), with relative positions of DRACH motif sites under statistically significant peaks plotted, as well as the most highly enriched motif under peaks. **(B)** The percent of genes modified by m^{6}A in the expressed transcriptome, genes with mRNA induction ≥ 4-fold in response to IFN-β treatment (ISGs), a group of core ISGs conserved in vertebrate species [260], or a subset of these core ISGs with antiviral functions [260]. **(C-F)** Read coverage plots of MeRIP (red) and input (black) reads in *IFITM1* (C), *MX1* (D), *ISG15* (E), and *EIF2AK2* (F) transcripts. Variance between biological replicates is represented by red and black shading around read coverage. Gray shading represents coding sequence, yellow shading represents m^{6}A peaks called by MeTDiff [262] and meRIPPer (https://sourceforge.net/projects/meripper/) software. All analyses are performed on 3 biological replicates. See also Figure 13.

Table 3: m^{6}A peaks in the IFN-β induced transcriptome.

Table 3.1: Input RNA-seq Analysis (IFN / Mock)
Table 3.2: MeTDiff m^{6}A Peaks
Table 3.3: meRIPPer m^{6}A Peaks
Due to size, this table has not been included in this document. It can be downloaded from this link: Table 3

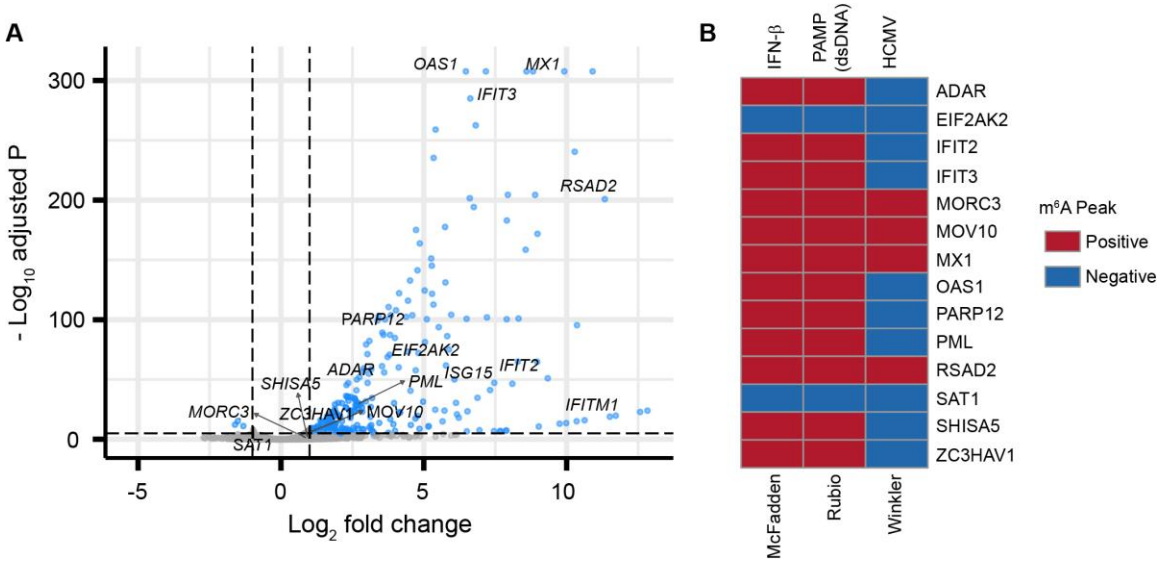

Figure 13: Related to Figure 12.
(A) Volcano plot showing gene expression changes (58,037 total genes) following IFN-β treatment (8 h) compared to mock treatment, with core antiviral ISGs labeled. Analysis was performed on 3 biological replicates of each condition. **(B)** Analysis of MeRIP-seq data from this study and two previous studies [231,232] showing m^{6}A peak presence or absence in core antiviral ISGs following induction of IFN pathways. IFN responses were induced by IFN-β (this study), double stranded DNA ([231]), or HCMV ([232]).

2.2.3 m^{6}A modification in the 3'UTR of IFITM1 enhances its translation.

m^{6}A is known to enhance the translation of certain mRNAs [183,257,264-266]. Specifically, the m^{6}A reader protein YTHDF1 can recognize m^{6}A within 3' UTRs and associate with eukaryotic translation initiation factors such as eIF3 to enhance the

translation of m^{6}A-modified transcripts [183]. To determine whether the translational regulation of ISGs by METTL3/14 is elicited through m^{6}A, we used *IFITM1* as a model METTL3/14-regulated ISG. We first determined the effect of METTL3/14 depletion on m^{6}A modification of *IFITM1*. MeRIP-RT-qPCR revealed that *IFITM1* mRNA was enriched above the m^{6}A-negative ISG *EIF2AK2* and a spiked-in m^{6}A-negative synthetic RNA, confirming that it contains m^{6}A. METTL3/14 depletion reduced the m^{6}A-enrichment of *IFITM1* mRNA but not of the m^{6}A-negative *EIF2AK2* transcript or the m^{6}A-negative synthetic RNA (Figure 14A-B). These data reveal that *IFITM1* is m^{6}A-modified by METTL3/14.

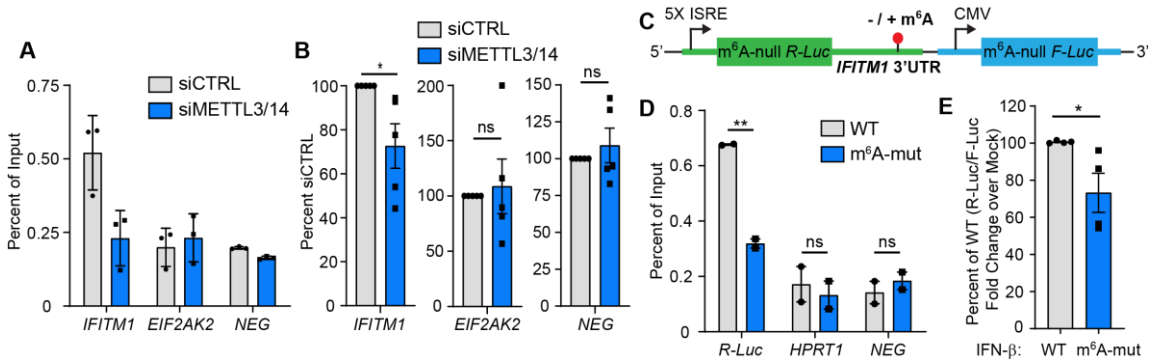

Figure 14: m^{6}A modification of the IFITM1 3'UTR enhances translation.
(A) Representative MeRIP-RT-qPCR analysis of relative m^{6}A level of *ISGs* induced by IFN-β (8 h) in Huh7 cells treated with non-targeting control (siCTRL) or METTL3/14 siRNA and spiked-in m^{6}A-negative (NEG) oligonucleotides. **(B)** Relative percent enrichment of each gene in (A), normalized to siCTRL, from 5 biological replicates. **(C)** Schematic of WT and mutant ISRE-m^{6}A-null *Renilla* luciferase (R-Luc) *IFITM1* 3' UTR reporters that also express m^{6}A-null firefly luciferase (F-Luc) from a separate promoter. **(D)** MeRIP-RT-qPCR analysis of relative m^{6}A level of WT and m^{6}A-mut *IFITM1* 3' UTR reporter RNA from transfected Huh7 cells treated with IFN-β (8 h). **(E)** Relative luciferase activity (R-Luc/F-Luc) in IFN-β induced (8 h, relative to mock) WT and m^{6}A-mut *IFITM1* 3' UTR reporters. Values are the mean ± SD of 3 technical replicates representative of 5 biological replicates (A); the mean ± SEM of 5 biological replicates (B); the mean ± SEM of 2 biological replicates (D), or mean ± SEM of 4 biological replicates (E). * $p < 0.05$, ** $p < 0.01$ by unpaired Student's t test. ns = not significant.

Having confirmed that *IFITM1* is m^{6}A modified, we next generated a luciferase reporter that contains an IFN-stimulated response element (ISRE) promoter-driven *Renilla* luciferase in which all DRAC motifs were ablated (m^{6}A-null *R-Luc*) [257] fused to the wild type (WT) *IFITM1* 3' UTR, or an analogous 3' UTR sequence in which the four putative m^{6}A motifs under the m^{6}A peak in the 3' UTR in *IFITM1* were inactivated by A→G transitions (m^{6}A-mut) (Figure 14C). These constructs also express a CMV promoter-driven m^{6}A-null firefly luciferase gene as a control. The m^{6}A modification status of the *IFITM1* 3' UTR reporter was first assessed using MeRIP-RT-qPCR after IFN-β treatment. The WT *IFITM1* 3' UTR reporter had increased m^{6}A modification compared to the m^{6}A-mut *IFITM1* 3' UTR reporter, as well as the negative controls: *HPRT1*, which does not contain m^{6}A [184], and an m^{6}A-negative synthetic RNA control (Figure 14D). We next compared the production of the *Renilla* luciferase protein, relative to firefly luciferase, from the WT and m^{6}A-mut IFITM1 3' UTR reporters by measuring luciferase activity. We found that the relative luciferase activity of the m^{6}A-mut IFITM1 3'UTR reporter was significantly decreased following IFN-β treatment compared to the WT IFITM1 3' UTR reporter (Figure 14E). Together, these data suggest that METTL3/14 regulates *IFITM1* translation through addition of m^{6}A to the 3' UTR and that m^{6}A within the *IFITM1* 3' UTR is sufficient to enhance its translation.

2.2.4 YTHDF1 binds *IFITM1* mRNA and enhances IFITM1 protein expression in an m^{6}A-dependent fashion.

The m^{6}A binding protein YTHDF1 enhances translation of a number of m^{6}A-modified genes [183]. To test if YTHDF1 elicited the translation-promoting effects of m^{6}A on ISGs, we stably overexpressed YTHDF1 (Y1^{OE}) or an m^{6}A binding-deficient YTHDF1 protein [267] (Y1mut^{OE}) in Huh7 cells and measured the IFN-induced expression of ISGs

24 hours later. Overexpression of YTHDF1 was sufficient to increase IFITM1 protein expression in response to IFN-β, while overexpression of the m^{6}A binding-deficient YTHDF1 protein (Y1mut^{OE}) did not increase IFITM1 abundance (Figure 15A-B). Importantly, wild-type and mutant YTHDF1 overexpression did not significantly affect the levels of *IFITM1* mRNA following IFN-β treatment, suggesting that YTHDF1 does not directly regulate IFN signaling or *IFITM1* mRNA stability (Figure 15C). Neither the IFN-induced expression of the m^{6}A-containing ISG MX1, nor the non-m^{6}A containing ISGs ISG15 and EIF2AK2, were significantly altered by YTHDF1 overexpression (Figure 15A-B). Interestingly, we found that WT YTHDF1 bound to the transcripts of *IFITM1*, *MX1*, *ISG15*, and the m^{6}A-positive control *SON* [184], while the m^{6}A-binding-defective YTHDF1 mutant protein did not. The non-m^{6}A containing mRNAs *EIF2AK2* and *RPL30* [183] did not bind to either protein (Figure 15D-E). Together, these results reveal that YTHDF1 binds to m^{6}A on *IFITM1* and enhances its translation. The apparent m^{6}A-dependent binding of YTHDF1 to *ISG15* suggests that *ISG15* is actually m^{6}A-modified. In fact, plotting MeRIP-seq reads over input reads for *ISG15* did show a potential region of m^{6}A enrichment in its 3' UTR (Figure 11E), although this was not identified as significant by two peak callers (Table 3). Taken together, these data suggest that YTHDF1 has transcript-specific roles in promoting translation, as it bound *IFITM1*, *MX1*, and *ISG15*, but its overexpression was only sufficient to significantly increase the protein production of IFITM1.

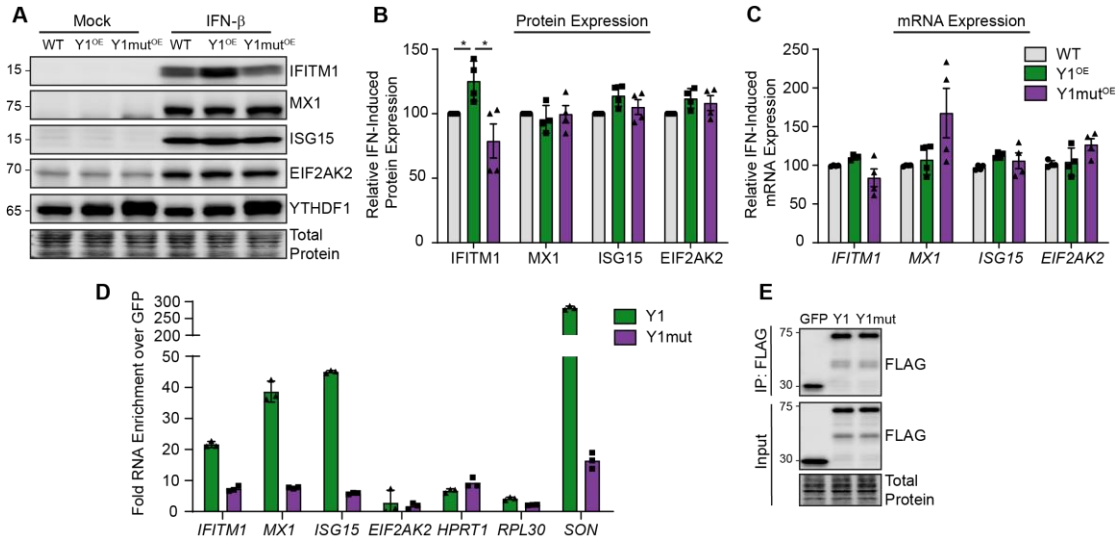

Figure 15: YTHDF1 enhances IFITM1 protein expression in an m^{6}A-dependent fashion.
(A) Immunoblot analysis of extracts from Huh7 cells stably overexpressing FLAG-YTHDF1 WT (Y1^{OE}) or FLAG-YTHDF1 W465A [267] (Y1mut^{OE}) following mock or IFN-β (24 h) treatment. **(B)** Quantification of ISG expression following IFN-β from 3 independent experiments of (A), normalized to total protein and graphed relative to siCTRL. **(C)** RT-qPCR analysis of ISG mRNA expression normalized to HPRT1 in Huh7 cells stably overexpressing FLAG-YTHDF1 WT (Y1^{OE}) or W465A (Y1mut^{OE}) after IFN-β (24 h) treatment **(D)** RT-qPCR analysis of enrichment of mRNAs following immunoprecipitation of FLAG-YTHDF1 WT (Y1) or W465A (Mut) compared to FLAG-GFP from Huh7 cells following IFN-β (8 h). IP values are normalized to input values and plotted as fold enrichment over GFP. **(E)** Immunoblot of FLAG-immunoprecipitated and input fractions used in (D). Values in (B-C) are the mean ± SEM of 3 biological replicates. * $p < 0.05$, by Kruskal-Wallis with Dunn's multiple comparisons test. Everything unlabeled was not significant with $p > 0.05$. Values in (D) are the mean ± SD of 3 technical replicates and are representative of 4 independent experiments.

2.2.5 METTL3/14 and m^{6}A promote the translation of a subset of ISGs.

Having demonstrated that m^{6}A supports the translation of two ISGs (*IFITM1* and *MX1*), and that m^{6}A is present on many ISGs, we next sought to identify additional ISGs whose protein expression is regulated by METTL3/14. To this end, we employed quantitative mass spectrometry-based proteomics with stable isotope labeling of amino acids (SILAC) to compare the proteomes of siCTRL and siMETTL3/14 cells after IFN-β

treatment (Table 4). The effect of siMETTL3/14 compared to siCTRL on protein abundance is centered at a log ratio of 0 for the majority of proteins (Figure 17A), demonstrating that METTL3/14 depletion does not have a global effect on protein levels after IFN-β treatment. We determined which proteins are ISGs by defining ISGs as genes upregulated >2-fold by IFN-β treatment in our previous RNA-seq experiment (Table 2). While mass spectrometry detection of ISGs was limited (n=18), we did identify a number of METTL3/14-regulated ISGs (Figure 16A, MS). The protein expression of most of these ISGs was decreased following METTL3/14 depletion, and these ISGs included the previously identified m^6A-modified IFITM1 (peptides corresponding to IFITM1/2/3) and MX1, as well as additional antiviral ISGs such as OAS2 and the different HLA-C chains (Figure 16A), which are also m^6A-modified. We also compared these data to our previous RNA-seq experiment (Table 2) to determine whether the effects of METTL3/14 on the protein level of these ISGs is determined by regulation of their mRNA expression. Importantly, following METTL3/14 depletion, the ISGs in this experiment that were decreased at the protein level did not also have a decrease in mRNA abundance, suggesting they may be regulated at the translation level, as our earlier polysome profiling indicated for IFITM1 and MX1 (Figure 9C-D; 16A, RNA). We note that not all m^6A-modified ISGs identified by mass spectrometry were regulated by METTL3/14 depletion (Figure 16A, m^6A). This suggests that METTL3/14 and m^6A regulate a subset of ISGs and support their protein expression.

As a complementary approach, we also used Ribo-seq to more broadly define the role of METTL3/14 in translational regulation of ISGs (Table 5). As ribosome profiling relies on digestion of mRNA that is not ribosome-bound, we first confirmed that reads in the untranslated regions were depleted (Figure 17B). Then we analyzed the top 100

most highly-induced ISGs (Table 2) that were actively translated (base mean >25) and compared the effect of METTL3/14 depletion on ribosome density (Ribo) to mRNA abundance from our previous RNA-seq analysis (RNA) (Figure 16B; Figure 17C; Table 2). METTL3/14 depletion overall appeared to result in decreased ribosome occupancy among many of these ISGs (66/100, including *IFITM1*), without having any generalized effect on their mRNA abundance (Figure 17C). In many cases, METTL3/14 depletion affected both the mRNA abundance and ribosome protection of individual ISGs similarly (Figure 16B, Quadrants I and III). However, for roughly a third of these genes (33/100), METTL3/14 depletion resulted in decreased ribosome protection, despite greater mRNA abundance (Figure 16B, Quadrant IV). Alternatively, very few (4/100) ISGs had both increased ribosome protection and decreased mRNA abundance following METTL3/14 depletion (Figure 16B, Quadrant II). We note that, of these 100 ISGs, 85 were m^6A-modified, roughly consistent with the 74% of genes that we had identified in the total expressed transcriptome as containing m^6A (Table 3). Interestingly, a number of m^6A-modified ISGs were not regulated by METTL3/14, as measured by ribosome protection or mRNA abundance, supporting a role for METTL3/14 and m^6A in regulation of only certain ISGs. These data, taken together with our quantitative mass spectrometry and RNA-seq analysis, suggest that METTL3/14 regulates the translation of a subset of ISGs to support their protein expression during the type I IFN response.

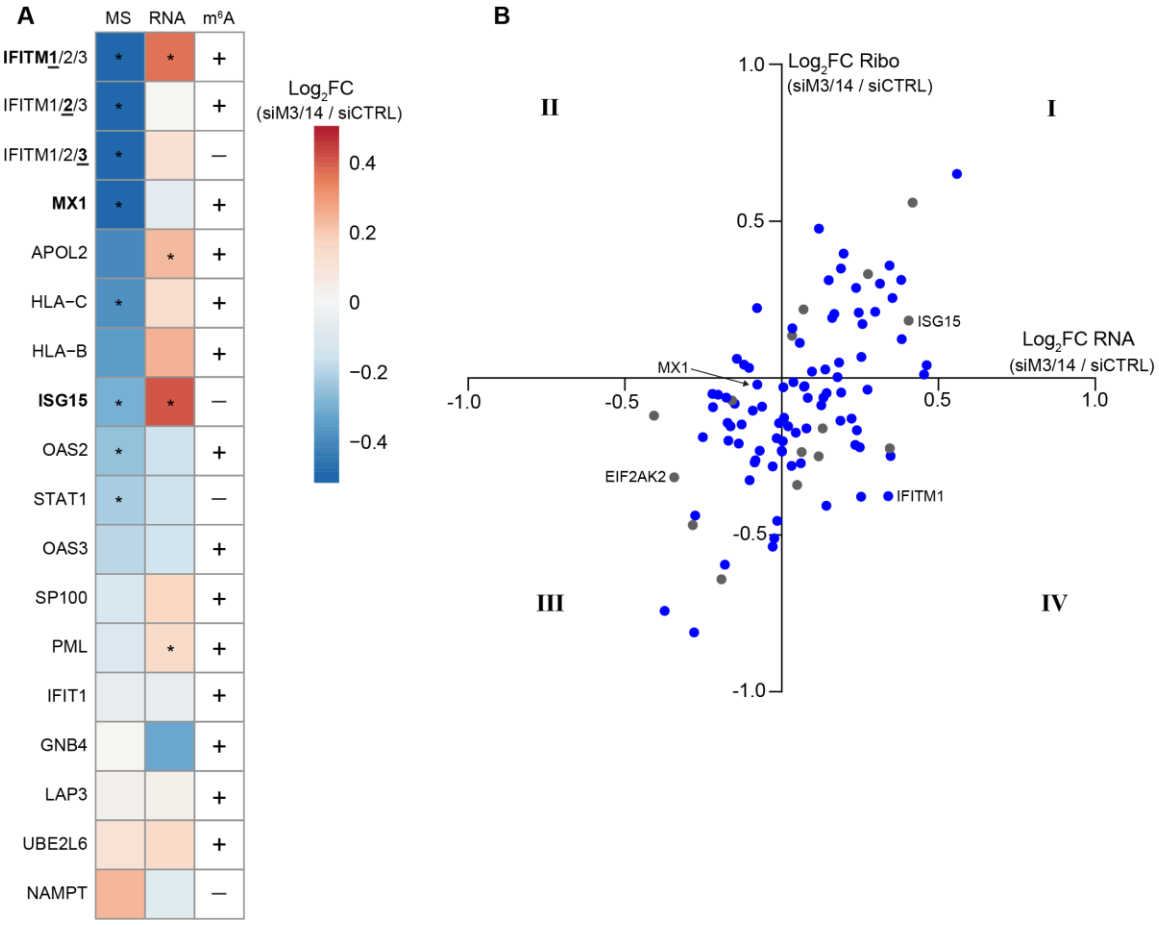

Figure 16: METTL3/14 regulates the translation of a subset of ISGs.
(A) 3-column heatmap shows the effect of METTL3/14 depletion on the expression of ISGs in Huh7 cells following IFN-β treatment. The first column shows the $\log_2$ fold change of protein estimates from quantitative mass spectrometry (siMETTL3/14 over siCTRL + IFN-β 24 h; n=2 biological replicates). The second column shows $\log_2$ fold change of mRNA reads from an independent RNA-seq experiment (siMETTL3/14 over siCTRL + IFN-β 8 h; n=3 biological replicates), and the third column indicates m^6A status (+ indicates m^6A-positive; - indicates m^6A-negative) from MeRIP-seq (+ IFN-β 8 h; n=3 biological replicates). Genes include any ISGs induced more than 2-fold by IFN from RNA-seq that were also detected by mass spectrometry. ISGs investigated in other figures are shown in bold. Because IFITM1/2/3 are similar, we used this notation to indicate peptides detected from this family of proteins; however, RNA-seq fold change and m^6A status correspond to the underlined number. * adjusted $P < 0.05$. **(B)** Four-quadrant scatterplot showing the effect of METTL3/14 on the expression of ISGs. The y-axis is the $\log_2$ fold change of ribosome protected fragments from Ribo-seq (siMETTL3/14 over siCTRL), and the x-axis is the $\log_2$ fold change of mRNA reads from an independent RNA-seq experiment (siMETTL3/14 over siCTRL). m^6A-modified (blue) or m^6A-negative (gray) genes are noted. ISGs investigated in other figures are labeled. See also Figure 17.

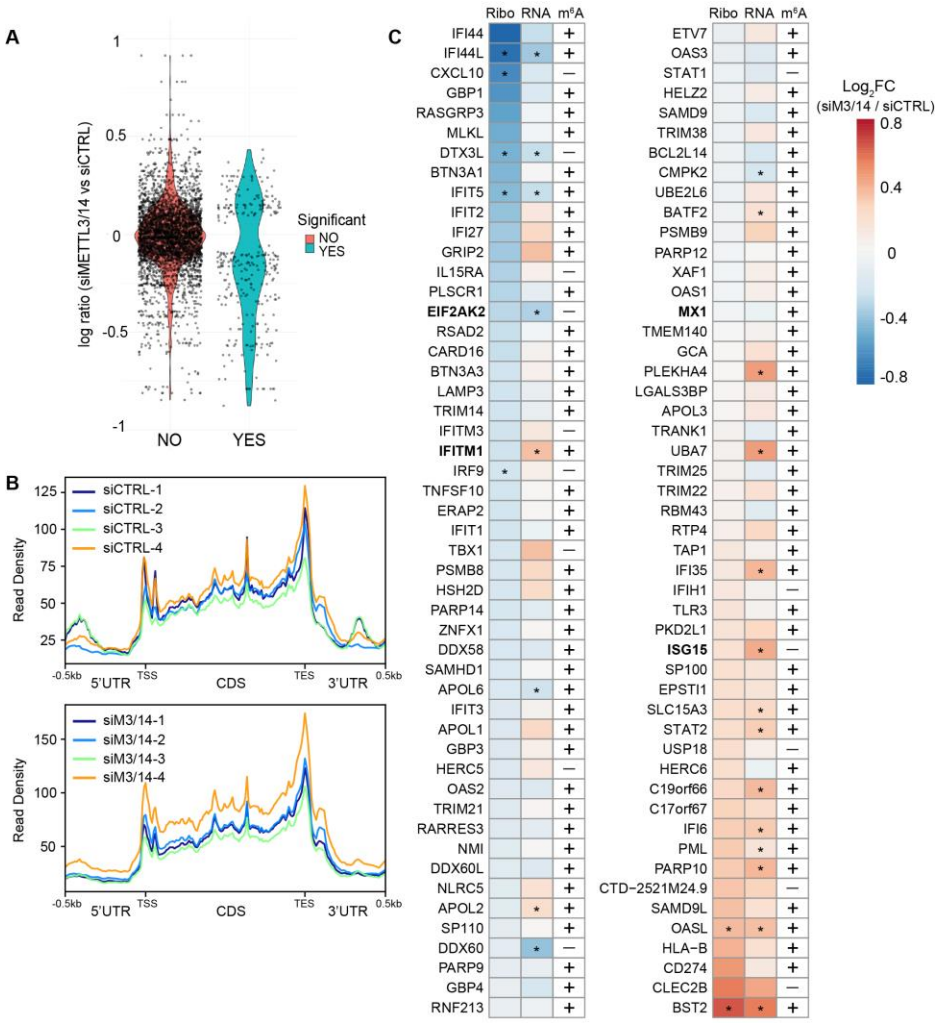

Figure 17: Related to Figure 16.

(A) Violin plot of the effect of siMETTL3/14 treated Huh7 cells compared to siCTRL treatment (+ IFN-β 24 h; 2 biological replicates each), expressed as log ratio, separated in two groups: non-significant (NO) with an adjusted p value > 0.01, or significant (YES) with an adjusted p value < 0.01. **(B)** Metagene plot showing ribosome protected fragment abundance 500 base pairs upstream and downstream of the translation start site (TSS) and translation end site (TES), and along the open reading frame (CDS; scaled to 1000 bp) for all siCTRL IFN and all siMETTL3/14 IFN replicates (+ IFN-β 8 h; n=4 biological replicates). **(C)** 3-column heatmap shows the effect of METTL3/14 depletion on the expression of 100 ISGs. The first column shows the log_2fold change of Ribo-seq reads (siMETTL3/14 over siCTRL). The second column shows log_2 fold change of mRNA reads from an independent RNA-seq experiment (siMETTL3/14 over siCTRL), and the third column indicates m^{6}A status (+ indicates m^{6}A-positive; - indicates m^{6}A-negative) from MeRIP-seq. Genes include the top 100 most highly-induced genes by IFN treatment from RNA-seq (see also Table S1) with base mean > 25, as

determined by DEseq2 [268] in all conditions (Ribo-seq, RNA-seq, MeRIP-seq). ISGs investigated in other figures are shown in bold. * adjusted $P < 0.05$.

Table 4: Analysis of METTL3/14 depletion effect on protein expression using quantitative mass spectrometry.

Due to size, this table has not been included in this document. It can be downloaded from this link: Table 4

Table 5: Analysis of Ribo-seq data from METTL3/14 depletion and IFN-β treatment.

Due to size, this table has not been included in this document. It can be downloaded from this link: Table 5

2.2.6 METTL3/14 augments the antiviral effects of the IFN response.

The fact that METTL3/14 enhances the expression of a subset of ISGs during the type I IFN response suggests that METTL3/14 could be required for an optimal antiviral response. To determine whether METTL3/14 contributes to viral restriction by type I IFN, we measured the ability of type I IFN to restrict infection by the negative-sense stranded RNA virus, vesicular stomatitis virus (VSV), following METTL3/14 perturbation. The VSV genome contains the m^6A_m cap modification, but as the deposition of this modification is not controlled by METTL3/14 [269-271], we would not expect VSV replication to be directly affected by changes in the levels of METTL3/14. Rather, any impact on VSV replication would likely be mediated by methylation of host factors. We perturbed the expression of METTL3/14 using siRNAs or by overexpression and then determined the percent of cells infected by VSV at 6 hours post-infection in the presence and absence of a low dose of IFN-β pretreatment (6 hours; 25 U/mL). Measuring VSV infection at early time points after infection allowed us to measure viral replication prior to cellular

upregulation of ISGs induced directly in response to infection. Indeed, in the absence of IFN-β pretreatment, we saw no induction of ISGs by VSV in any condition (Figure 18A-B). Additionally, as anticipated, we found that the replication of VSV, as measured by immunoblotting or quantifying the percent of cells infected, was not altered by depletion or overexpression of METTL3/14 in cells in the absence of IFN-β pretreatment (Figure 18). As observed earlier, following IFN-β pretreatment, METTL3/14 depletion led to decreased expression of METTL3/14-regulated ISGs (Figure 18A), while METTL3/14 overexpression increased the expression of these ISGs (Figure 18B). As expected, IFN-β pretreatment resulted in overall less replication of VSV, as IFN-β is known to inhibit VSV replication [272] (Figure 18). However, upon depletion of METTL3/14, the ability of IFN-β to restrict VSV was reduced (Figure 18A, 18C). Conversely, METTL3/14 overexpression enhanced IFN-mediated restriction of VSV (Figure 18B, 18D). These data indicate that METTL3/14 enhances the antiviral properties of type I IFN and is required for an efficient IFN-mediated antiviral response.

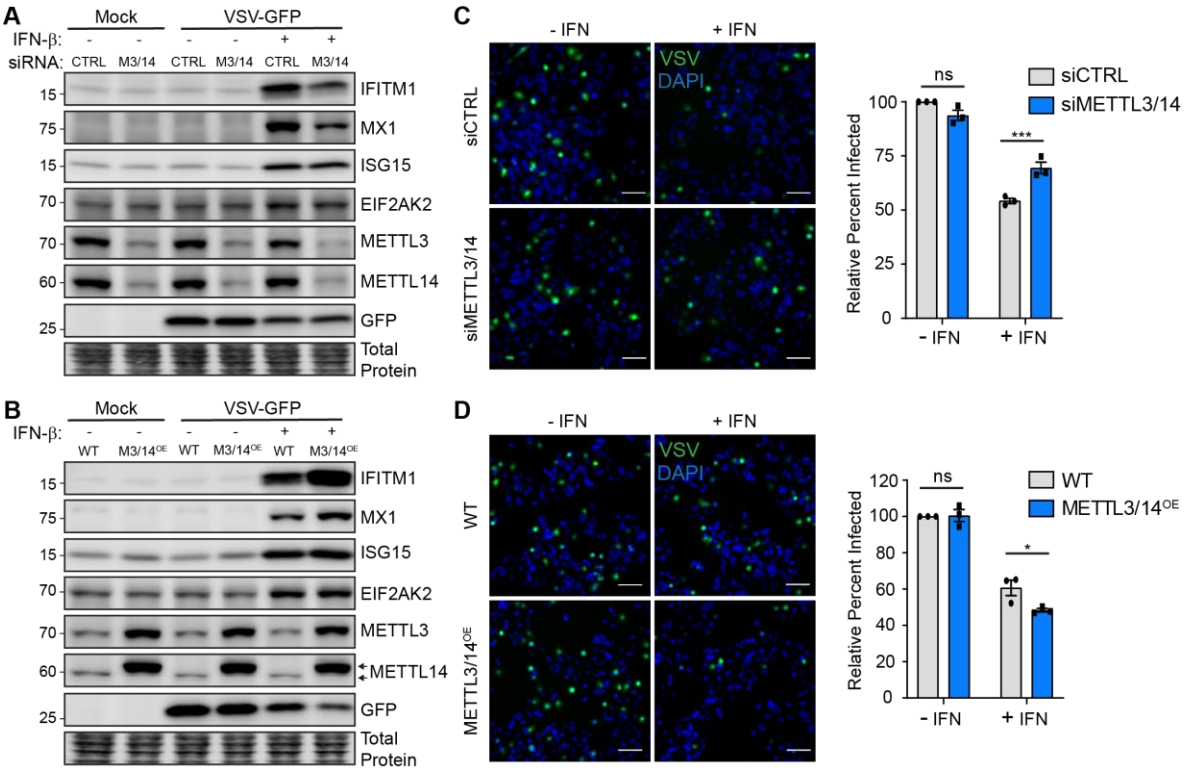

Figure 18: METTL3/14 augments the antiviral effects of the type I IFN response. **(A, B)** Representative immunoblot analysis (n=3) of extracts from Huh7 cells transfected with siRNAs (A) or stably overexpressing FLAG-METTL14, which also enhances METTL3 expression (M3/14^{OE}); (B), then treated with IFN-β (6 h) or mock, followed by infection with VSV (MOI=2; 6 h). Arrows denote FLAG-METTL14 (top) and endogenous METLL14 (bottom). **(C, D)** Representative micrographs of Huh7 cells treated with non-targeting control (siCTRL) or METTL3/14 siRNA (C) or stably overexpressing FLAG-METTL14 (METTL3/14^{OE}; D), that were pre-treated with IFN-β (6 h), and then infected with VSV (MOI=2; 6 h), with quantification of percent of cells infected from 3 independent experiments with 5 fields per condition, with >150 cells per field, normalized to siCTRL or WT with no IFN treatment, shown on the right. Scale Bar, 100 µm. Values are the mean ± SEM of 3 biological replicates. * $p < 0.05$, *** $p < 0.001$ by 2-way ANOVA with Sidak's multiple comparisons test. ns = not significant.

2.3 Discussion

Post-transcriptional control of the type I IFN response remains poorly understood, and most of our existing knowledge centers around miRNA-mediated regulation of the IFN-induced JAK-STAT signaling pathway [250] or a few examples of

alternative splicing of ISG transcripts [251]. While a number of reports have documented non-canonical activation or delayed stimulation of subsets of ISGs during viral infection, the molecular pathways that can control these subsets of ISGs are not well understood [122,124]. However, a number of studies have identified transcriptional regulators of subsets of ISGs [252-254], and the mRNA Cap1 methyltransferase CMTR1 was recently shown to regulate the expression of certain ISGs [134]. These studies demonstrate the complexity of regulation of expression of ISGs that extends beyond transcriptional induction of ISGs from signaling of the JAK-STAT pathway. Here, we identify a novel post-transcriptional regulatory mechanism for the expression of a subset of antiviral ISGs. We found that the m^{6}A methyltransferase complex of METTL3/14 methylates certain antiviral ISGs to facilitate their translation to promote an antiviral cellular state.

The transcript-specific effects of m^{6}A can modulate gene expression to coordinate cellular responses. Indeed, we found that the presence of m^{6}A on ISGs can elicit different mechanisms of post-transcriptional regulation. For *IFITM1*, m^{6}A in the 3' UTR led to an increase in its translation, via METTL3/14 and the reader protein YTHDF1. Consistent with our results, previous reports have shown that 3' UTR m^{6}A modification enhances translation initiation and that YTHDF1 likely mediates this enhancement by recruiting eIF3 to m^{6}A-modified mRNAs [183]. Interestingly, while the m^{6}A-modified *MX1* is also upregulated at the protein level by METTL3/14, YTHDF1 overexpression was not sufficient to elicit this upregulation. This may indicate that MX1 requires other factors or additional readers to enhance its expression. Indeed, YTHDF3 has recently been shown to have roles in promoting translation of m^{6}A-modified genes, perhaps by its interaction with proteins of the 40S and 60S ribosomal subunits [185,273], and YTHDC2 can recognize m^{6}A within coding sequence to enhance translation [266].

Of note, others have found that YTHDF3 inhibits ISG production in murine models through its enhancement of *FOXO3* translation, although this apparently occurred independently of m^{6}A [233]. Therefore, m^{6}A and its related proteins can regulate ISG expression through a variety of mechanisms. Indeed, only a subset of our identified m^{6}A-modified ISGs were translationally enhanced by METTL3/14, as shown by a combination of Ribo-seq, quantitative mass spectrometry, and RNA-seq (Figure 16). As m^{6}A has multiple functions in mRNA metabolism, it is possible that m^{6}A affects processes other than translation for these other modified ISGs, for example by modulating their splicing, nuclear export, secondary structure, or stability [255]. Indeed, it is likely that *ISG15* mRNA stability is regulated by m^{6}A, as we found that this transcript is bound by YTHDF1, appears to have an m^{6}A site in its 3' UTR, and its mRNA levels are increased following METTL3/14 depletion. m^{6}A may also regulate mRNA trafficking or turnover of ISGs at later timepoints after IFN stimulation or may contribute to alternative splicing of antiviral genes in response to IFN.

Disentangling the regulatory effects of m^{6}A on viral infection has been challenging, as both viral and host transcripts contain m^{6}A [178]. Recent work by our group and others revealed that m^{6}A regulates several aspects of the host response to infection [231,232,257]. For example, when the *IFNB1* transcript is induced, which can occur in response to viral infection, it is modified by m^{6}A, and this destabilizes the transcript. This regulation of *IFNB1* may serve as an intrinsic mechanism to dampen and control the innate immune response [231,232]. Interestingly, HCMV appears to hijack this arm of immune regulation by upregulating METTL3/14 expression to increase m^{6}A on *IFNB1*, which ultimately decreases IFN-β production, resulting in enhanced viral replication [231,232]. However, in our work, by directly stimulating ISGs with IFN-β, we

reveal additional m^{6}A-mediated regulation of certain ISGs downstream of IFN-β production. Specifically, we show that METTL3/14 depletion reduces the ability of IFN to restrict VSV infection, while METTL3/14 overexpression enhances the ability of IFN to inhibit VSV infection (Figure 18). Importantly, as VSV replication was not affected by changes in METTL3/14 expression in the absence of IFN, this suggests that the differential ability of IFN to restrict VSV following perturbation of METTL3/14 expression is not mediated by direct regulation of the viral RNA (Figure 18). Rather, these data support the idea that METTL3/14 augments the antiviral response by enhancing the production of ISGs. Identifying the factors that control m^{6}A addition to a specific subset of ISGs will be an important future pursuit and may clarify why only a subset of these antiviral genes become methylated. Many type I IFN-stimulated genes are also induced by type II (IFN-γ) and type III (IFN-λ) IFNs. Future studies may uncover whether signaling downstream of these IFN families also leads to similar m^{6}A-mediated modulation of ISG expression. Additionally, exploring whether viruses employ strategies to counter METTL3/14-mediated enhancement of ISGs will shed further light on the interplay between viral and host RNA processes and how RNA modifications regulate these processes.

In addition to regulating type I IFN pathways, m^{6}A tunes other cellular responses to viral infection. We recently showed changes to the m^{6}A status of certain host transcripts in response to infection by *Flaviviridae*. Further, we found that many of these m^{6}A-altered genes regulate *Flaviviridae* infection [257]. Some of the alterations in m^{6}A during infection were driven by innate immune sensing pathways, revealing that innate immune activation can affect cellular m^{6}A distribution during infection. Others have recently shown that VSV infection impairs the demethylase activity of ALKBH5, resulting

in increased m^{6}A modification and destabilization of the *OGDH* transcript. This resulted in less production of the metabolite itaconate, which appeared to be required for VSV replication [177]. While these effects of m^{6}A on VSV replication occurred independently of IFN signaling, our work revealed that m^{6}A can also inhibit VSV replication by promoting ISG expression during IFN signaling. While we did not find an effect of m^{6}A on VSV replication in the absence of IFN signaling, as described above [177], we did not investigate a role for ALKBH5. Taken together, our findings add to the knowledge of the diverse regulatory functions of m^{6}A during host-pathogen interactions.

In summary, we reveal a subset of ISGs that are post-transcriptionally regulated by METTL3/14 through m^{6}A modification. Additionally, we show that the translation of these ISGs is enhanced by m^{6}A and postulate that m^{6}A may be utilized during the IFN response as a strategy for efficient production of antiviral proteins and the establishment of an antiviral cellular state. Together, these data provide a new molecular understanding of type I IFN response regulation that will ultimately broaden our understanding of innate immunity and host-pathogen interactions. In addition to their functions in antiviral innate immunity, ISGs are also known to regulate inflammation and cell death and recent reports have discovered roles for ISGs in cancer and embryonic development [114,116,117]. Therefore, characterizing the molecular mechanisms that govern ISG expression will be essential for understanding their dysregulation and this information could be harnessed to develop therapeutics to alter ISG expression, which will be relevant to multiple diseases.

2.4 Materials and methods

2.4.1 Cell lines.

Human hepatoma Huh7 cells, lung carcinoma A549 cells, neonatal human dermal fibroblast (NHDF) cells, Vero cells, and embryonic kidney 293T cells were grown in Dulbecco's modification of Eagle's medium (DMEM; Mediatech) supplemented with 10% fetal bovine serum (Thermo Fisher Scientific), 1X minimum essential medium non-essential amino acids (Thermo Fisher Scientific), and 25 mM HEPES (Thermo Fisher Scientific) (cDMEM). The identity of the Huh7 cells used in this study was verified by using the GenePrint STR kit (Promega) (DNA Analysis Facility, Duke University, Durham, NC, USA). A549 cells, 293T, and Vero cells (CCL-185, CRL-3216, and CCL-81) were obtained from American Type Culture Collection (ATCC), NHDF cells (CC-2509) were obtained from Lonza, and Huh7 cells were a gift of Dr. Michael Gale. All cell lines were verified as mycoplasma free by the LookOut Mycoplasma PCR detection kit (Sigma).

2.4.2 IFN-β treatment.

All IFN-β (PBL Assay Science) treatments were performed at a concentration of 50 units/mL in cDMEM, unless otherwise noted.

2.4.3 VSV infection.

GFP-expressing VSV [274] was obtained from Dr. Sean Whelan and propagated by infecting Vero cells grown in cDMEM for 48 hours, after which infectious supernatant was harvested and cleared by centrifugation (1,000 X g for 10 minutes at 4°C) and frozen at -80°C prior to titering. To determine the titer of viral stocks, confluent Vero cells were inoculated with serial dilutions of VSV in serum-free DMEM for 2 hours, overlaid

with cDMEM containing 2% SeaPlaque Agarose (Lonza), and incubated at 37°C for an additional 24 hours. Cells were then fixed using 4% formaldehyde and visualized to count GFP-expressing plaques and calculate plaque forming units/mL. Experimental VSV infections were performed at a multiplicity of infection of 2 in serum-free DMEM for 1.5 h, after which cDMEM was replenished. Cells were fixed in 4% formaldehyde, washed with PBS, and stained for DAPI (4′,6-diamidino-2-phenylindole) (Life Technologies, 1:1000). For each condition, 5 images were acquired at 10X magnification on a Zeiss Axio Observer Z1 microscope, and images were processed using ZEN 2 (Zeiss). The percent of cells infected was calculated by counting the number of GFP-positive cells / the number of nuclei (DAPI).

2.4.4 Plasmids.

These plasmids have been described previously: pLEX-FLAG-YTHDF1 [275], psiCheck2-m^{6}A-null [257], psPAX2 (Addgene plasmid #12260; RRID:Addgene_12260), and pMD2.G (Addgene plasmid # 12259; RRID:Addgene_12259). The following plasmids were constructed in this study: pLEX-FLAG-METTL14, pLEX-FLAG-YTHDF1 W465A, and psiCheck2-m^{6}A-null-ISRE-*IFITM1* 3’ UTR reporter (wild-type and m^{6}A-mut). pLEX-FLAG-METTL14 was generated by cloning the PCR-amplified FLAG-tagged METTL14 coding sequence into the BamHI and XhoI restriction sites of the pLEX expression vector. pLEX-FLAG-YTHDF1 W465A was generated by site-directed mutagenesis of pLEX-FLAG-YTHDF1. WT and m^{6}A-mut IFITM1 3’ UTR reporter plasmids (psiCheck2-m^{6}A-null-ISRE-*IFITM1* 3’ UTR reporter) were generated by inserting either wild-type *IFITM1* 3’ UTR cDNA or *IFITM1* 3’ UTR cDNA with 4 A-to-G mutations at potential m^{6}A sites (obtained as IDT gBlocks) into the XhoI and NotI restriction sites of psiCheck2-m^{6}A-null [257]. The 5X ISRE promoter was PCR-amplified

from pISREluc [276] then inserted into the KpnI and NheI sites. All DNA sequences were verified by sequencing.

2.4.5 Transfection.

siRNAs directed against METTL3 (SI04317096), METTL14 (SI00459942), or non-targeting AllStars negative control siRNA (1027280) were purchased from Qiagen. All siRNA transfections were performed using the Lipofectamine RNAiMax reagent (Invitrogen), according to manufacturer's instructions. siMETTL3/14 co-transfections were performed at a ratio of 1:2 siMETTL3:siMETTL14. Huh7 and A549 cells were transfected with 25 pmol of siRNA at a final concentration of 0.0125 μM, and NHDF cells were transfected with 250 pmol of siRNA at a final concentration of 0.25 μM. Media was changed 4 hours post-transfection, and cells were incubated for 36 h post-transfection prior to each experimental treatment. Plasmid transfections of IFITM1 3' UTR reporter plasmids (500 ng per single well of a 6-well plate) were performed using the FuGENE 6 (Promega), according to manufacturer's instructions.

2.4.6 Generation of overexpression cell lines.

Lentiviral particles were generated by harvesting supernatant 72 h post-transfection of 293T cells with pLEX-FLAG-METTL14, pLEX-FLAG-YTHDF1, or pLEX-FLAG-YTHDF1 W465A, and the packaging plasmids psPAX2 and pMD2.G (provided by Duke Functional Genomics Facility). This supernatant was then used to transduce Huh7 cells for 48 hours. Following transduction, cells were selected in 2 μg/mL puromycin (Sigma) for 48 hours and then single cell colonies were isolated. Overexpression of FLAG-tagged proteins in selected colonies was verified by immunoblotting, and we also verified that METTL14 overexpression stabilized METTL3 [167], creating METTL3/14

overexpression cell lines. These clones were maintained in cDMEM containing 1 µg/mL puromycin.

2.4.7 Immunoblotting.

Cells were lysed in a modified radioimmunoprecipitation assay (RIPA) buffer (10 mM Tris [pH 7.5], 150 mM NaCl, 0.5% sodium deoxycholate, and 1% Triton X-100) supplemented with protease inhibitor cocktail (Sigma) and phosphatase inhibitor cocktail II (Millipore), and post-nuclear lysates were harvested by centrifugation. Quantified protein (between 5 and 15 µg) was added to a 4X SDS protein sample buffer (40% glycerol, 240 mM Tris-HCl [pH 6.8], 8% SDS, 0.04% bromophenol blue, 5% beta-mercaptoethanol), resolved by SDS/PAGE, and transferred to nitrocellulose membranes in a 25 mM Tris-192 mM glycine-0.01% SDS buffer. Membranes were stained with Revert 700 total protein stain (LI-COR Biosciences), then blocked in 3% bovine serum albumin. Membranes were incubated with primary antibodies for 2 hours at room temperature or overnight at 4°C. After washing with PBS-T buffer (1× PBS, 0.05% Tween 20), membranes were incubated with species-specific horseradish peroxidase-conjugated antibodies (Jackson ImmunoResearch, 1:5000) for 1 hour at room temperature, followed by treatment of the membrane with Clarity enhanced chemiluminescence (Bio-Rad) and imaging on an Odyssey Fc imaging system (LI-COR Biosciences). The following antibodies were used for immunoblotting: mouse anti-IFITM1 (Proteintech 60074-1-Ig, 1:1000; recognizes IFITM1 but not IFITM2 or IFITM3 [277,278]), rabbit anti-MX1 (Abcam ab207414, 1:1000), mouse anti-ISG15 (Santa Cruz sc-166755, 1:5000), rabbit anti-EIF2AK2 (Abcam ab32506, 1:1000), rabbit anti-METTL14 (Sigma HPA038002, 1:2500), mouse anti-METTL3 (Abnova H00056339-B01P, 1:1000), rabbit anti-YTHDF1 (Proteintech 17479-1-AP, 1:1000), mouse anti-

FLAG-HRP (Sigma A8592, 1:5000), rabbit anti-GFP (Thermo Fisher Scientific A-11122, 1:1000).

2.4.8 Quantification of immunoblots.

Following imaging using the LI-COR Odyssey Fc, immunoblots were quantified using ImageStudio Lite software, and raw values were normalized to total protein (Revert 700 total protein stain) for each condition.

2.4.9 MeRIP-seq and analysis.

Following mock or IFN-β treatment of Huh7 cells for 8 hours, cellular RNA was harvested using TRIzol (Thermo Fisher Scientific), polyA-tailed mRNA was selected using the Dynabeads mRNA Purification kit (Thermo Fisher Scientific), and MeRIP-seq was performed using the NEB EpiMark m^6A-enrichment kit as previously described [257] with the following modifications. Briefly, 25 mL Protein G Dynabeads (Thermo Fisher) per sample were washed three times in MeRIP buffer (150 mM NaCl, 10 mM Tris-HCl [pH 7.5], 0.1% NP-40), and incubated with 1 mL anti-m6 A antibody for 2 h at 4C with rotation. After washing three times with MeRIP buffer, anti-m6 A conjugated beads were incubated with purified mRNA with rotation at 4C overnight in 300 mL MeRIP buffer with 1 mL RNase inhibitor (recombinant RNasin; Promega). 10% of the mRNA sample was saved as the input fraction. Beads were then washed twice with 500 mL MeRIP buffer, twice with low salt wash buffer (50 mM NaCl, 10 mM Tris-HCl [pH 7.5], 0.1% NP-40), twice with high salt wash buffer (500 mM NaCl, 10 mM Tris-HCl [pH 7.5], 0.1% NP-40), and once again with MeRIP buffer. m6 A-modified RNA was eluted twice in 100 mL of MeRIP buffer containing 5 mM m6 A salt (Santa Cruz Biotechnology) for 30 min at 4C with rotation. Eluates were pooled and concentrated by ethanol purification. RNA-seq

libraries were prepared from both eluate and 10% input mRNA using the TruSeq mRNA library prep kit (Illumina), subjected to quality control (MultiQC), and sequenced on the HiSeq 4000 instrument. Reads were trimmed using Trimmomatic [279] and aligned to the hg38 genome using the splice-aware STAR aligner [280]. Changes in gene expression between Mock and IFN-β treated samples were then identified using DESeq2 [268] based on differences in read counts from featureCounts [281] and plotted in Figure S2A. m^6A peaks were identified in IFN-β treated samples using the MeTDiff peak caller [262] and additionally with meRIPPer software, available at the following URL: (https://sourceforge.net/projects/meripper/). Presented data are from MeTDiff analysis unless otherwise noted. Raw data from Winkler et al. [232] and Rubio et al. [231] were similarly processed (Figure S2B). Coverage plots were generated using CovFuzze [222] and a metagene plot for peak locations produced as previously described [257]. Motif enrichment was calculated using HOMER [282]. Full methods and scripts for data processing are open-source and online on GitHub (https://github.com/al-mcintyre/merip_reanalysis_scripts) [241].

2.4.10 RT-qPCR.

Total cellular RNA was extracted using the Qiagen RNeasy kit (Life Technologies) or TRIzol extraction (Thermo Fisher Scientific). RNA was then reverse transcribed using the iScript cDNA synthesis kit (Bio-Rad) as per the manufacturer's instructions. The resulting cDNA was diluted 1:5 in nuclease-free H2O. RT-qPCR was performed in triplicate using the Power SYBR Green PCR master mix (Thermo Fisher Scientific) and the Applied Biosystems Step One Plus or QuantStudio 6 Flex RT-PCR systems. The oligonucleotide sequences used are listed in Table S5.

2.4.11 Nuclear/cytoplasmic fractionation.

Following siRNA treatment (36 h) and IFN-β treatment (20 h), cells were harvested and lysed in 200 µL lysis buffer (10 mM Tris-HCl [pH 7.4], 140 mM NaCl, 1.5 mM MgCl2, 10 mM EDTA, 0.5% Nonidet P-40 (NP-40)) on ice for 10 minutes. Following centrifugation at 12000 X g at 4°C for 5 minutes, the supernatant (cytoplasmic fraction) was collected, and the nuclear pellet was rinsed twice with lysis buffer. RNA was extracted from cytoplasmic and nuclear pellets using TRIzol reagent and analyzed by RT-qPCR.

2.4.12 Protein stability analysis.

Following siRNA treatment (36 h), Huh7 cells were treated with IFN-β for 16 hours to induce ISGs. IFN-β was then replenished at half the dose in cDMEM containing either DMSO as a control, or 50 µg/mL cycloheximide (CHX, Sigma-Aldrich). Cells were harvested over a timecourse (0, 2, 4, 6, 8, 12 hours post-CHX) and subjected to immunoblotting. Protein stability was determined by measuring the protein remaining at each timepoint following CHX treatment.

2.4.13 Polysome profiling.

Cells treated with siRNAs (36 h) were treated with IFN-β for 6 hours, then pulsed with CHX (50 µg/mL) for 10 minutes. Cells were harvested using trypsin and then lysed in cytoplasmic lysis buffer (200 mM KCl, 25 mM HEPES [pH 7.0], 10 mM MgCl2, 2% n-Dodecyl β-D-maltoside (DDM; Chem-Impex), 0.2 mM CHX, 1 mM DTT, 40 U RNasin) for 15 minutes on ice. Following clarification, lysates were ultracentrifuged on 15-50% sucrose gradients prepared in polysome gradient buffer (200 mM KCl, 25 mM HEPES [pH 7.0], 15 mM MgCl2, 1 mM DTT, 0.2 mM CHX) at 35,000 X g for 3.5 hours at 4°C.

Following ultracentrifugation, 24 fractions were collected from each sample using a BioComp Piston Gradient Fractionator instrument fitted with a TRIAX flow cell to measure absorbance. RNA was extracted from each fraction using TRIzol LS reagent (Thermo Fisher Scientific), and RNA quality was checked on a 1% agarose gel. Following cDNA synthesis using the iScript cDNA synthesis kit (Bio-Rad), RT-qPCR was performed using primers specific for each gene.

2.4.14 MeRIP-RT-qPCR.

Total cellular RNA was harvested using TRIzol reagent and normalized to equal input concentrations. m^6A-positive and m^6A-negative control oligonucleotides (EpiMark N6-Methyladenosine Enrichment Kit, New England Biolabs) were spiked into total RNA prior to immunoprecipitation. RNA was then immunoprecipitated with anti-m^6A antibody (New England Biolabs) overnight at 4°C with head-over-tail rotation, and then washed twice with 1X reaction buffer (150mM NaCl, 10mM Tris-HCl, pH 7.5, 0.1% NP40), twice with low salt wash buffer (50 mM NaCl, 10 mM Tris-HCl, pH 7.5, 0.1% NP-40), twice with high salt wash buffer (500 mM NaCl, 10 mM Tris-HCl, pH 7.5, 0.1% NP-40), and once with 1X reaction buffer. RNA was eluted from beads in elution buffer twice for 1 hour at 4°C, and then precipitated in isopropanol overnight at -20°C, pelleted by centrifugation, and resuspended in nuclease-free water. Equal volumes of eluted RNA and input RNA were used for cDNA synthesis and quantified by RT-qPCR. IP efficiency was normalized by relative pulldown of spike-in positive controls.

2.4.15 Luciferase assays.

Following plasmid transfection of WT and m^6A-mut IFITM1 3’ UTR reporters and mock or IFN-β treatment (12 h), a dual luciferase assay (Promega) was performed

according to manufacturer's instructions. Data was normalized as fold-change (IFN-β over mock) of the value of *Renilla* luminescence divided by firefly luminescence, and values for WT IFITM1 3' UTR reporter were set as 1.

2.4.16 RNA immunoprecipitation.

Following DNA transfection (16 h) and IFN-β treatment (8 h), cells were harvested and lysed in polysome lysis buffer (100 mM KCl, 5 mM MgCl2, 10 mM HEPES [pH 7.0], 0.5% NP-40) supplemented with protease inhibitor cocktail (Sigma) and RNasin ribonuclease inhibitor (Promega), and lysates were cleared by centrifugation. Ribonucleoprotein complexes were immunoprecipitated with anti-FLAG M2 beads (Sigma) overnight at 4°C with head-over-tail rotation, and then washed five times in ice-cold NT2 buffer (50 mM Tris-HCl [pH 7.4], 150 mM NaCl, 1 mM MgCl2, 0.05% NP-40). Protein for immunoblotting was eluted from 25 percent of beads by boiling in 2X Laemmli sample buffer (Bio-Rad). RNA was extracted from 75 percent of beads using TRIzol reagent (Thermo Fisher Scientific). Equal volumes of eluted RNA were used for cDNA synthesis, quantified by RT-qPCR, and normalized to RNA levels in input samples. Enrichment over GFP was then calculated and plotted.

2.4.17 RNA-seq.

Following siRNA treatment (36 h), Huh7 cells seeded in 10-cm^2 plates were stimulated with IFN-β or mock treated (8 h), then harvested and RNA extraction was performed using TRIzol reagent (Thermo Fisher Scientific). Samples were then treated with Turbo DNase I (Thermo Fisher Scientific) according to manufacturer protocol and incubated at 37°C for 30 min, followed by phenol/chloroform extraction and ethanol precipitation overnight. RNA concentrations were then normalized. Sequencing libraries

were prepared using the KAPA Stranded mRNA-Seq Kit (Roche) and sequenced on an Illumina HiSeq 4000 with 100 bp paired-end reads by the Duke University Center for Genomic and Computational Biology.

2.4.18 Ribo-seq.

Following siRNA treatment (36 h), Huh7 cells seeded in 15-cm^2 plates were stimulated with IFN-β (8 h), then washed with ice cold PBS, and flash frozen in liquid nitrogen. Cells were then lysed in plates with polysome lysis buffer (20 mM Tris-HCl [pH 7.4], 150 mM NaCl, 5 mM $MgCl_2$, 1 mM DTT, 1% Triton X-100, 25 U/mL Turbo DNase I (Thermo Fisher Scientific)), scraped, and passed through a 25 gauge needle before collection in microfuge tubes and incubation for 15 minutes on ice. Cytoplasmic lysates were clarified by centrifugation. 5% of lysate was taken for western blotting, and the remaining cytoplasmic lysate was supplemented with 0.4M $CaCl_2$ and 4000 gel units micrococcal nuclease (New England Biolabs), and incubated at 37°C (30 min) to generate ribosome protected fragments (RPF RNA). RPF RNA was then ultracentrifuged (35000 X g at 4°C for 3.5 h), over 15-50% sucrose gradients in polysome gradient buffer (20 mM Tris-HCl [pH 7.4], 150 mM NaCl, 5 mM $MgCl_2$, 1 mM DTT), after which 12 fractions were collected from each sample using a BioComp Piston Gradient Fractionator instrument fitted with a TRIAX flow cell to measure absorbance. Monosome fractions (fractions 6 and 7) were then pooled and loaded onto a 100 kD molecular weight cut-off filter (Vivaspin 20) and centrifuged at 3000 X g at 4°C for 35 minutes to concentrate monosome-bound RPF RNA. The flow-through was discarded and retained monosomes were separated from RPF RNA by adding polysome lysis buffer supplemented with 50 mM EDTA and incubation on ice for 15 minutes. The resulting RPF RNA solution was then re-applied to the emptied 100 kD molecular weight cut-off

filter and centrifuged at 3000 X g at 4°C for 15 minutes to separate RPF RNA from monosomes. The flow-through containing the RPF RNA was then collected, phenol-chloroform extracted, and ethanol precipitated. Precipitated RPF RNA samples were then run on a 15% TBE-Urea gel (Invitrogen), and a band corresponding to 28-32 nucleotides was excised, crushed, and incubated in 0.4M NaCl with 40 units of RNasin ribonuclease inhibitor (Promega) for 8 hours shaking at 4°C 1100 RPM. RNA was recovered by filtration through Corning Costar Spin-X columns (Sigma-Aldrich) then isopropanol precipitated overnight. After resuspension, the remaining RNA was T4 Polynucleotide Kinase (New England Biolabs) treated, phenol-chloroform extracted, and precipitated in ethanol overnight. Sequencing libraries for RPF samples were then generated using the NEB Next small RNA library prep kit and these libraries were sequenced on an Illumina NextSeq 500 High-output 75 bp with paired end reads by the Duke University Center for Genomic and Computational Biology.

2.4.19 RNA-seq and Ribo-seq data analysis.

Reads were evaluated using FastQC and trimmed using cutadapt [283], followed by alignment to the hg38 human reference genome using the STAR aligner with default parameters. The number of read fragments uniquely aligned to each gene were counted with the Gencode v21 main comprehensive gene annotation file (aggregated by gene_name) using featureCounts. Using a python script, the raw counts from each replicate and condition were merged to generate a count matrix with N rows/genes and M samples/columns (python scripts for count-matrix generation are open-source and on GitHub (https://github.com/hmourelatos/McFadden_ISG_m6a_countMatricies)). To identify differentially expressed genes between various groups, we used DESeq2 [268] to perform three pairwise contrasts. First, with RNA-seq we compared the effects of IFN-

β and mock treatment in cells transfected with siCTRL (Table S1.1). Additional RNA-seq analyses included comparison of siMETTL3/14 and siCTRL treated cells after both IFN-β and mock treatment (Tables S1.2 and S1.3, respectively). Finally, with Ribo-seq, we compared siMETTL3/14 and siCTRL treated cells following IFN-β treatment (Table S4). In each case, DESeq2 was applied with no additional covariates and results shown in Tables S1.1, S1.2, and S3 respectively. Metagene plots from Ribo-seq reads were composed using deepTools v3.1 [284] with the computeMatrix utility. RNA-seq heatmap was generated using R software, and the heatmap for Ribo-seq was generated using ClustVis [285].

2.4.20 Mass spectrometry.

Prior to the siRNA experiments, cells were grown for at least 12 generations in DMEM medium without Lysine and Arginine (#PI88420), supplemented with Dialyzed FBS (#26000044), either light or heavy L-Arginine and L-Lysine (L-Arginine-HCl #PI88427; L-Arginine-HCl, 13C6, 15N4 #PI88434; L-Lysine-2HCl #PI88429; L-Lysine-2HCl, 13C6, 15N2 #PI88432), and 100 U/ml penicillin, 100 µg/ml streptomycin and 2 mM L-glutamine. Following stable isotope labeling, siRNA-treated cells (36 h) were stimulated with IFN-β for 24 hours prior to harvest by trypsinization and lysis in RIPA buffer supplemented with protease inhibitor cocktail (Sigma) and phosphatase inhibitor cocktail II (Millipore), and post-nuclear lysates were harvested by centrifugation. 5 µL at 1 µg/µL of siMETTL3/14 (Heavy) extracts were mixed with 5 µL at 1 µg/µL of siCTRL (Light) extracts for the Forward experiment, and 5 µL at 1 µg/µL of siMETTL3/14 (Light) extracts were mixed with 5 µL at 1 µg/µL of siCTRL (Heavy) extracts for the Reverse experiment. The lysates were run on a 4-12% Bis-Tris gel for 30 min. The gel was stained with Colloidal Coomassie and a single patch was cut and processed for each

sample. The gel patches were digested with trypsin. The resulting peptides were cleaned with a C18 tip. Liquid chromatography was performed with an EASY-nLC™ 1000 Integrated Ultra High Pressure Nano-HPLC System and MS/MS with a Q-EXACTIVE System equipped with a Nanospray Flex Ion Source, as previously described [286].

2.4.21 Mass spectrometry data analysis.

Four RAW files representing two replicates each of Forward and Reverse SILAC experiments were retrieved from the Orbitrap. Heavy/light label ratios were quantified across all samples using MaxQuant v1.6.7.0 with the Andromeda search engine and default parameters other than specifying SILAC labels [287,288]. For all analyses, the "H/L Ratio – Normalized" field containing median-centered label ratios was extracted for each peptide and/or protein and compared across replicates (Table S3). Heatmaps for mass spectrometry were generated using ClustVis [285].

Peptide regression modeling:

To take advantage of the measurement independence of unique peptides, we applied a simple linear mixed model to identify significant shifts in labeling ratio between conditions while accounting for peptide-specific effects. First, we merge all proteins that are described by the same set of peptide ratios (e.g. protein sequences from the same gene for which all detected peptides are shared). Then, for each protein (defined now as a set of peptide ratios), we fit a linear model of the following form using lme4 in R [289]

$$r \sim Zu_{pep} + X\beta_{label} + \epsilon$$

where:

- *r* is the median-normalized heavy/light label ratio derived from MaxQuant

- Z is a binary design matrix indicating the peptide identity of each ratio measurement
- X is a binary design vector indicating condition (forward or reverse)
- u_{pep} is a vector of random effects corresponding to each peptide effect
- β_{label} is the fixed effect of condition

Thus, each peptide ratio is described as the sum of a peptide-level random effect and a condition (forward vs reverse) fixed effect, and some error. We extract effect size estimates and p-values from unmodified Wald tests on the fixed effect of condition, and adjust across all proteins with the Benjamini-Hochberg (BH) procedure. Note that in the less-powerful case of proteins with only one measured peptide, the random peptide effect is just a constant and the model reduces to simply comparing the means of the forward and reverse replicate ratios for the single peptide.

Aggregating proteins for gene-level results:

Peptide regression modeling generates one test for each protein, so many genes are tested multiple times at each of their proteins. Annotated reference protein sequences often contain multiple entries per gene with varying degrees of similarity. After applying the procedure above, we observe as expected that the vast majority of genes contain either all significant or all non-significant protein results. We conservatively describe as significant any gene with a significant maximum p-value (meaning all tested proteins are significant) following multiple test correction.

2.4.22 Oligonucleotides and siRNAs used in this study.

Table 6: List of oligonucleotides and siRNAs used in this study.

Due to size, this table has not been included in this document. It can be downloaded from this link: Table 6

2.5 Data availability

Data availability. All raw data from RNA-seq, MeRIP-seq, and Ribo-seq are available through GEO (accession number: GSE155448).

Raw data from mass spectrometry are available at the following URLs:

https://web.corral.tacc.utexas.edu/xhemalce/Forward1.raw

https://web.corral.tacc.utexas.edu/xhemalce/Forward2.raw

https://web.corral.tacc.utexas.edu/xhemalce/Reverse1.raw

https://web.corral.tacc.utexas.edu/xhemalce/Reverse2.raw

3. FTO is a transcriptional suppressor of a subset of ISGs

3.1 Introduction

The fat mass and obesity-associated (FTO) gene encodes an enzyme whose function is crucial for human health, and variants of this gene are associated with obesity and body mass index, type 2 diabetes, inflammation, and cardiovascular disease [290-293]. Additionally, genetic variants that result in full loss of enzymatic function cause severe defects in the development of the central nervous system and cardiovascular system that can result in lethality [294]. Despite its essential functions for human development and health, the molecular functions of FTO that regulate these biological processes are incompletely understood. Analysis of the sequence homology of FTO revealed similarity to alpha-ketoglutarate oxygenase enzymes, particularly the AlkB homolog family (ALKBH) proteins [295]. This study also uncovered a role for FTO in nucleic acid demethylation. Subsequently, the RNA modification m^6A was found to be a major substrate of FTO [172], a function shared by ALKBH5 [173]. FTO can also catalyze the removal of the cap-adjacent m^6Am modification [296]. Through these

functions, FTO can regulate the biology of many m^{6}A-modified RNAs [145]. These discoveries have led to many studies describing functions for FTO and its m^{6}A demethylase activity in regulation of cellular and biological processes, including neurogenesis, dopamine signaling and appetite regulation, adipogenesis, oncogenesis, and viral infection [178,205,297-301].

We previously reported a role for FTO in regulation of infection by HCV [187]. However, the role of FTO in regulation of host response pathways to viral infection has not been elucidated. Interestingly, FTO was recently shown to regulate the response of melanoma cells to IFN-γ treatment, suggesting a role in the response to IFNs [301]. Given its link to inflammation and obesity, it will be important to determine how FTO regulates IFN pathways, as these are major inflammatory cytokines. Additionally, having found a role for m^{6}A in regulation of the type I IFN response (Chapter 2; [244]), we sought to determine whether FTO also regulates the type I IFN response through its role as an m^{6}A demethylase.

Here, we found that depletion of FTO results in increased production of a subset of ISGs, some of which are METTL3/14-regulated. However, unlike METTL3/14, FTO regulates the mRNA levels of these ISGs. Additionally, FTO appears to regulate a distinct subset of ISGs from those regulated by METTL3/14, and these include many proinflammatory genes. By labeling nascent RNA, we found that FTO regulates the transcription of ISGs and that FTO-depleted cells are primed to respond to type I IFN treatment. Finally, we found that FTO regulation of ISGs is not dependent on its m^{6}Am demethylase activity, as deletion of the m^{6}Am writer enzyme did not impact the phenotypic effect of FTO depletion on ISG expression. Taken together, these results reveal a novel role for FTO in the transcriptional suppression of a subset of ISGs,

including genes that regulate inflammation. These results may have important implications for our understanding of the role of FTO in disease.

3.2 Results

3.2.1 FTO regulates the mRNA expression of a subset of ISGs.

Having demonstrated that METTL3/14 and m^{6}A regulate the translation of a subset of ISGs (Chapter 2; [244]), we hypothesized that FTO could mediate the removal of m^{6}A on these ISGs and suppress their translation. To test this hypothesis, we used siRNAs to deplete METTL3/14 or FTO and stimulated the expression of ISGs with IFN-β treatment (12 hours) and measured the expression of a subset of ISGs by immunoblotting. As expected, depletion of FTO resulted in increased protein expression of a subset of ISGs, including IFITM1, GBP1, and IFIT3, all of which were decreased by METTL3/14 depletion (Figure 19A). However, while MX1 protein expression was decreased by METTL3/14 depletion, as expected, it was unaffected by FTO depletion. The ISGs ISG15 and EIF2AK2 were unaffected by either METTL3/14 or FTO depletion (Figure 19A). These results seemed to support our hypothesis that FTO suppresses the translation of ISGs. However, FTO depletion also resulted in a similar increase at the mRNA level of the ISGs that it regulated, whereas METTL3/14 depletion did impact the mRNA levels of ISGs (Figure 19B). These results suggested that FTO regulates a subset of ISGs by a mechanism distinct from METTL3/14 and m^{6}A-mediated translation enhancement of ISGs.

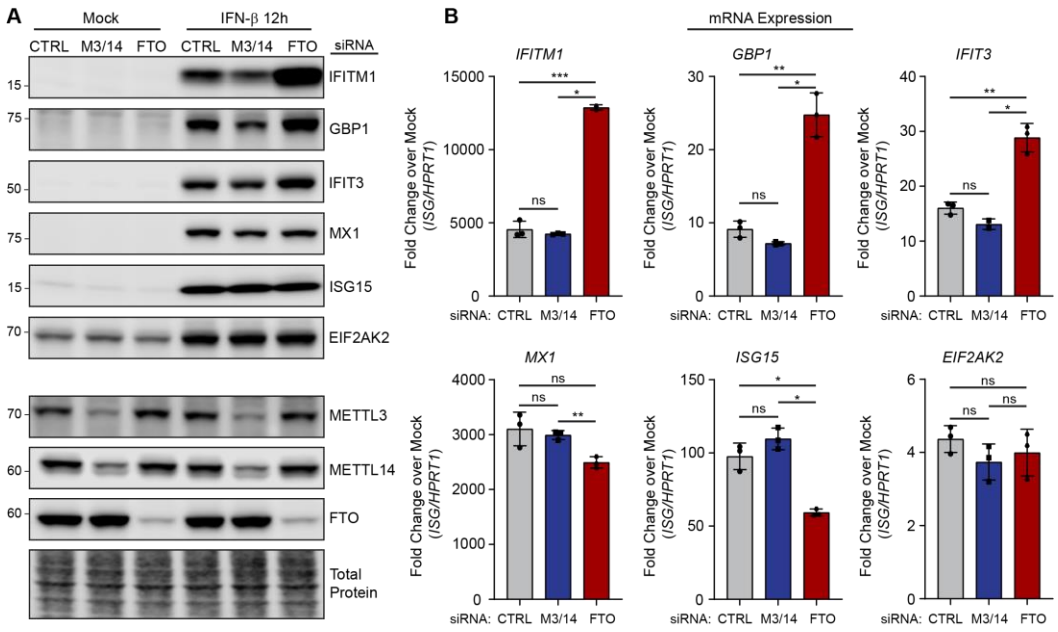

Figure 19: FTO regulates the mRNA expression of a subset of ISGs.
(A) Immunoblot analysis of extracts from Huh7 cells transfected with siRNAs to control (CTRL), METTL3/14 (M3/14), or FTO prior to mock or IFN-β (12 h) treatment. Data are representative of 3 biological experiments. **(B)** RT-qPCR analysis of ISG induction normalized to *HPRT1* following IFN-β treatment of Huh7 cells treated with non-targeting control (CTRL) or METTL3/14 siRNA plotted as fold change over mock treatment for each ISG. Values are the mean ± SD of 3 technical replicates, representative of 3 biological experiments. * $p < 0.05$, ** $p < 0.01$, *** $p < 0.005$ by one way ANOVA with Dunnett's multiple comparisons test (C-E).

3.2.2 FTO regulates the transcription of a subset of ISGs

Having determined that FTO regulates the mRNA levels of certain of ISGs, we next used RNA-seq to profile gene expression in FTO-depleted cells, following IFN-β stimulation (8 hours) (Table 7). Gene ontology analysis of the genes significantly regulated by FTO (adjusted $P < 0.01$) revealed that FTO-regulated genes are enriched in biological categories involved in transcription and signal transduction. Immune processes were also particularly enriched, including antigen presentation, chemokine production, response to type I IFN and IFN-γ, viral defense, and regulation of immune

cell activation (Table 7). This suggested that FTO regulates many ISGs and other genes involved in immune processes. We plotted the effect of FTO depletion on the top 300 most highly induced ISGs (Figure 20A). This revealed that a majority of ISGs are upregulated at the mRNA level following FTO depletion. Indeed, of these 300 ISGs, 114 were significantly regulated by FTO (adjusted $P < 0.01$) (Figure 20B). Interestingly, the expression of all but 2 of these FTO-regulated ISGs was increased upon FTO depletion, confirming that FTO is a suppressor of a subset of ISGs (Figure 20B). Among the most highly induced of these genes were the proinflammatory cytokines CXCL10 and CXCL11. Genes among the FTO-regulated subset in Figure 19 (IFITM1, IFIT3, and GBP1) were also upregulated by FTO in these data (Figure 20B). These data reveal that FTO is a suppressor of a subset of ISGs.

Table 7: RNA-seq analysis of mRNA expression following IFN-β treatment and FTO depletion.

Table 7.1: siFTO IFN / siCTRL IFN
Table 7.2: Gene Ontology analysis of FTO-regulated genes
Due to size, this table has not been included in this document. It can be downloaded from this link: Table 7

To determine how FTO regulates the mRNA expression of ISGs, we pulsed CTRL, METTL3/14, or FTO-depleted cells with 4-thiouridine (4-sU) and IFN-β for 1 hour to metabolically label nascent transcripts produced in response to IFN stimulation. We then purified the nascent RNA and performed RT-qPCR to quantify relative transcription. These experiments revealed that depletion of FTO led to a marked increase of the transcription of *IFITM1*, an FTO-regulated ISG, during the pulse. Interestingly, the transcription of *ISG15* and *EIF2AK2* were also slightly increased by FTO depletion,

although this was not statistically significant (Figure 20C). Alternatively, METTL3/14 depletion did affect the transcription of any of these ISGs, and the transcription of a housekeeping gene, *CREBBP*, was not affected in any condition (Figure 20C). We next performed an additional similar experiment with 4-sU and IFN-β pulses of both 1 hour and 12 hours and measured the transcription of additional ISGs (Figure 20D-E). Interestingly, nearly all ISGs tested (*IFITM1*, *MX1*, *ISG15*, *EIF2AK2*, *GBP1*, *IFIT3*, and *CXCL10*) had a slight increase in transcription following FTO depletion at 1 hour, but these effects were not observed after a 12 hour pulse for the ISGs *MX1*, *ISG15*, and *EIF2AK2*, none of which were regulated in Figure 19 or in our RNA-seq data. These data likely indicate that FTO-depleted cells are primed to respond to IFN-β, as they transcribe ISGs more rapidly, but negative regulators of the type I IFN response seem to be functional, as these early effects normalize to siCTRL cells after 12 hours.

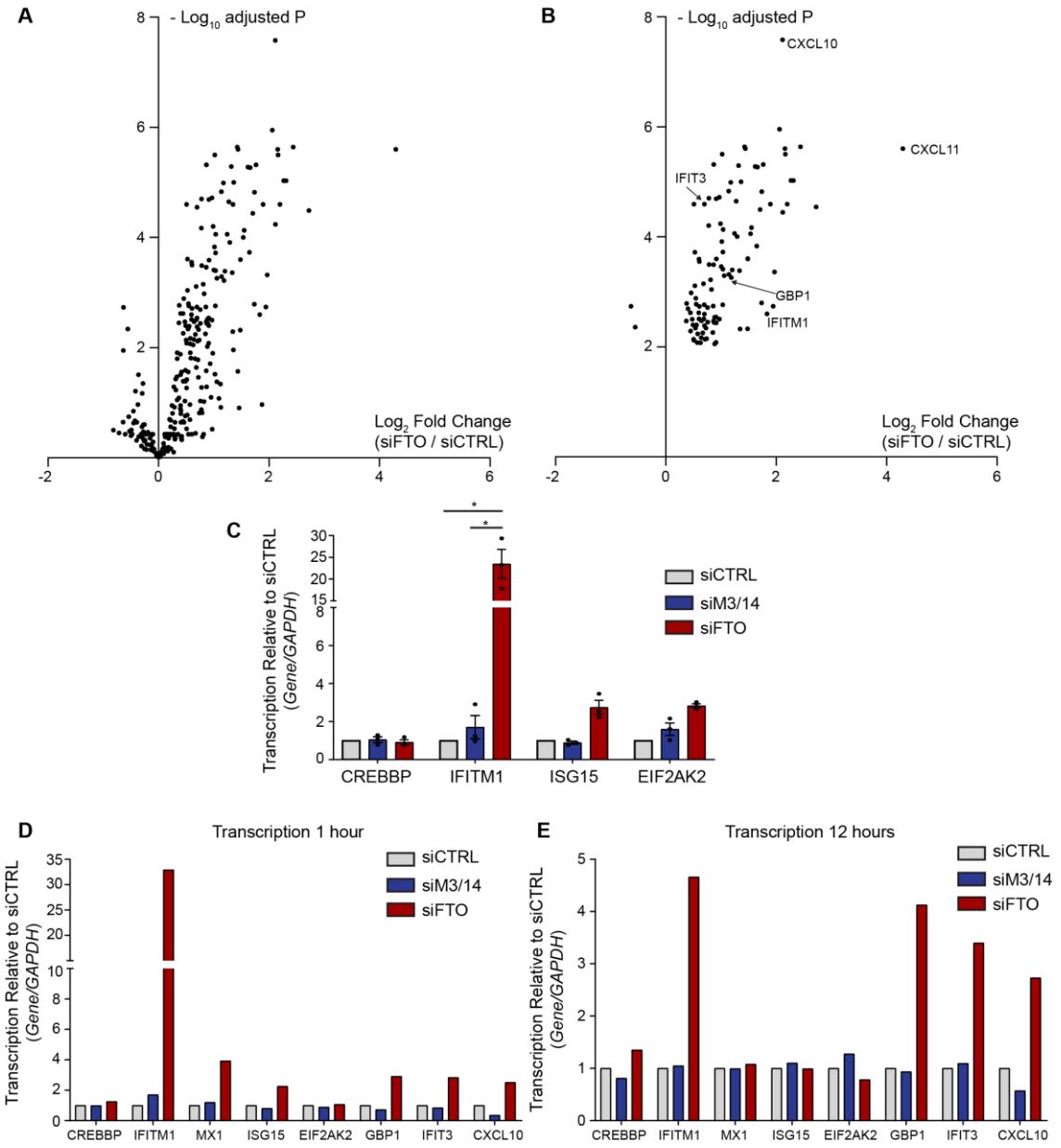

Figure 20: FTO regulates the transcription of ISGs.
(A-B) RNA-seq analysis following siRNA transfection and IFN-β treatment (3 biological replicates). (A) Volcano plot of FTO depletion effect (siFTO / siCTRL) on the 300 most highly induced ISGs. (B) Volcano plot of significantly FTO-regulated ISGs (adjusted P < 0.01). **(C)** Relative transcription measured by 4-sU pulse labeling for 1 hour. Values are the mean ± SEM of 3 biological experiments. * P < 0.01; all other comparisons not significant (P < 0.05) by 2-way ANOVA with Tukey's multiple comparisons. **(D-E)** Relative transcription measured by 4-sU pulse labeling for 1 hour (D) or 12 hours (E). Values are the mean of 3 technical replicates.

3.2.3 FTO regulation of ISGs occurs independently of the RNA modification m^{6}Am

The role of FTO as an RNA demethylase is among its major molecular functions, and recent work suggests that the cap-adjacent m^{6}Am modification, which can regulate transcript stability, may be the primary substrate for FTO demethylation [296]. m^{6}Am deposition is catalyzed by the enzyme PCIF1 [270,271]. We used PCIF1 knockout cells [270] to determine whether this modification is responsible for FTO regulation of ISGs. We would hypothesize that the phenotypic effect of FTO depletion would be lost in PCIF1 knockout cells, if m^{6}Am were involved in this regulation. However, IFITM1 expression was similarly affected by FTO depletion in both wild-type and PCIF1 knockout 293T cells (Figure 21). These data reveal that FTO regulates ISGs via an m^{6}Am-independent mechanism.

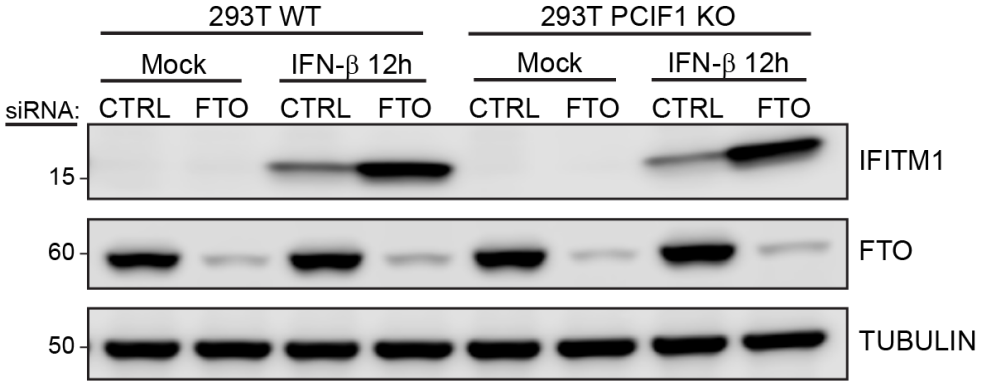

Figure 21: FTO regulation of IFITM1 occurs independently of m^{6}Am.
Immunoblot analysis of extracts from wild-type (WT) or PCIF1 knockout 293T cells transfected with siRNAs to control (CTRL) or FTO prior to mock or IFN-β (12 h) treatment.

3.3 Discussion

Through these experiments, we have identified a novel role for FTO in regulating the expression of ISGs. We had previously discovered that METTL3/14 and m^{6}A

regulate the translation of a subset of ISGs [244], but here we report that, surprisingly, FTO-regulated ISGs are distinct from those regulated by METTL3/14 and are regulated at the level of transcription. FTO-regulated ISGs include many proinflammatory factors, and FTO-depleted cells appear to be primed to respond to type I IFNs. This transcription regulatory role of FTO is independent of its ability to demethylate m^6Am. These data reveal important roles for FTO in type I IFN response regulation, which may have important implications for inflammatory and antiviral responses.

The function of FTO as an RNA demethylase appears to be important for a number of biological processes [145]. The relative contributions of its m^6A versus m^6Am demethylase activity in the biological functions of FTO have recently been a source of debate [296,302], and other molecular functions of FTO are understudied. A recent study found that FTO can mediate transcriptional repression activity, as FTO can bind to its own promoter to inhibit its transcription in an auto-regulatory feedback loop [303]. Here, we describe a novel function of FTO in transcriptional repression of ISGs, although the mechanisms by which FTO represses these ISGs remains unknown. We found that m^6Am is not involved in this regulation, although the contributions of m^6A have not been explored. It is unlikely that FTO demethylation of m^6A sites on ISGs exerts *cis*-regulatory control of their transcription. Rather, FTO may modulate the expression of a *trans*-regulatory factor, such as a transcription factor or epigenetic modifier, through its m^6A demethylase activity.

It is possible that FTO binds to the promoters of ISGs to exert its transcription repression activity. FTO is known to localize to nuclear speckles, which are transcription hubs [172,304], thus FTO binding to DNA would not be surprising. FTO may also either directly or indirectly recruit epigenetic modifiers, such as chromatin silencers, to the

promoters of ISGs. Thus, it will be important to profile the chromatin landscape of FTO-depleted cells to determine whether ISG promoters are primed for transcription. Indeed, our data suggest that FTO-depleted cells respond more efficiently to IFN treatment, although negative regulation of the type I IFN response is likely intact (Figure 20).

There are many mechanistic possibilities for the role of FTO in transcriptional regulation of ISGs, as well as transcriptional regulation of the genome more broadly. Future studies to determine how FTO represses transcription and what other classes of genes are transcriptionally regulated by FTO will be very important for our understanding of the molecular functions of FTO and how FTO regulates biological processes. These results may have broad implications for the involvement of FTO in human disease, especially inflammation-related conditions.

3.4 Materials and methods

3.4.1 Cell lines.

Human hepatoma Huh7 cells and embryonic kidney 293T cells were grown in Dulbecco's modification of Eagle's medium (DMEM; Mediatech) supplemented with 10% fetal bovine serum (Thermo Fisher Scientific), 1X minimum essential medium non-essential amino acids (Thermo Fisher Scientific), and 25 mM HEPES (Thermo Fisher Scientific) (cDMEM). Huh7 cells used in this study were a gift of Dr. Michael Gale, and their identity was verified by using the GenePrint STR kit (Promega) (DNA Analysis Facility, Duke University, Durham, NC, USA). Wild-type and PCIF1 knockout 293T cells [270] were a gift of Dr. Eric Greer. All cell lines were verified as mycoplasma free by the LookOut Mycoplasma PCR detection kit (Sigma).

3.4.2 IFN-β treatment.

All IFN-β (PBL Assay Science) treatments were performed at a concentration of 50 units/mL in cDMEM.

3.4.3 Transfection.

siRNAs directed against FTO (SI04177530), METTL3 (SI04317096), METTL14 (SI00459942), or non-targeting AllStars negative control siRNA (1027280) were purchased from Qiagen. All siRNA transfections were performed using the Lipofectamine RNAiMax reagent (Invitrogen), according to manufacturer's instructions. siMETTL3/14 co-transfections were performed at a ratio of 1:2 siMETTL3:siMETTL14. Transfections were performed with 25 pmol of siRNA at a final concentration of 0.0125 μM. Media was changed 4 hours post-transfection, and cells were incubated for 36 h post-transfection prior to each experimental treatment.

3.4.4 Immunoblotting.

Cells were lysed in a modified radioimmunoprecipitation assay (RIPA) buffer (10 mM Tris [pH 7.5], 150 mM NaCl, 0.5% sodium deoxycholate, and 1% Triton X-100) supplemented with protease inhibitor cocktail (Sigma) and phosphatase inhibitor cocktail II (Millipore), and post-nuclear lysates were harvested by centrifugation. Quantified protein (between 5 and 15 μg) was added to a 4X SDS protein sample buffer (40% glycerol, 240 mM Tris-HCl [pH 6.8], 8% SDS, 0.04% bromophenol blue, 5% beta-mercaptoethanol), resolved by SDS/PAGE, and transferred to nitrocellulose membranes in a 25 mM Tris-192 mM glycine-0.01% SDS buffer. Membranes were stained with Revert 700 total protein stain (LI-COR Biosciences), then blocked in 3% bovine serum albumin. Membranes were incubated with primary antibodies for 2 hours at room

temperature or overnight at 4°C. After washing with PBS-T buffer (1× PBS, 0.05% Tween 20), membranes were incubated with species-specific horseradish peroxidase-conjugated antibodies (Jackson ImmunoResearch, 1:5000) for 1 hour at room temperature, followed by treatment of the membrane with Clarity enhanced chemiluminescence (Bio-Rad) and imaging on an Odyssey Fc imaging system (LI-COR Biosciences). The following antibodies were used for immunoblotting: mouse anti-IFITM1 (Proteintech 60074-1-Ig, 1:1000; recognizes IFITM1 but not IFITM2 or IFITM3 [277,278]), rabbit anti-MX1 (Abcam ab207414, 1:1000), mouse anti-ISG15 (Santa Cruz sc-166755, 1:5000), rabbit anti-EIF2AK2 (Abcam ab32506, 1:1000), rabbit anti-GBP1 (Abcam EPR8285), mouse anti-IFIT3 (Abcam ab76818), rabbit anti-METTL14 (Sigma HPA038002, 1:2500), mouse anti-METTL3 (Abnova H00056339-B01P, 1:1000), rabbit anti-FTO (Abcam EPR6895, 1:1000), mouse anti-TUBULIN (Sigma T5168, 1:5000).

3.4.5 RT-qPCR.

Total cellular RNA was extracted using the Qiagen RNeasy kit (Life Technologies) or TRIzol extraction (Thermo Fisher Scientific). RNA was then reverse transcribed using the iScript cDNA synthesis kit (Bio-Rad) as per the manufacturer's instructions. The resulting cDNA was diluted 1:5 in nuclease-free H2O. RT-qPCR was performed in triplicate using the Power SYBR Green PCR master mix (Thermo Fisher Scientific) and the Applied Biosystems Step One Plus or QuantStudio 6 Flex RT-PCR systems. Primer sequences for RT-qPCR are listed in Table 8.

Table 8: RT-qPCR primers used in this study.

Target	**Forward Primer (5'-3')**	**Reverse Primer (5'-3')**
GAPDH	AAGGTGAAGGTCGGAGTCAAC	GGGGTCATTGATGGCAACAATA

HPRT1	TGACACTGGCAAAACAATGCA	GGTCCTTTTCACCAGCAAGCT
CREBBP	CTCAGCTGTGACCTCATGGA	AGGTCGTAGTCCTCGCACAC
IFITM1	ACTAGTAGCCGCCCATAGCC	GCACGTGCACTTTATTGAATG
MX1	TTCAGCACCTGATGGCCTATC	TGGATGATCAAAGGGATGTGG
ISG15	GCGAACTCATCTTTGCCAGTA	CCAGCA TCTTCACCGTCAG
EIF2AK2	TCGCTGGTATCACTCGTCTG	GATTCTGAAGACCGCCAGAG
GBP1	GTGGAACGTGTGAAAGCTGA	CAACTGGACCCTGTCGTTCT
IFIT3	AGTCTAGTCACTTGGGGAAAC	ATAAATCTGAGCATCTGAGAGTC
CXCL10	AGCAGAGGAACCTCCAGTCT	ATGCAGGTACAGCGTACAGT

3.4.6 RNA-seq and analysis.

Following siRNA treatment (36 h), Huh7 cells seeded in 10-cm^2 plates were stimulated with IFN-β or mock treated (8 h), then harvested and RNA extraction was performed using TRIzol reagent (Thermo Fisher Scientific). Samples were then treated with Turbo DNase I (Thermo Fisher Scientific) according to manufacturer protocol and incubated at 37°C for 30 min, followed by phenol/chloroform extraction and ethanol precipitation overnight. RNA concentrations were then normalized. Sequencing libraries were prepared using the KAPA Stranded mRNA-Seq Kit (Roche) and sequenced on an Illumina HiSeq 4000 with 100 bp paired-end reads by the Duke University Center for Genomic and Computational Biology. Reads were evaluated using FastQC and trimmed using cutadapt [283], followed by alignment to the hg38 human reference genome using the STAR aligner with default parameters. The number of read fragments uniquely aligned to each gene were counted with the Gencode v21 main comprehensive gene

annotation file (aggregated by gene_name) using featureCounts. Limma software [305] was then used to analyze differential expression.

3.4.7 Metabolic labeling of nascent transcripts with 4-sU

siRNA-treated cells were pulsed with 4-sU at a final concentration of 200 uM (-/+ IFN-β) for the indicated amount of time before harvest in TRIzol and RNA extraction. Purification of newly transcribed, 4-sU labeled RNA was performed as previously described [306]. Briefly, 50 ug of RNA were biotinylated in biotinylation buffer (10 mM Tris-HCl pH 7.4, 1 mM EDTA, 20 ng/ul MTSEA Biotin-XX (Biotium)) for 30 minutes at room temperature, shaking at 800 rpm. A phenol/chloroform extraction was performed, and RNA was precipitated in isopropanol for 1 hour at -20°C. Following centrifugation for 20 minutes at 12000 X g at 4°C, RNA was resuspended, and 20% of each sample was taken for input samples. The remaining RNA was then incubated with Streptavidin MyOne C1 Dynabeads (Thermo Fisher Scientific), which were prewashed with 0.1M NaCl, in streptavidin binding buffer (final concentration 5 mM Tris-HCl pH 7.4, 0.5 mM EDTA, 1M NaCl) for 30 minutes at room temperature, shaking at 800 rpm. The supernatant containing unbound “pre-existing” RNA was then collected, and the beads were washed 4X with wash buffer (100 mM Tris-HCl pH 7.4, 10 mM EDTA, 1M NaCl, 0.1% Tween-20), and each wash was collected. Two additional washes were performed and supernatant was discarded. To elute biotinylated RNA, 100 mM DTT (freshly prepared) was added and the supernatant was collected. This was repeated 3 times to collect all labeled RNA. Finally, both the “pre-existing” and “newly transcribed” fractions were precipitated in isopropanol for 1 hour at -20°C. Following centrifugation for 20 minutes at 12000 X g at 4°C, RNA was resuspended, and cDNA was synthesized for each RNA fraction using the iScript cDNA synthesis kit (BioRad). RT-qPCR was then

performed for total and newly transcribed fractions and used to determine the relative transcription rate of genes of interest, compared to GAPDH.

3.5 Data availability

Raw data from the FTO RNA-seq experiment are available at the following URL: https://duke.box.com/s/bpwq9ouhklc5p1obxfmymwcdbnk146e6

4. Conclusion

4.1 Summary

In my dissertation research, I investigated a role for the RNA modification m^{6}A in regulation of the type I IFN response. At the time that I began my research, it was becoming clear that m^{6}A was an important regulator of viral infection, however it was not clear how m^{6}A regulates host pathways following infection. Type I IFNs induce many antiviral genes to establish an antiviral cellular state and limit viral replication. Therefore, understanding the role of m^{6}A in the type I IFN response was essential for our overall understanding of the functions of m^{6}A at the virus-host interface. By perturbing the expression of the m^{6}A methyltransferase components METTL3 and METTL14 using siRNA depletion or stable ectopic overexpression and measuring the protein expression of ISGs following IFN-β stimulation, I found that METTL3/14 regulates the production of a subset of ISGs, including the antiviral genes IFITM1 and MX1. This work was innovative in that it was the first study to explore the role of METTL3/14 in the response to exogenous IFN, thus eliminating potential confounding effects of m^{6}A on endogenous IFN production. Next, I investigated at what level of gene expression METTL3/14 regulates these ISGs. RT-qPCR revealed that METTL3/14 did not regulate the mRNA levels of the ISGs whose protein expression was regulated. Additionally, RNA-seq revealed that METTL3/14 does not regulate the activation of the JAK-STAT pathway or ISG mRNA levels generally, although some transcript-specific effects were observed, which may be a product of METTL3/14 regulation of the mRNA stability on certain ISGs. I then used polysome profiling to determine whether METTL3/14 regulates the translation of ISGs. Indeed, *IFITM1* and *MX1* transcripts were less associated with the

highest molecular weight polysome fractions and also with the 80S fraction, possibly revealing that METTL3/14 regulates translation initiation of these genes.

To investigate whether METTL3/14 regulation of a subset of ISGs may be a product of m^{6}A on the transcripts of these ISGs, we mapped m^{6}A in the IFN-β induced transcriptome using meRIP-seq, which revealed the *IFITM1* and *MX1* transcripts are both modified by m^{6}A in their 3'UTRs. Using IFITM1 as a model METTL3/14-regulated ISG, I undertook mutational studies in a reporter system to ablate m^{6}A within the 3'UTR of IFITM1 and found that m^{6}A regulates its translation, suggesting that the observed effects of METTL3/14 are indeed a product of m^{6}A on this subset of ISGs. We then hypothesized that the m^{6}A reader protein YTHDF1 could bind to m^{6}A on ISGs and enhance their translation. We found that YTHDF1 binds to the mRNA of *IFITM1*, *MX1*, and *ISG15* in an m^{6}A-dependent manner, whereas *EIF2AK2* mRNA was not bound by YTHDF1. Further, wild-type YTHDF1 overexpression was sufficient to enhance IFITM1 expression, while the m^{6}A binding mutant was not. These data suggest YTHDF1 binds m^{6}A on *IFITM1* mRNA and enhances its translation. Interestingly, YTHDF1 overexpression was not sufficient to enhance MX1 expression, despite the ability of YTHDF1 to bind to *MX1* mRNA.

To identify additional ISGs whose translation is regulated by METTL3/14, we used stable isotope labeling with amino acids in cell culture followed by quantitative mass spectrometry following METTL3/14 depletion and IFN-β treatment to identify proteins whose expression is altered by METTL3/14 depletion. This approach identified several additional METTL3/14-regulated ISGs, most of whose expression was decreased following METTL3/14 depletion, without a similar decrease in mRNA abundance, suggesting that METTL3/14 promotion of ISG translation may be fairly

common. Additionally, using ribosome profiling and assessing the effect of METTL3/14 depletion on the translation of the top 100 most highly induced ISGs, we found evidence that more than one third of these ISGs are likely translationally regulated by METTL3/14, and many of these ISGs are m^{6}A-modified. Given that METTL3/14 enhanced the translation of a subset of antiviral ISGs, we hypothesized that this regulation could be required for the full potency of the IFN response. Indeed, METTL3/14 depletion allowed increased infection by VSV, specifically in IFN pretreated cells, likely as these cells had less expression of ISGs. METTL3/14 overexpression, conversely, led to increased potency of the IFN response against VSV. These experiments demonstrate that METTL3/14 and m^{6}A enhance the antiviral effects of the IFN response.

Next, we were interested in understanding the role of the m^{6}A demethylase protein, FTO, in regulating the type I IFN response. Interestingly, we found that FTO regulates a distinct subset of ISGs and that their mRNA levels are affected by FTO, unlike METTL3/14 regulation of ISGs. Using RNA-seq, we identified the full subset of FTO-regulated ISGs, which include many proinflammatory genes. We then asked how FTO might regulate the RNA levels of ISGs and, using metabolic labeling of nascent transcripts, we found that FTO regulates the transcription of these ISGs and that FTO-depleted cells are primed to respond to IFN-β. Finally, we found that FTO regulation of ISGs occurs independently of the RNA modification m^{6}Am, which is a substrate for FTO demethylation. Taken together, these results identify FTO as a transcriptional suppressor of ISGs and proinflammatory genes.

Through my research, I have identified both positive and negative molecular regulators of the type I IFN response. While METTL3/14 and m^{6}A promote the translation of ISGs and contribute to the antiviral effects of the IFN response, FTO

suppresses the transcription of ISGs. This research adds valuable layers to our understanding of the functions of m^{6}A and its related machinery in immunity and at the virus-host interface. However, many important questions remain regarding this research and these research fields. I will discuss future directions that will enhance our understanding of the phenomena described in this dissertation, as well as our overall understanding of m^{6}A and its functions in immunity and infection.

4.2 Future directions and discussion

4.2.1 Through what mechanisms does m^{6}A enhance ISG translation?

We found that METTL3/14 and m^{6}A enhance the translation of a subset of ISGs and determined that YTHDF1 likely mediates this enhancement for *IFITM1*. However, YTHDF1 overexpression did not enhance MX1 expression. There are multiple possibilities that may explain why YTHDF1 overexpression was not sufficient to enhance MX1 expression – (1) YTHDF1 strongly associates with *MX1* mRNA at basal levels, thus it is difficult to achieve increased binding of YTHDF1 to this transcript; (2) YTHDF1 requires other interacting proteins to enhance *MX1* translation, and would require co-expression of these proteins to have an observable effect, or (3) YTHDF1 binding to *MX1* mRNA is not involved in enhancing its translation, and instead other reader proteins recognize m^{6}A on MX1 and enhance its translation. Tethering of YTHDF1 to MX1 mRNA by adding a BoxB motif and FLAG tag to *MX1* mRNA and co-expressing this with YTHDF1 fused to λ peptide (or GFP as a control) would likely help determine if forcing increased YTHDF1 binding to *MX1* mRNA can enhance its translation.

Despite the fact that YTHDF1 is perhaps the most well characterized m^{6}A reader protein with translation enhancing activity, the mechanisms by which it facilitates

translation are not well understood. The model that YTHDF1 recruits translation initiation factors to m^{6}A-modified RNA is based on experiments demonstrating that YTHDF1 interacts with translation initiation factors such as proteins within the 40S and 60S ribosomal subunits, as well as subunits of the translation initiation factor complex eIF3 [183]. While our data likely point to METTL3/14 enhancing translation initiation of m^{6}A-modified ISGs (see Figure 9), further mechanistic studies to demonstrate that YTHDF1-eIF3 interaction, for example, is required for the translation promotion of *IFITM1* would be informative of the mechanisms by which YTHDF1 regulates the translation of ISGs and translation generally.

We have not investigated the effect of YTHDF1 on ISGs globally, thus it is unclear how many METTL3/14-regulated ISGs are regulated in a similar way by YTHDF1. Is YTHDF1 the major reader protein involved in enhancing the translation of m^{6}A-modified ISGs? Other reader proteins have been found to promote translation of m^{6}A-modified mRNAs, as well. METTL3 itself has been reported to bind m^{6}A sites and interact with the translation initiation factor eIF3H to enhance translation [264,307]. YTHDC2 is an additional m^{6}A reader protein with the ability to enhance translation [266]. Other translation-promoting m^{6}A reader RNA binding proteins likely have yet to be discovered. To determine whether YTHDF1 is the primary reader protein involved in promoting the translation of m^{6}A-modified ISGs, it would be useful to perform ribosome profiling with YTHDF1 depletion, or with wild-type and m^{6}A binding mutant YTHDF1 overexpression and overlap the translationally regulated ISGs with those regulated by METTL3/14. This would inform how prevalent YTHDF1 regulation of m^{6}A modified ISGs is, and how likely it is that other reader proteins are important for this function.

A number of RNA binding proteins are IFN-inducible. It would be fascinating to discover an IFN-induced m^{6}A binding protein that could enhance the translation of m^{6}A-modified RNAs in a positive feedback loop for efficient ISG translation. Indeed, a number of IFN-inducible proteins and even long non-coding RNAs are involved in regulating the activation of the response (see Chapter 1.2.2). A number of viruses are known to activate cellular responses that inhibit cellular translation, such as through activation of EIF2AK2 [308]. Some reports suggest that certain mRNAs, such as those encoding cytokines or ISGs, can be preferentially translated during cellular translation arrest [309]. Whether m^{6}A may be capable of mediating such preferential translation of ISGs during translation arrest could be interesting to explore, especially as it would benefit cells to produce antiviral genes during these virus-activated translation inhibitory states.

4.2.2 What features of ISGs allow some to become m^{6}A-modified, while others are not?

Our meRIP-seq data revealed that a majority of ISGs (approximately 85%) are m^{6}A-modified. While m^{6}A modification is common, the minimal sequence requirement for m^{6}A modification ([G/A]AC) is far more common [157,158,162]. This raises the question of why and how certain genes are m^{6}A modified, while others are not. It is likely that additional factors within the m^{6}A methyltransferase complex guide its specificity and preference for certain motifs [168-170]. Still, despite knowing the core m^{6}A motif and the core components of the methyltransferase complex, we cannot accurately predict sites where m^{6}A modification will occur without experimental mapping of m^{6}A. Perhaps as a small group of genes whose expression can be easily and strongly induced by IFN treatment, ISGs could present an interesting opportunity to study how m^{6}A modification occurs only on some genes and not others.

In terms of the functionality of m^{6}A modification of ISGs, a post-transcriptional control to mediate efficient translation of antiviral factors during viral infection (especially as cellular translation is often impaired during viral infection [308]) has obvious utility. Thus, the high percentage of m^{6}A modification among ISGs is not surprising, but some ISGs are not m^{6}A modified. EIF2AK2 was an m^{6}A-negative ISG from our meRIP-seq data that also showed no evidence of m^{6}A modification in our functional experiments. EIF2AK2 has many functions in addition to its roles in the antiviral response, such as regulation of mitosis [310]. It is also not as strongly IFN-induced as many ISGs (see Figure 10D). Perhaps the m^{6}A status of ISGs can be further related to their functions or their IFN inducibility, although these ideas warrant further investigation.

4.2.3 Does m^{6}A have additional effects on the transcripts of ISGs?

Our mass spectrometry and ribosome profiling experiments revealed that not all m^{6}A-modified ISGs are impacted at the level of translation by METTL3/14 depletion. In some cases, it may be that depletion of METTL3/14 is not sufficient to reveal its full impact on the expression of certain ISGs, and that full METTL3 knockout could produce stronger phenotypes, especially as METTL3 can catalyze m^{6}A deposition at low levels [168]. However, it is likely that m^{6}A has additional regulatory effects on certain ISGs, aside from its role in translational regulation. Indeed, while our RNA-seq data revealed that METTL3/14 depletion did not impair the activation of the JAK-STAT pathway or have generalized effects on the mRNA abundance of ISGs, it did have transcript-specific effects on certain ISGs (see Figure 10, Table 2). Therefore, m^{6}A may impact the mRNA stability of a subset of ISGs, and this question could be further explored by depleting METTL3/14, stimulating cells with IFN-β to induce ISGs, and then blocking transcription with actinomycin D and performing RNA-seq at multiple timepoints to measure the decay

of ISG transcripts. It may also be interesting to explore whether m^{6}A could regulate the localization of ISG transcripts in P bodies or stress granules [184,311] using METTL3/14 depletion experiments and visualizing the localization of ISG transcripts using FISH probes.

4.2.4 Do viruses subvert m^{6}A modification of ISGs to facilitate their replication?

We found that METTL3/14 could augment the antiviral effects of IFN-β pretreatment on VSV. It is worth noting that type I IFNs induce paracrine signaling, thus "pretreatment" of cells with a low dose of IFN, prior to infection, does have implications for biological infections. This contribution of m^{6}A to the efficient establishment of an antiviral cellular state may be important for viral infection and, indeed, paracrine effects would be difficult for a virus to subvert. Many viruses limit IFN production in infected cells [112], however type I IFN responses are still crucial and effective for restriction of viral infection [94,95]. HCMV was recently shown to induce the expression of the m^{6}A machinery in infected cells, which hypermethylated and destabilized the *IFNB1* transcript, resulting in a defective IFN response [231,232]. This is an example of a virus exploiting host m^{6}A functions to benefit its replication. Other viruses induce alterations of the m^{6}A machinery, including cytoplasmic relocalization or post-translational modifications, which can result in altered m^{6}A patterns in the host transcriptome [175,177,243]. Might some viruses use similar or additional strategies to subvert the m^{6}A machinery from the transcripts of ISGs and preclude their modification by m^{6}A? This will be an important area to explore using diverse viruses and approaches like meRIP-seq, or quantitative mass spectrometry to analyze the m^{6}A status of ISGs and their expression during viral infection.

4.2.5 By what mechanisms does FTO suppress the transcription of a subset of ISGs?

I found that FTO inhibits the transcription of a subset of ISGs and, through metabolic labeling of nascent transcripts following IFN-β stimulation, I also found that FTO-depleted cells are primed to respond to IFN stimulation. However, the mechanisms by which FTO regulates transcription require further investigation. There are many possible mechanisms through which this could occur, and I will discuss some systematic experimental approaches to test several (non-mutually exclusive) hypotheses that may elucidate these mechanisms.

4.2.5.1 Is FTO regulation of ISGs mediated by m^6A?

The RNA demethylase activities of FTO are likely one of its key molecular functions. FTO is capable of demethylating the RNA modifications m^6A and m^6Am, and recent literature suggests that m^6Am may be the preferred substrate of FTO [296]. m^6Am deposition is controlled by PCIF1 [270,271]. By comparing the phenotypic effect of FTO depletion on IFITM1 expression in wild-type and PCIF1 knockout cells, in which m^6Am should be absent [270], we found that FTO had the same effect in both cell types, thus FTO regulation of ISGs is m^6Am-independent. We have not yet determined whether FTO regulation of ISGs is dependent on METTL3-mediated m^6A modifications. METTL3 genetic knockout cells would be ideal to test this hypothesis, however METTL3 seems to be required for the proliferation of cancer cells, thus full genetic knockout of METTL3 in Huh7 cells would probably not produce viable cells [312]. Embryonic stem cells do tolerate METTL3 knockout but exhibit phenotypic abnormalities [141]. Nevertheless, these cells may be ideal for determining whether FTO suppression of ISGs is dependent

on METTL3-mediated m^{6}A modification, as long as this phenotype is intact in embryonic stem cells.

FTO removal of m^{6}A would not likely impact the transcription of ISGs in *cis* but may control the expression of a *trans*-regulatory factor. Indeed, a recent report revealed that METTL3 and m^{6}A can regulate global transcription through regulation of the expression of a class of chromatin-associated regulatory RNAs (carRNAs) [313]. Specifically, m^{6}A modification of these carRNAs, such as LINE1 elements, and destabilizes these RNAs. carRNAs can associate with chromatin and recruit transcription enhancer proteins, such as EP300 or YY1. Thus, METTL3 appears to indirectly regulate transcription through destabilization of carRNAs, at least in mouse embryonic stem cells [313]. In this specific model, FTO would likely promote transcription, as removal of m^{6}A would stabilize these carRNAs and promote open chromatin. Our identification of FTO as a transcriptional repressor likely indicates that this model does not explain this phenotype. However, the discovery of a role for m^{6}A in transcriptional regulation may still shed some light on how FTO could suppress the transcription of ISGs.

4.2.5.2 FTO as a regulator of NF-κB

The ISGs whose transcription is regulated by FTO include many proinflammatory factors and genes that are also subject to NF-κB regulation (see Figure 20). Therefore, FTO could modulate the activation of NF-κB signaling. A few studies have linked FTO to NF-κB activation, or vice versa, but the regulatory mechanisms are not understood [301,314,315]. To test whether FTO regulates NF-κB signaling, we could utilize an NF-κB promoter luciferase reporter system with perturbation of FTO by siRNA or overexpression. Additionally, we could perturb certain known factors within the NF-κB pathway to determine whether any of these perturbations phenocopy FTO depletion.

4.2.5.3 FTO regulation of a non-canonical factor regulating a subset of ISGs.

As discussed previously (see Chapter 1.2.2), a number of reports have described separate regulation of subsets of ISGs, some of which discovered regulatory factors such as the transcription factor ETV7 [122-127]. While FTO does not appear to regulate the overall activation of the JAK-STAT pathway, given that many ISGs are induced to normal levels following FTO depletion (see Figure 20), it is possible that it could regulate a non-canonical transcription factor or epigenetic modifier that regulates this subset of ISGs. In this case, this factor may be difficult to identify, although a targeted siRNA screen of transcription factors whose expression was regulated by FTO in my RNA-seq data set (Table 6) may be a useful initial experiment. These results would build on our discovery of FTO as a novel suppressor of ISG transcription and also uncover additional non-canonical regulators of ISG expression.

4.2.5.4 FTO as a transcription factor

Another possible mechanism by which FTO could suppress the transcription of ISGs is by binding directly to their promoters and repressing their transcription, perhaps by recruiting chromatin silencing factors. A transcriptional repression function was recently discovered for FTO in a report that found that FTO binds its own promoter and suppresses its transcription in an auto-regulatory feedback loop [303]. However, this study did not test whether FTO regulates the transcription of other genes. To test which genes are transcriptionally regulated globally by FTO, we could employ 4-sU pulse labeling followed by RNA-seq after FTO depletion and IFN-β stimulation. Additionally, chIP-qPCR and chIP-seq will be useful experiments to determine at what promoter sites does FTO bind within the genome.

4.2.5.5 Epigenetic regulation by FTO

The priming of FTO depleted cells to respond to IFN (see Figure 20) may suggest epigenetic priming that allows fast activation of transcription from the promoters of ISGs. FTO is primarily a nuclear protein that localizes to nuclear speckles, which are transcriptional hubs [172,304]. Therefore, it would not be surprising if FTO can interact with epigenetic modifiers to regulate chromatin accessibility. To test this hypothesis, it would be useful to perform IP-mass spectrometry to identify proteins that interact with FTO. This may reveal chromatin modifiers that can be recruited by FTO. Additionally, there are many chemical compounds that can inhibit classes of epigenetic modifiers [316], which, if used in combination with FTO depletion experiments, may reveal whether FTO suppression of ISG transcription depends on these epigenetic modifiers.

4.3 Broader impacts of this research

Overall, the results presented in this dissertation are important discoveries for our understanding of interferon biology and regulation of inflammatory genes, post-transcriptional gene regulation, and the roles of m^6A at the virus-host interface. Post-transcriptional regulation of ISGs is poorly understood and these results suggest that studying the translation of ISGs will enhance our understanding of the type I IFN response and viral restriction, with potential implications for inflammatory conditions and cancer biology. Additionally, discovering a novel role for FTO as a transcriptional regulator of ISGs may be an important revelation for understanding its roles in human health, especially as FTO is linked to inflammation and a number of human diseases. There are many important questions associated with my findings, and I look forward to seeing the progress of this field in the future.

References

1. McFadden MJ, Gokhale NS, Horner SM: Protect this house: cytosolic sensing of viruses. *Curr Opin Virol* 2017, 22:36-43.

2. Beachboard DC, Horner SM: Innate immune evasion strategies of DNA and RNA viruses. *Curr Opin Microbiol* 2016, 32:113-119.

3. Chan YK, Gack MU: Viral evasion of intracellular DNA and RNA sensing. *Nat Rev Microbiol* 2016, 14:360-373.

4. Gack MU: Mechanisms of RIG-I-like receptor activation and manipulation by viral pathogens. *J Virol* 2014, 88:5213-5216.

5. Hou F, Sun L, Zheng H, Skaug B, Jiang QX, Chen ZJ: MAVS forms functional prion-like aggregates to activate and propagate antiviral innate immune response. *Cell* 2011, 146:448-461.

6. Liu S, Chen J, Cai X, Wu J, Chen X, Wu YT, Sun L, Chen ZJ: MAVS recruits multiple ubiquitin E3 ligases to activate antiviral signaling cascades. *Elife* 2013, 2:e00785.

7. Schoggins JW, Wilson SJ, Panis M, Murphy MY, Jones CT, Bieniasz P, Rice CM: A diverse range of gene products are effectors of the type I interferon antiviral response. *Nature* 2011, 472:481-485.

8. Metz P, Dazert E, Ruggieri A, Mazur J, Kaderali L, Kaul A, Zeuge U, Windisch MP, Trippler M, Lohmann V, et al.: Identification of type I and type II interferon-induced effectors controlling hepatitis C virus replication. *Hepatology* 2012, 56:2082-2093.

9. Schoggins JW: Interferon-stimulated genes: roles in viral pathogenesis. *Curr Opin Virol* 2014, 6:40-46.

10. Jensen S, Thomsen AR: Sensing of RNA viruses: a review of innate immune receptors involved in recognizing RNA virus invasion. *J Virol* 2012, 86:2900-2910.

11. Kell AM, Gale M, Jr.: RIG-I in RNA virus recognition. *Virology* 2015, 479-480:110-121.

12. Yoneyama M, Kikuchi M, Natsukawa T, Shinobu N, Imaizumi T, Miyagishi M, Taira K, Akira S, Fujita T: The RNA helicase RIG-I has an essential function in double-stranded RNA-induced innate antiviral responses. *Nat Immunol* 2004, 5:730-737.

13. Hornung V, Ellegast J, Kim S, Brzozka K, Jung A, Kato H, Poeck H, Akira S, Conzelmann KK, Schlee M, et al.: 5'-Triphosphate RNA is the ligand for RIG-I. *Science* 2006, 314:994-997.

14. Goubau D, Schlee M, Deddouche S, Pruijssers AJ, Zillinger T, Goldeck M, Schuberth C, Van der Veen AG, Fujimura T, Rehwinkel J, et al.: Antiviral immunity via RIG-I-mediated recognition of RNA bearing 5'-diphosphates. *Nature* 2014, 514:372-375.

15. Spengler JR, Patel JR, Chakrabarti AK, Zivcec M, Garcia-Sastre A, Spiropoulou CF, Bergeron E: RIG-I Mediates an Antiviral Response to Crimean-Congo Hemorrhagic Fever Virus. *J Virol* 2015, 89:10219-10229.

16. Schuberth-Wagner C, Ludwig J, Bruder AK, Herzner AM, Zillinger T, Goldeck M, Schmidt T, Schmid-Burgk JL, Kerber R, Wolter S, et al.: A Conserved Histidine in the RNA Sensor RIG-I Controls Immune Tolerance to N1-2'O-Methylated Self RNA. *Immunity* 2015, 43:41-51.

17. Devarkar SC, Wang C, Miller MT, Ramanathan A, Jiang F, Khan AG, Patel SS, Marcotrigiano J: Structural basis for m7G recognition and 2'-O-methyl discrimination in capped RNAs by the innate immune receptor RIG-I. *Proc Natl Acad Sci U S A* 2016, 113:596-601.

18. Habjan M, Hubel P, Lacerda L, Benda C, Holze C, Eberl CH, Mann A, Kindler E, Gil-Cruz C, Ziebuhr J, et al.: Sequestration by IFIT1 impairs translation of 2'O-unmethylated capped RNA. *PLoS Pathog* 2013, 9:e1003663.

19. Daffis S, Szretter KJ, Schriewer J, Li J, Youn S, Errett J, Lin TY, Schneller S, Zust R, Dong H, et al.: 2'-O methylation of the viral mRNA cap evades host restriction by IFIT family members. *Nature* 2010, 468:452-456.

20. Decroly E, Ferron F, Lescar J, Canard B: Conventional and unconventional mechanisms for capping viral mRNA. *Nat Rev Microbiol* 2012, 10:51-65.

21. Saito T, Hirai R, Loo YM, Owen D, Johnson CL, Sinha SC, Akira S, Fujita T, Gale M, Jr.: Regulation of innate antiviral defenses through a shared repressor domain in RIG-I and LGP2. *Proc Natl Acad Sci U S A* 2007, 104:582-587.

22. Jiang F, Ramanathan A, Miller MT, Tang GQ, Gale M, Jr., Patel SS, Marcotrigiano J: Structural basis of RNA recognition and activation by innate immune receptor RIG-I. *Nature* 2011, 479:423-427.

23. Kowalinski E, Lunardi T, McCarthy AA, Louber J, Brunel J, Grigorov B, Gerlier D, Cusack S: Structural basis for the activation of innate immune pattern-recognition receptor RIG-I by viral RNA. *Cell* 2011, 147:423-435.

24. Ramanathan A, Devarkar SC, Jiang F, Miller MT, Khan AG, Marcotrigiano J, Patel SS: The autoinhibitory CARD2-Hel2i Interface of RIG-I governs RNA selection. *Nucleic Acids Res* 2016, 44:896-909.

25. Oshiumi H, Matsumoto M, Hatakeyama S, Seya T: Riplet/RNF135, a RING finger protein, ubiquitinates RIG-I to promote interferon-beta induction during the early phase of viral infection. *J Biol Chem* 2009, 284:807-817.

26. Oshiumi H, Miyashita M, Inoue N, Okabe M, Matsumoto M, Seya T: The ubiquitin ligase Riplet is essential for RIG-I-dependent innate immune responses to RNA virus infection. *Cell Host Microbe* 2010, 8:496-509.

27. Gack MU, Shin YC, Joo CH, Urano T, Liang C, Sun L, Takeuchi O, Akira S, Chen Z, Inoue S, et al.: TRIM25 RING-finger E3 ubiquitin ligase is essential for RIG-I-mediated antiviral activity. *Nature* 2007, 446:916-920.

28. Kuniyoshi K, Takeuchi O, Pandey S, Satoh T, Iwasaki H, Akira S, Kawai T: Pivotal role of RNA-binding E3 ubiquitin ligase MEX3C in RIG-I-mediated antiviral innate immunity. *Proc Natl Acad Sci U S A* 2014, 111:5646-5651.

29. Yan J, Li Q, Mao AP, Hu MM, Shu HB: TRIM4 modulates type I interferon induction and cellular antiviral response by targeting RIG-I for K63-linked ubiquitination. *J Mol Cell Biol* 2014, 6:154-163.

30. Peisley A, Wu B, Xu H, Chen ZJ, Hur S: Structural basis for ubiquitin-mediated antiviral signal activation by RIG-I. *Nature* 2014, 509:110-114.

31. Choi SJ, Lee HC, Kim JH, Park SY, Kim TH, Lee WK, Jang DJ, Yoon JE, Choi YI, Kim S, et al.: HDAC6 regulates cellular viral RNA sensing by deacetylation of RIG-I. *Embo j* 2016, 35:429-442.

32. Liu HM, Jiang F, Loo YM, Hsu S, Hsiang TY, Marcotrigiano J, Gale M, Jr.: Regulation of Retinoic Acid Inducible Gene-I (RIG-I) Activation by the Histone Deacetylase 6. *EBioMedicine* 2016, 9:195-206.

33. Wies E, Wang MK, Maharaj NP, Chen K, Zhou S, Finberg RW, Gack MU: Dephosphorylation of the RNA sensors RIG-I and MDA5 by the phosphatase PP1 is essential for innate immune signaling. *Immunity* 2013, 38:437-449.

34. Horner SM, Liu HM, Park HS, Briley J, Gale M, Jr.: Mitochondrial-associated endoplasmic reticulum membranes (MAM) form innate immune synapses and are targeted by hepatitis C virus. *Proc Natl Acad Sci U S A* 2011, 108:14590-14595.

35. Liu HM, Loo YM, Horner SM, Zornetzer GA, Katze MG, Gale M, Jr.: The mitochondrial targeting chaperone 14-3-3epsilon regulates a RIG-I translocon that mediates membrane association and innate antiviral immunity. *Cell Host Microbe* 2012, 11:528-537.

36. Chan YK, Gack MU: RIG-I-like receptor regulation in virus infection and immunity. *Curr Opin Virol* 2015, 12:7-14.

37. Kang DC, Gopalkrishnan RV, Wu Q, Jankowsky E, Pyle AM, Fisher PB: mda-5: An interferon-inducible putative RNA helicase with double-stranded RNA-dependent ATPase activity and melanoma growth-suppressive properties. *Proc Natl Acad Sci U S A* 2002, 99:637-642.

38. Kato H, Takeuchi O, Mikamo-Satoh E, Hirai R, Kawai T, Matsushita K, Hiiragi A, Dermody TS, Fujita T, Akira S: Length-dependent recognition of double-stranded ribonucleic acids by retinoic acid-inducible gene-I and melanoma differentiation-associated gene 5. *J Exp Med* 2008, 205:1601-1610.

39. Zust R, Cervantes-Barragan L, Habjan M, Maier R, Neuman BW, Ziebuhr J, Szretter KJ, Baker SC, Barchet W, Diamond MS, et al.: Ribose 2'-O-methylation provides a molecular signature for the distinction of self and non-self mRNA dependent on the RNA sensor Mda5. *Nat Immunol* 2011, 12:137-143.

40. Wu B, Peisley A, Richards C, Yao H, Zeng X, Lin C, Chu F, Walz T, Hur S: Structural basis for dsRNA recognition, filament formation, and antiviral signal activation by MDA5. *Cell* 2013, 152:276-289.

41. Motz C, Schuhmann KM, Kirchhofer A, Moldt M, Witte G, Conzelmann KK, Hopfner KP: Paramyxovirus V proteins disrupt the fold of the RNA sensor MDA5 to inhibit antiviral signaling. *Science* 2013, 339:690-693.

42. Yoneyama M, Kikuchi M, Matsumoto K, Imaizumi T, Miyagishi M, Taira K, Foy E, Loo YM, Gale M, Jr., Akira S, et al.: Shared and unique functions of the DExD/H-box helicases RIG-I, MDA5, and LGP2 in antiviral innate immunity. *J Immunol* 2005, 175:2851-2858.

43. Rothenfusser S, Goutagny N, DiPerna G, Gong M, Monks BG, Schoenemeyer A, Yamamoto M, Akira S, Fitzgerald KA: The RNA helicase Lgp2 inhibits TLR-independent sensing of viral replication by retinoic acid-inducible gene-I. *J Immunol* 2005, 175:5260-5268.

44. Bruns AM, Leser GP, Lamb RA, Horvath CM: The innate immune sensor LGP2 activates antiviral signaling by regulating MDA5-RNA interaction and filament assembly. *Mol Cell* 2014, 55:771-781.

45. Uchikawa E, Lethier M, Malet H, Brunel J, Gerlier D, Cusack S: Structural Analysis of dsRNA Binding to Anti-viral Pattern Recognition Receptors LGP2 and MDA5. *Mol Cell* 2016, 62:586-602.

46. Venkataraman T, Valdes M, Elsby R, Kakuta S, Caceres G, Saijo S, Iwakura Y, Barber GN: Loss of DExD/H box RNA helicase LGP2 manifests disparate antiviral responses. *J Immunol* 2007, 178:6444-6455.

47. Unterholzner L: The interferon response to intracellular DNA: why so many receptors? *Immunobiology* 2013, 218:1312-1321.

48. Ishii KJ, Coban C, Kato H, Takahashi K, Torii Y, Takeshita F, Ludwig H, Sutter G, Suzuki K, Hemmi H, et al.: A Toll-like receptor-independent antiviral response induced by double-stranded B-form DNA. *Nat Immunol* 2006, 7:40-48.

49. Stetson DB, Medzhitov R: Recognition of cytosolic DNA activates an IRF3-dependent innate immune response. *Immunity* 2006, 24:93-103.

50. Burdette DL, Monroe KM, Sotelo-Troha K, Iwig JS, Eckert B, Hyodo M, Hayakawa Y, Vance RE: STING is a direct innate immune sensor of cyclic di-GMP. *Nature* 2011, 478:515-518.

51. Ishikawa H, Ma Z, Barber GN: STING regulates intracellular DNA-mediated, type I interferon-dependent innate immunity. *Nature* 2009, 461:788-792.

52. Saitoh T, Fujita N, Hayashi T, Takahara K, Satoh T, Lee H, Matsunaga K, Kageyama S, Omori H, Noda T, et al.: Atg9a controls dsDNA-driven dynamic translocation of STING and the innate immune response. *Proc Natl Acad Sci U S A* 2009, 106:20842-20846.

53. Mukai K, Konno H, Akiba T, Uemura T, Waguri S, Kobayashi T, Barber GN, Arai H, Taguchi T: Activation of STING requires palmitoylation at the Golgi. *Nat Commun* 2016, 7:11932.

54. Liu S, Cai X, Wu J, Cong Q, Chen X, Li T, Du F, Ren J, Wu YT, Grishin NV, et al.: Phosphorylation of innate immune adaptor proteins MAVS, STING, and TRIF induces IRF3 activation. *Science* 2015, 347:aaa2630.

55. Chen H, Sun H, You F, Sun W, Zhou X, Chen L, Yang J, Wang Y, Tang H, Guan Y, et al.: Activation of STAT6 by STING is critical for antiviral innate immunity. *Cell* 2011, 147:436-446.

56. Sun L, Wu J, Du F, Chen X, Chen ZJ: Cyclic GMP-AMP synthase is a cytosolic DNA sensor that activates the type I interferon pathway. *Science* 2013, 339:786-791.

57. Wu J, Sun L, Chen X, Du F, Shi H, Chen C, Chen ZJ: Cyclic GMP-AMP is an endogenous second messenger in innate immune signaling by cytosolic DNA. *Science* 2013, 339:826-830.

58. Orzalli MH, Broekema NM, Diner BA, Hancks DC, Elde NC, Cristea IM, Knipe DM: cGAS-mediated stabilization of IFI16 promotes innate signaling during herpes simplex virus infection. *Proc Natl Acad Sci U S A* 2015, 112:E1773-1781.

59. Ma Z, Damania B: The cGAS-STING Defense Pathway and Its Counteraction by Viruses. *Cell Host Microbe* 2016, 19:150-158.

60. Gao D, Wu J, Wu YT, Du F, Aroh C, Yan N, Sun L, Chen ZJ: Cyclic GMP-AMP synthase is an innate immune sensor of HIV and other retroviruses. *Science* 2013, 341:903-906.

61. Schoggins JW, MacDuff DA, Imanaka N, Gainey MD, Shrestha B, Eitson JL, Mar KB, Richardson RB, Ratushny AV, Litvak V, et al.: Pan-viral specificity of IFN-induced genes reveals new roles for cGAS in innate immunity. *Nature* 2014, 505:691-695.

62. Maringer K, Fernandez-Sesma A: Message in a bottle: lessons learned from antagonism of STING signalling during RNA virus infection. *Cytokine Growth Factor Rev* 2014, 25:669-679.

63. Sun B, Sundström KB, Chew JJ, Bist P, Gan ES, Tan HC, Goh KC, Chawla T, Tang CK, Ooi EE: Dengue virus activates cGAS through the release of mitochondrial DNA. *Sci Rep* 2017, 7:3594.

64. Civril F, Deimling T, de Oliveira Mann CC, Ablasser A, Moldt M, Witte G, Hornung V, Hopfner KP: Structural mechanism of cytosolic DNA sensing by cGAS. *Nature* 2013, 498:332-337.

65. Kranzusch PJ, Lee AS, Berger JM, Doudna JA: Structure of human cGAS reveals a conserved family of second-messenger enzymes in innate immunity. *Cell Rep* 2013, 3:1362-1368.

66. Ablasser A, Goldeck M, Cavlar T, Deimling T, Witte G, Rohl I, Hopfner KP, Ludwig J, Hornung V: cGAS produces a 2'-5'-linked cyclic dinucleotide second messenger that activates STING. *Nature* 2013, 498:380-384.

67. Diner EJ, Burdette DL, Wilson SC, Monroe KM, Kellenberger CA, Hyodo M, Hayakawa Y, Hammond MC, Vance RE: The innate immune DNA sensor cGAS produces a noncanonical cyclic dinucleotide that activates human STING. *Cell Rep* 2013, 3:1355-1361.

68. Zhang X, Shi H, Wu J, Zhang X, Sun L, Chen C, Chen ZJ: Cyclic GMP-AMP containing mixed phosphodiester linkages is an endogenous high-affinity ligand for STING. *Mol Cell* 2013, 51:226-235.

69. Tsuchida T, Zou J, Saitoh T, Kumar H, Abe T, Matsuura Y, Kawai T, Akira S: The ubiquitin ligase TRIM56 regulates innate immune responses to intracellular double-stranded DNA. *Immunity* 2010, 33:765-776.

70. Zhang J, Hu MM, Wang YY, Shu HB: TRIM32 protein modulates type I interferon induction and cellular antiviral response by targeting MITA/STING protein for K63-linked ubiquitination. *J Biol Chem* 2012, 287:28646-28655.

71. Takaoka A, Wang Z, Choi MK, Yanai H, Negishi H, Ban T, Lu Y, Miyagishi M, Kodama T, Honda K, et al.: DAI (DLM-1/ZBP1) is a cytosolic DNA sensor and an activator of innate immune response. *Nature* 2007, 448:501-505.

72. DeFilippis VR, Alvarado D, Sali T, Rothenburg S, Fruh K: Human cytomegalovirus induces the interferon response via the DNA sensor ZBP1. *J Virol* 2010, 84:585-598.

73. Upton JW, Kaiser WJ, Mocarski ES: DAI/ZBP1/DLM-1 complexes with RIP3 to mediate virus-induced programmed necrosis that is targeted by murine cytomegalovirus vIRA. *Cell Host Microbe* 2012, 11:290-297.

74. Zhang W, Zhou Q, Xu W, Cai Y, Yin Z, Gao X, Xiong S: DNA-dependent activator of interferon-regulatory factors (DAI) promotes lupus nephritis by activating the calcium pathway. *J Biol Chem* 2013, 288:13534-13550.

75. Ishii KJ, Kawagoe T, Koyama S, Matsui K, Kumar H, Kawai T, Uematsu S, Takeuchi O, Takeshita F, Coban C, et al.: TANK-binding kinase-1 delineates innate and adaptive immune responses to DNA vaccines. *Nature* 2008, 451:725-729.

76. Wang Z, Choi MK, Ban T, Yanai H, Negishi H, Lu Y, Tamura T, Takaoka A, Nishikura K, Taniguchi T: Regulation of innate immune responses by DAI (DLM-1/ZBP1) and other DNA-sensing molecules. *Proc Natl Acad Sci U S A* 2008, 105:5477-5482.

77. Radoshevich L, Dussurget O: Cytosolic Innate Immune Sensing and Signaling upon Infection. *Front Microbiol* 2016, 7:313.

78. Zhang T, Yin C, Boyd DF, Quarato G, Ingram JP, Shubina M, Ragan KB, Ishizuka T, Crawford JC, Tummers B, et al.: Influenza Virus Z-RNAs Induce ZBP1-Mediated Necroptosis. *Cell* 2020, 180:1115-1129.e1113.

79. Unterholzner L, Keating SE, Baran M, Horan KA, Jensen SB, Sharma S, Sirois CM, Jin T, Latz E, Xiao TS, et al.: IFI16 is an innate immune sensor for intracellular DNA. *Nat Immunol* 2010, 11:997-1004.

80. Kerur N, Veettil MV, Sharma-Walia N, Bottero V, Sadagopan S, Otageri P, Chandran B: IFI16 acts as a nuclear pathogen sensor to induce the inflammasome in response to Kaposi Sarcoma-associated herpesvirus infection. *Cell Host Microbe* 2011, 9:363-375.

81. Hornung V, Ablasser A, Charrel-Dennis M, Bauernfeind F, Horvath G, Caffrey DR, Latz E, Fitzgerald KA: AIM2 recognizes cytosolic dsDNA and forms a caspase-1-activating inflammasome with ASC. *Nature* 2009, 458:514-518.

82. Jones JW, Kayagaki N, Broz P, Henry T, Newton K, O'Rourke K, Chan S, Dong J, Qu Y, Roose-Girma M, et al.: Absent in melanoma 2 is required for innate immune recognition of Francisella tularensis. *Proc Natl Acad Sci U S A* 2010, 107:9771-9776.

83. Rathinam VA, Jiang Z, Waggoner SN, Sharma S, Cole LE, Waggoner L, Vanaja SK, Monks BG, Ganesan S, Latz E, et al.: The AIM2 inflammasome is essential for

host defense against cytosolic bacteria and DNA viruses. *Nat Immunol* 2010, 11:395-402.

84. Guo H, Callaway JB, Ting JP: Inflammasomes: mechanism of action, role in disease, and therapeutics. *Nat Med* 2015, 21:677-687.

85. Johnson KE, Chikoti L, Chandran B: Herpes simplex virus 1 infection induces activation and subsequent inhibition of the IFI16 and NLRP3 inflammasomes. *J Virol* 2013, 87:5005-5018.

86. Jakobsen MR, Bak RO, Andersen A, Berg RK, Jensen SB, Tengchuan J, Laustsen A, Hansen K, Ostergaard L, Fitzgerald KA, et al.: IFI16 senses DNA forms of the lentiviral replication cycle and controls HIV-1 replication. *Proc Natl Acad Sci U S A* 2013, 110:E4571-4580.

87. Orzalli MH, DeLuca NA, Knipe DM: Nuclear IFI16 induction of IRF-3 signaling during herpesviral infection and degradation of IFI16 by the viral ICP0 protein. *Proc Natl Acad Sci U S A* 2012, 109:E3008-3017.

88. Li T, Chen J, Cristea IM: Human cytomegalovirus tegument protein pUL83 inhibits IFI16-mediated DNA sensing for immune evasion. *Cell Host Microbe* 2013, 14:591-599.

89. Gray EE, Winship D, Snyder JM, Child SJ, Geballe AP, Stetson DB: The AIM2-like Receptors Are Dispensable for the Interferon Response to Intracellular DNA. *Immunity* 2016, 45:255-266.

90. Isaacs A, Lindenmann J: Virus interference. I. The interferon. *Proc R Soc Lond B Biol Sci* 1957, 147:258-267.

91. Isaacs A, Lindenmann J, Valentine RC: Virus interference. II. Some properties of interferon. *Proc R Soc Lond B Biol Sci* 1957, 147:268-273.

92. Stark GR, Darnell JE, Jr.: The JAK-STAT pathway at twenty. *Immunity* 2012, 36:503-514.

93. Schoggins JW: Interferon-Stimulated Genes: What Do They All Do? *Annu Rev Virol* 2019, 6:567-584.

94. Bastard P, Manry J, Chen J, Rosain J, Seeleuthner Y, AbuZaitun O, Lorenzo L, Khan T, Hasek M, Hernandez N, et al.: Herpes simplex encephalitis in a patient with a distinctive form of inherited IFNAR1 deficiency. *J Clin Invest* 2020.

95. Bastard P, Rosen LB, Zhang Q, Michailidis E, Hoffmann HH, Zhang Y, Dorgham K, Philippot Q, Rosain J, Béziat V, et al.: Auto-antibodies against type I IFNs in patients with life-threatening COVID-19. *Science* 2020.

96. Larner AC, Jonak G, Cheng YS, Korant B, Knight E, Darnell JE, Jr.: Transcriptional induction of two genes in human cells by beta interferon. *Proc Natl Acad Sci U S A* 1984, 81:6733-6737.

97. Bolen CR, Ding S, Robek MD, Kleinstein SH: Dynamic expression profiling of type I and type III interferon-stimulated hepatocytes reveals a stable hierarchy of gene expression. *Hepatology* 2014, 59:1262-1272.

98. Uze G, Lutfalla G, Gresser I: Genetic transfer of a functional human interferon alpha receptor into mouse cells: cloning and expression of its cDNA. *Cell* 1990, 60:225-234.

99. Novick D, Cohen B, Rubinstein M: The human interferon alpha/beta receptor: characterization and molecular cloning. *Cell* 1994, 77:391-400.

100. Cohen B, Novick D, Barak S, Rubinstein M: Ligand-induced association of the type I interferon receptor components. *Mol Cell Biol* 1995, 15:4208-4214.

101. Velazquez L, Fellous M, Stark GR, Pellegrini S: A protein tyrosine kinase in the interferon alpha/beta signaling pathway. *Cell* 1992, 70:313-322.

102. Muller M, Briscoe J, Laxton C, Guschin D, Ziemiecki A, Silvennoinen O, Harpur AG, Barbieri G, Witthuhn BA, Schindler C, et al.: The protein tyrosine kinase JAK1 complements defects in interferon-alpha/beta and -gamma signal transduction. *Nature* 1993, 366:129-135.

103. Improta T, Schindler C, Horvath CM, Kerr IM, Stark GR, Darnell JE, Jr.: Transcription factor ISGF-3 formation requires phosphorylated Stat91 protein, but Stat113 protein is phosphorylated independently of Stat91 protein. *Proc Natl Acad Sci U S A* 1994, 91:4776-4780.

104. Leung S, Qureshi SA, Kerr IM, Darnell JE, Jr., Stark GR: Role of STAT2 in the alpha interferon signaling pathway. *Mol Cell Biol* 1995, 15:1312-1317.

105. Fu XY, Schindler C, Improta T, Aebersold R, Darnell JE, Jr.: The proteins of ISGF-3, the interferon alpha-induced transcriptional activator, define a gene family involved in signal transduction. *Proc Natl Acad Sci U S A* 1992, 89:7840-7843.

106. Veals SA, Schindler C, Leonard D, Fu XY, Aebersold R, Darnell JE, Jr., Levy DE: Subunit of an alpha-interferon-responsive transcription factor is related to interferon regulatory factor and Myb families of DNA-binding proteins. *Mol Cell Biol* 1992, 12:3315-3324.

107. Platanitis E, Demiroz D, Schneller A, Fischer K, Capelle C, Hartl M, Gossenreiter T, Müller M, Novatchkova M, Decker T: A molecular switch from STAT2-IRF9 to ISGF3 underlies interferon-induced gene transcription. *Nat Commun* 2019, 10:2921.

108. Schneider WM, Chevillotte MD, Rice CM: Interferon-stimulated genes: a complex web of host defenses. *Annu Rev Immunol* 2014, 32:513-545.

109. Hervas-Stubbs S, Perez-Gracia JL, Rouzaut A, Sanmamed MF, Le Bon A, Melero I: Direct effects of type I interferons on cells of the immune system. *Clin Cancer Res* 2011, 17:2619-2627.

110. Makris S, Paulsen M, Johansson C: Type I Interferons as Regulators of Lung Inflammation. *Front Immunol* 2017, 8:259.

111. Ak AK, Mendez MD: Herpes Simplex Encephalitis. In *StatPearls*. Edited by: StatPearls Publishing

112. Beachboard DC, Horner SM: Innate immune evasion strategies of DNA and RNA viruses. *Curr Opin Microbiol* 2016, 32:113-119.

113. Wong G, Qiu XG: Type I interferon receptor knockout mice as models for infection of highly pathogenic viruses with outbreak potential. *Zool Res* 2018, 39:3-14.

114. Cheon H, Borden EC, Stark GR: Interferons and their stimulated genes in the tumor microenvironment. *Semin Oncol* 2014, 41:156-173.

115. Zamanian-Daryoush M, Der SD, Williams BR: Cell cycle regulation of the double stranded RNA activated protein kinase, PKR. *Oncogene* 1999, 18:315-326.

116. Buchrieser J, Degrelle SA, Couderc T, Nevers Q, Disson O, Manet C, Donahue DA, Porrot F, Hillion KH, Perthame E, et al.: IFITM proteins inhibit placental syncytiotrophoblast formation and promote fetal demise. *Science* 2019, 365:176-180.

117. Yockey LJ, Iwasaki A: Interferons and Proinflammatory Cytokines in Pregnancy and Fetal Development. *Immunity* 2018, 49:397-412.

118. Rodero MP, Crow YJ: Type I interferon-mediated monogenic autoinflammation: The type I interferonopathies, a conceptual overview. *J Exp Med* 2016, 213:2527-2538.

119. Starr R, Willson TA, Viney EM, Murray LJ, Rayner JR, Jenkins BJ, Gonda TJ, Alexander WS, Metcalf D, Nicola NA, et al.: A family of cytokine-inducible inhibitors of signalling. *Nature* 1997, 387:917-921.

120. Krebs DL, Hilton DJ: SOCS proteins: negative regulators of cytokine signaling. *Stem Cells* 2001, 19:378-387.

121. Malakhova OA, Kim KI, Luo JK, Zou W, Kumar KG, Fuchs SY, Shuai K, Zhang DE: UBP43 is a novel regulator of interferon signaling independent of its ISG15 isopeptidase activity. *Embo j* 2006, 25:2358-2367.

122. Pulit-Penaloza JA, Scherbik SV, Brinton MA: Type 1 IFN-independent activation of a subset of interferon stimulated genes in West Nile virus Eg101-infected mouse cells. *Virology* 2012, 425:82-94.

123. Schroeder L, Herwartz C, Jordanovski D, Steger G: ZNF395 Is an Activator of a Subset of IFN-Stimulated Genes. *Mediators Inflamm* 2017, 2017:1248201.

124. Rose KM, Elliott R, Martinez-Sobrido L, Garcia-Sastre A, Weiss SR: Murine coronavirus delays expression of a subset of interferon-stimulated genes. *J Virol* 2010, 84:5656-5669.

125. Froggatt HM, Harding AT, Heaton NS: ETV7 represses a subset of interferon-stimulated genes that restrict influenza viruses. *bioRxiv* 2019.

126. Cui K, Tailor P, Liu H, Chen X, Ozato K, Zhao K: The chromatin-remodeling BAF complex mediates cellular antiviral activities by promoter priming. *Mol Cell Biol* 2004, 24:4476-4486.

127. Liu H, Kang H, Liu R, Chen X, Zhao K: Maximal induction of a subset of interferon target genes requires the chromatin-remodeling activity of the BAF complex. *Mol Cell Biol* 2002, 22:6471-6479.

128. Fang TC, Schaefer U, Mecklenbrauker I, Stienen A, Dewell S, Chen MS, Rioja I, Parravicini V, Prinjha RK, Chandwani R, et al.: Histone H3 lysine 9 di-methylation as an epigenetic signature of the interferon response. *J Exp Med* 2012, 209:661-669.

129. Ivashkiv LB, Donlin LT: Regulation of type I interferon responses. *Nat Rev Immunol* 2014, 14:36-49.

130. Gregersen LH, Jacobsen AB, Frankel LB, Wen J, Krogh A, Lund AH: MicroRNA-145 targets YES and STAT1 in colon cancer cells. *PLoS One* 2010, 5:e8836.

131. Jiang S, Zhang HW, Lu MH, He XH, Li Y, Gu H, Liu MF, Wang ED: MicroRNA-155 functions as an OncomiR in breast cancer by targeting the suppressor of cytokine signaling 1 gene. *Cancer Res* 2010, 70:3119-3127.

132. Li A, Song W, Qian J, Li Y, He J, Zhang Q, Li W, Zhai A, Kao W, Hu Y, et al.: MiR-122 modulates type I interferon expression through blocking suppressor of cytokine signaling 1. *Int J Biochem Cell Biol* 2013, 45:858-865.

133. Rothamel K, Arcos S, Kim B, Reasoner C, Mukherjee N, Ascano M: ELAVL1 Exclusively Couples mRNA Stability with the 3'UTRs of Interferon Stimulated Genes. *bioRxiv* 2020.

134. Williams GD, Gokhale NS, Snider DL, Horner SM: The mRNA Cap 2'-O-Methyltransferase CMTR1 Regulates the Expression of Certain Interferon-Stimulated Genes. *mSphere* 2020, 5.

135. Zhou J, Wan J, Gao X, Zhang X, Jaffrey SR, Qian SB: Dynamic m(6)A mRNA methylation directs translational control of heat shock response. *Nature* 2015, 526:591-594.

136. Meyer KD, Patil DP, Zhou J, Zinoviev A, Skabkin MA, Elemento O, Pestova TV, Qian SB, Jaffrey SR: 5' UTR m(6)A Promotes Cap-Independent Translation. *Cell* 2015, 163:999-1010.

137. Xiang Y, Laurent B, Hsu CH, Nachtergaele S, Lu Z, Sheng W, Xu C, Chen H, Ouyang J, Wang S, et al.: RNA m(6)A methylation regulates the ultraviolet-induced DNA damage response. *Nature* 2017, 543:573-576.

138. Fry NJ, Law BA, Ilkayeva OR, Holley CL, Mansfield KD: N(6)-methyladenosine is required for the hypoxic stabilization of specific mRNAs. *Rna* 2017, 23:1444-1455.

139. Zhou J, Wan J, Shu XE, Mao Y, Liu XM, Yuan X, Zhang X, Hess ME, Brüning JC, Qian SB: N(6)-Methyladenosine Guides mRNA Alternative Translation during Integrated Stress Response. *Mol Cell* 2018, 69:636-647.e637.

140. Engel M, Eggert C, Kaplick PM, Eder M, Roh S, Tietze L, Namendorf C, Arloth J, Weber P, Rex-Haffner M, et al.: The Role of m(6)A/m-RNA Methylation in Stress Response Regulation. *Neuron* 2018, 99:389-403.e389.

141. Geula S, Moshitch-Moshkovitz S, Dominissini D, Mansour AA, Kol N, Salmon-Divon M, Hershkovitz V, Peer E, Mor N, Manor YS, et al.: m6A mRNA methylation facilitates resolution of naïve pluripotency toward differentiation. *Science* 2015, 347:1002-1006.

142. Zhang M, Zhai Y, Zhang S, Dai X, Li Z: Roles of N6-Methyladenosine (m(6)A) in Stem Cell Fate Decisions and Early Embryonic Development in Mammals. *Front Cell Dev Biol* 2020, 8:782.

143. Gagliardi D, Dziembowski A: 5' and 3' modifications controlling RNA degradation: from safeguards to executioners. *Philos Trans R Soc Lond B Biol Sci* 2018, 373.

144. Boo SH, Kim YK: The emerging role of RNA modifications in the regulation of mRNA stability. *Exp Mol Med* 2020, 52:400-408.

145. Roundtree IA, Evans ME, Pan T, He C: Dynamic RNA Modifications in Gene Expression Regulation. *Cell* 2017, 169:1187-1200.

146. Cowling VH: Regulation of mRNA cap methylation. *Biochem J* 2009, 425:295-302.

147. Baralle FE, Giudice J: Alternative splicing as a regulator of development and tissue identity. *Nat Rev Mol Cell Biol* 2017, 18:437-451.

148. Wigington CP, Williams KR, Meers MP, Bassell GJ, Corbett AH: Poly(A) RNA-binding proteins and polyadenosine RNA: new members and novel functions. *Wiley Interdiscip Rev RNA* 2014, 5:601-622.

149. Keene JD: RNA regulons: coordination of post-transcriptional events. *Nat Rev Genet* 2007, 8:533-543.

150. Song J, Yi C: Reading Chemical Modifications in the Transcriptome. *J Mol Biol* 2019.

151. Meyer KD, Jaffrey SR: Rethinking m(6)A Readers, Writers, and Erasers. *Annu Rev Cell Dev Biol* 2017, 33:319-342.

152. Lavi S, Shatkin AJ: Methylated simian virus 40-specific RNA from nuclei and cytoplasm of infected BSC-1 cells. *Proc Natl Acad Sci U S A* 1975, 72:2012-2016.

153. Sommer S, Salditt-Georgieff M, Bachenheimer S, Darnell JE, Furuichi Y, Morgan M, Shatkin AJ: The methylation of adenovirus-specific nuclear and cytoplasmic RNA. *Nucleic Acids Res* 1976, 3:749-765.

154. Krug RM, Morgan MA, Shatkin AJ: Influenza viral mRNA contains internal N6-methyladenosine and 5'-terminal 7-methylguanosine in cap structures. *J Virol* 1976, 20:45-53.

155. Moss B, Gershowitz A, Stringer JR, Holland LE, Wagner EK: 5'-Terminal and internal methylated nucleosides in herpes simplex virus type 1 mRNA. *J Virol* 1977, 23:234-239.

156. Zhu ZM, Huo FC, Pei DS: Function and evolution of RNA N6-methyladenosine modification. *Int J Biol Sci* 2020, 16:1929-1940.

157. Meyer KD, Saletore Y, Zumbo P, Elemento O, Mason CE, Jaffrey SR: Comprehensive analysis of mRNA methylation reveals enrichment in 3' UTRs and near stop codons. *Cell* 2012, 149:1635-1646.

158. Dominissini D, Moshitch-Moshkovitz S, Schwartz S, Salmon-Divon M, Ungar L, Osenberg S, Cesarkas K, Jacob-Hirsch J, Amariglio N, Kupiec M, et al.: Topology of the human and mouse m6A RNA methylomes revealed by m6A-seq. *Nature* 2012, 485:201-206.

159. Mayr C: What Are 3' UTRs Doing? *Cold Spring Harb Perspect Biol* 2019, 11.

160. Liu N, Parisien M, Dai Q, Zheng G, He C, Pan T: Probing N6-methyladenosine RNA modification status at single nucleotide resolution in mRNA and long noncoding RNA. *Rna* 2013, 19:1848-1856.

161. Harcourt EM, Ehrenschwender T, Batista PJ, Chang HY, Kool ET: Identification of a selective polymerase enables detection of N(6)-methyladenosine in RNA. *J Am Chem Soc* 2013, 135:19079-19082.

162. Linder B, Grozhik AV, Olarerin-George AO, Meydan C, Mason CE, Jaffrey SR: Single-nucleotide-resolution mapping of m6A and m6Am throughout the transcriptome. *Nat Methods* 2015, 12:767-772.

163. Chen K, Lu Z, Wang X, Fu Y, Luo GZ, Liu N, Han D, Dominissini D, Dai Q, Pan T, et al.: High-resolution N(6) -methyladenosine (m(6) A) map using photo-crosslinking-assisted m(6) A sequencing. *Angew Chem Int Ed Engl* 2015, 54:1587-1590.

164. Liu B, Merriman DK, Choi SH, Schumacher MA, Plangger R, Kreutz C, Horner SM, Meyer KD, Al-Hashimi HM: A potentially abundant junctional RNA motif stabilized by m(6)A and Mg(2). *Nat Commun* 2018, 9:2761.

165. Bokar JA, Shambaugh ME, Polayes D, Matera AG, Rottman FM: Purification and cDNA cloning of the AdoMet-binding subunit of the human mRNA (N6-adenosine)-methyltransferase. *Rna* 1997, 3:1233-1247.

166. Liu J, Yue Y, Han D, Wang X, Fu Y, Zhang L, Jia G, Yu M, Lu Z, Deng X, et al.: A METTL3-METTL14 complex mediates mammalian nuclear RNA N6-adenosine methylation. *Nat Chem Biol* 2014, 10:93-95.

167. Ping XL, Sun BF, Wang L, Xiao W, Yang X, Wang WJ, Adhikari S, Shi Y, Lv Y, Chen YS, et al.: Mammalian WTAP is a regulatory subunit of the RNA N6-methyladenosine methyltransferase. *Cell Res* 2014, 24:177-189.

168. Schwartz S, Mumbach MR, Jovanovic M, Wang T, Maciag K, Bushkin GG, Mertins P, Ter-Ovanesyan D, Habib N, Cacchiarelli D, et al.: Perturbation of m6A writers reveals two distinct classes of mRNA methylation at internal and 5' sites. *Cell Rep* 2014, 8:284-296.

169. Knuckles P, Lence T, Haussmann IU, Jacob D, Kreim N, Carl SH, Masiello I, Hares T, Villaseñor R, Hess D, et al.: Zc3h13/Flacc is required for adenosine methylation by bridging the mRNA-binding factor Rbm15/Spenito to the m(6)A machinery component Wtap/Fl(2)d. *Genes Dev* 2018, 32:415-429.

170. Patil DP, Chen CK, Pickering BF, Chow A, Jackson C, Guttman M, Jaffrey SR: m(6)A RNA methylation promotes XIST-mediated transcriptional repression. *Nature* 2016, 537:369-373.

171. Slobodin B, Han R, Calderone V, Vrielink J, Loayza-Puch F, Elkon R, Agami R: Transcription Impacts the Efficiency of mRNA Translation via Co-transcriptional N6-adenosine Methylation. *Cell* 2017, 169:326-337.e312.

172. Jia G, Fu Y, Zhao X, Dai Q, Zheng G, Yang Y, Yi C, Lindahl T, Pan T, Yang YG, et al.: N6-methyladenosine in nuclear RNA is a major substrate of the obesity-associated FTO. *Nat Chem Biol* 2011, 7:885-887.

173. Zheng G, Dahl JA, Niu Y, Fedorcsak P, Huang CM, Li CJ, Vågbø CB, Shi Y, Wang WL, Song SH, et al.: ALKBH5 is a mammalian RNA demethylase that impacts RNA metabolism and mouse fertility. *Mol Cell* 2013, 49:18-29.

174. Ke S, Pandya-Jones A, Saito Y, Fak JJ, Vagbo CB, Geula S, Hanna JH, Black DL, Darnell JE, Jr., Darnell RB: m(6)A mRNA modifications are deposited in nascent pre-mRNA and are not required for splicing but do specify cytoplasmic turnover. *Genes Dev* 2017, 31:990-1006.

175. Gokhale NS, McIntyre ABR, Mattocks MD, Holley CL, Lazear HM, Mason CE, Horner SM: Altered m(6)A Modification of Specific Cellular Transcripts Affects Flaviviridae Infection. *Mol Cell* 2020, 77:542-555.e548.

176. Zheng Q, Hou J, Zhou Y, Li Z, Cao X: The RNA helicase DDX46 inhibits innate immunity by entrapping m(6)A-demethylated antiviral transcripts in the nucleus. *Nat Immunol* 2017, 18:1094-1103.

177. Liu Y, You Y, Lu Z, Yang J, Li P, Liu L, Xu H, Niu Y, Cao X: N (6)-methyladenosine RNA modification-mediated cellular metabolism rewiring inhibits viral replication. *Science* 2019, 365:1171-1176.

178. Williams GD, Gokhale NS, Horner SM: Regulation of Viral Infection by the RNA Modification N6-Methyladenosine. *Annu Rev Virol* 2019, 6:235-253.

179. Liu N, Dai Q, Zheng G, He C, Parisien M, Pan T: N(6)-methyladenosine-dependent RNA structural switches regulate RNA-protein interactions. *Nature* 2015, 518:560-564.

180. Edupuganti RR, Geiger S, Lindeboom RGH, Shi H, Hsu PJ, Lu Z, Wang SY, Baltissen MPA, Jansen P, Rossa M, et al.: N(6)-methyladenosine (m(6)A) recruits and repels proteins to regulate mRNA homeostasis. *Nat Struct Mol Biol* 2017, 24:870-878.

181. Arguello AE, DeLiberto AN, Kleiner RE: RNA Chemical Proteomics Reveals the N(6)-Methyladenosine (m(6)A)-Regulated Protein-RNA Interactome. *J Am Chem Soc* 2017, 139:17249-17252.

182. Shi H, Wei J, He C: Where, When, and How: Context-Dependent Functions of RNA Methylation Writers, Readers, and Erasers. *Mol Cell* 2019, 74:640-650.

183. Wang X, Zhao BS, Roundtree IA, Lu Z, Han D, Ma H, Weng X, Chen K, Shi H, He C: N(6)-methyladenosine Modulates Messenger RNA Translation Efficiency. *Cell* 2015, 161:1388-1399.

184. Wang X, Lu Z, Gomez A, Hon GC, Yue Y, Han D, Fu Y, Parisien M, Dai Q, Jia G, et al.: N6-methyladenosine-dependent regulation of messenger RNA stability. *Nature* 2014, 505:117-120.

185. Shi H, Wang X, Lu Z, Zhao BS, Ma H, Hsu PJ, Liu C, He C: YTHDF3 facilitates translation and decay of N(6)-methyladenosine-modified RNA. *Cell Res* 2017, 27:315-328.

186. Tirumuru N, Zhao BS, Lu W, Lu Z, He C, Wu L: N(6)-methyladenosine of HIV-1 RNA regulates viral infection and HIV-1 Gag protein expression. *Elife* 2016, 5.

187. Gokhale NS, McIntyre ABR, McFadden MJ, Roder AE, Kennedy EM, Gandara JA, Hopcraft SE, Quicke KM, Vazquez C, Willer J, et al.: N6-Methyladenosine in Flaviviridae Viral RNA Genomes Regulates Infection. *Cell Host Microbe* 2016, 20:654-665.

188. Kasowitz SD, Ma J, Anderson SJ, Leu NA, Xu Y, Gregory BD, Schultz RM, Wang PJ: Nuclear m6A reader YTHDC1 regulates alternative polyadenylation and splicing during mouse oocyte development. *PLoS Genet* 2018, 14:e1007412.

189. Kretschmer J, Rao H, Hackert P, Sloan KE, Höbartner C, Bohnsack MT: The m(6)A reader protein YTHDC2 interacts with the small ribosomal subunit and the 5'-3' exoribonuclease XRN1. *Rna* 2018, 24:1339-1350.

190. Wang Y, Li Y, Toth JI, Petroski MD, Zhang Z, Zhao JC: N6-methyladenosine modification destabilizes developmental regulators in embryonic stem cells. *Nat Cell Biol* 2014, 16:191-198.

191. Batista PJ, Molinie B, Wang J, Qu K, Zhang J, Li L, Bouley DM, Lujan E, Haddad B, Daneshvar K, et al.: m(6)A RNA modification controls cell fate transition in mammalian embryonic stem cells. *Cell Stem Cell* 2014, 15:707-719.

192. Kan L, Grozhik AV, Vedanayagam J, Patil DP, Pang N, Lim KS, Huang YC, Joseph B, Lin CJ, Despic V, et al.: The m(6)A pathway facilitates sex determination in Drosophila. *Nat Commun* 2017, 8:15737.

193. Lin Z, Tong MH: m(6)A mRNA modification regulates mammalian spermatogenesis. *Biochim Biophys Acta Gene Regul Mech* 2019, 1862:403-411.

194. Meyer KD, Jaffrey SR: The dynamic epitranscriptome: N6-methyladenosine and gene expression control. *Nat Rev Mol Cell Biol* 2014, 15:313-326.

195. Cheng Y, Luo H, Izzo F, Pickering BF, Nguyen D, Myers R, Schurer A, Gourkanti S, Brüning JC, Vu LP, et al.: m(6)A RNA Methylation Maintains Hematopoietic Stem Cell Identity and Symmetric Commitment. *Cell Rep* 2019, 28:1703-1716.e1706.

196. Wang H, Hu X, Huang M, Liu J, Gu Y, Ma L, Zhou Q, Cao X: Mettl3-mediated mRNA m(6)A methylation promotes dendritic cell activation. *Nat Commun* 2019, 10:1898.

197. Li HB, Tong J, Zhu S, Batista PJ, Duffy EE, Zhao J, Bailis W, Cao G, Kroehling L, Chen Y, et al.: m(6)A mRNA methylation controls T cell homeostasis by targeting the IL-7/STAT5/SOCS pathways. *Nature* 2017, 548:338-342.

198. Tong J, Cao G, Zhang T, Sefik E, Amezcua Vesely MC, Broughton JP, Zhu S, Li H, Li B, Chen L, et al.: m(6)A mRNA methylation sustains Treg suppressive functions. *Cell Res* 2018, 28:253-256.

199. Chen M, Wong CM: The emerging roles of N6-methyladenosine (m6A) deregulation in liver carcinogenesis. *Mol Cancer* 2020, 19:44.

200. Fustin JM, Doi M, Yamaguchi Y, Hida H, Nishimura S, Yoshida M, Isagawa T, Morioka MS, Kakeya H, Manabe I, et al.: RNA-methylation-dependent RNA processing controls the speed of the circadian clock. *Cell* 2013, 155:793-806.

201. Li M, Zhao X, Wang W, Shi H, Pan Q, Lu Z, Perez SP, Suganthan R, He C, Bjørås M, et al.: Ythdf2-mediated m(6)A mRNA clearance modulates neural development in mice. *Genome Biol* 2018, 19:69.

202. Merkurjev D, Hong WT, Iida K, Oomoto I, Goldie BJ, Yamaguti H, Ohara T, Kawaguchi SY, Hirano T, Martin KC, et al.: Synaptic N(6)-methyladenosine (m(6)A) epitranscriptome reveals functional partitioning of localized transcripts. *Nat Neurosci* 2018, 21:1004-1014.

203. Shi H, Zhang X, Weng YL, Lu Z, Liu Y, Lu Z, Li J, Hao P, Zhang Y, Zhang F, et al.: m(6)A facilitates hippocampus-dependent learning and memory through YTHDF1. *Nature* 2018, 563:249-253.

204. Zaccara S, Ries RJ, Jaffrey SR: Reading, writing and erasing mRNA methylation. *Nat Rev Mol Cell Biol* 2019, 20:608-624.

205. Zhao X, Yang Y, Sun BF, Shi Y, Yang X, Xiao W, Hao YJ, Ping XL, Chen YS, Wang WJ, et al.: FTO-dependent demethylation of N6-methyladenosine regulates mRNA splicing and is required for adipogenesis. *Cell Res* 2014, 24:1403-1419.

206. Yue Y, Liu J, Cui X, Cao J, Luo G, Zhang Z, Cheng T, Gao M, Shu X, Ma H, et al.: VIRMA mediates preferential m(6)A mRNA methylation in 3'UTR and near stop codon and associates with alternative polyadenylation. *Cell Discov* 2018, 4:10.

207. Patil DP, Pickering BF, Jaffrey SR: Reading m(6)A in the Transcriptome: m(6)A-Binding Proteins. *Trends Cell Biol* 2018, 28:113-127.

208. Takeuchi O, Akira S: Pattern recognition receptors and inflammation. *Cell* 2010, 140:805-820.

209. Iwasaki A, Medzhitov R: Control of adaptive immunity by the innate immune system. *Nat Immunol* 2015, 16:343-353.

210. Schlee M, Hartmann G: Discriminating self from non-self in nucleic acid sensing. *Nat Rev Immunol* 2016, 16:566-580.

211. Decroly E, Ferron F, Lescar J, Canard B: Conventional and unconventional mechanisms for capping viral mRNA. *Nat Rev Microbiol* 2011, 10:51-65.

212. Karikó K, Buckstein M, Ni H, Weissman D: Suppression of RNA recognition by Toll-like receptors: the impact of nucleoside modification and the evolutionary origin of RNA. *Immunity* 2005, 23:165-175.

213. Durbin AF, Wang C, Marcotrigiano J, Gehrke L: RNAs Containing Modified Nucleotides Fail To Trigger RIG-I Conformational Changes for Innate Immune Signaling. *mBio* 2016, 7.

214. Chen YG, Chen R, Ahmad S, Verma R, Kasturi SP, Amaya L, Broughton JP, Kim J, Cadena C, Pulendran B, et al.: N6-Methyladenosine Modification Controls Circular RNA Immunity. *Mol Cell* 2019, 76:96-109.e109.

215. Wang J, Wang L, Diao J, Shi YG, Shi Y, Ma H, Shen H: Binding to m(6)A RNA promotes YTHDF2-mediated phase separation. *Protein Cell* 2020, 11:304-307.

216. Gao Y, Vasic R, Song Y, Teng R, Liu C, Gbyli R, Biancon G, Nelakanti R, Lobben K, Kudo E, et al.: m(6)A Modification Prevents Formation of Endogenous Double-Stranded RNAs and Deleterious Innate Immune Responses during Hematopoietic Development. *Immunity* 2020, 52:1007-1021.e1008.

217. Lu M, Zhang Z, Xue M, Zhao BS, Harder O, Li A, Liang X, Gao TZ, Xu Y, Zhou J, et al.: N(6)-methyladenosine modification enables viral RNA to escape recognition by RNA sensor RIG-I. *Nat Microbiol* 2020, 5:584-598.

218. Kim GW, Imam H, Khan M, Siddiqui A: N6-Methyladenosine Modification of Hepatitis B and C Viral RNAs Attenuates Host Innate Immunity via RIG-I Signaling. *J Biol Chem* 2020.

219. Feng Z, Li Q, Meng R, Yi B, Xu Q: METTL3 regulates alternative splicing of MyD88 upon the lipopolysaccharide-induced inflammatory response in human dental pulp cells. *J Cell Mol Med* 2018, 22:2558-2568.

220. Lester SN, Li K: Toll-like receptors in antiviral innate immunity. *J Mol Biol* 2014, 426:1246-1264.

221. Yu R, Li Q, Feng Z, Cai L, Xu Q: m6A Reader YTHDF2 Regulates LPS-Induced Inflammatory Response. *Int J Mol Sci* 2019, 20.

222. Imam H, Khan M, Gokhale NS, McIntyre ABR, Kim GW, Jang JY, Kim SJ, Mason CE, Horner SM, Siddiqui A: N6-methyladenosine modification of hepatitis B virus RNA differentially regulates the viral life cycle. *Proc Natl Acad Sci U S A* 2018, 115:8829-8834.

223. Pardi N, Hogan MJ, Pelc RS, Muramatsu H, Andersen H, DeMaso CR, Dowd KA, Sutherland LL, Scearce RM, Parks R, et al.: Zika virus protection by a single low-dose nucleoside-modified mRNA vaccination. *Nature* 2017, 543:248-251.

224. Pardi N, Parkhouse K, Kirkpatrick E, McMahon M, Zost SJ, Mui BL, Tam YK, Karikó K, Barbosa CJ, Madden TD, et al.: Nucleoside-modified mRNA immunization elicits influenza virus hemagglutinin stalk-specific antibodies. *Nat Commun* 2018, 9:3361.

225. Lieberman J: Tapping the RNA world for therapeutics. *Nat Struct Mol Biol* 2018, 25:357-364.

226. Imam H, Kim GW, Mir SA, Khan M, Siddiqui A: Interferon-stimulated gene 20 (ISG20) selectively degrades N6-methyladenosine modified Hepatitis B Virus transcripts. *PLoS Pathog* 2020, 16:e1008338.

227. Kumar P, Sweeney TR, Skabkin MA, Skabkina OV, Hellen CU, Pestova TV: Inhibition of translation by IFIT family members is determined by their ability to interact selectively with the 5'-terminal regions of cap0-, cap1- and 5'ppp-mRNAs. *Nucleic Acids Res* 2014, 42:3228-3245.

228. Takata MA, Gonçalves-Carneiro D, Zang TM, Soll SJ, York A, Blanco-Melo D, Bieniasz PD: CG dinucleotide suppression enables antiviral defence targeting non-self RNA. *Nature* 2017, 550:124-127.

229. Refolo G, Vescovo T, Piacentini M, Fimia GM, Ciccosanti F: Mitochondrial Interactome: A Focus on Antiviral Signaling Pathways. *Front Cell Dev Biol* 2020, 8:8.

230. Zhou KI, Shi H, Lyu R, Wylder AC, Matuszek Ż, Pan JN, He C, Parisien M, Pan T: Regulation of Co-transcriptional Pre-mRNA Splicing by m(6)A through the Low-Complexity Protein hnRNPG. *Mol Cell* 2019, 76:70-81.e79.

231. Rubio RM, Depledge DP, Bianco C, Thompson L, Mohr I: RNA m(6) A modification enzymes shape innate responses to DNA by regulating interferon beta. *Genes Dev* 2018, 32:1472-1484.

232. Winkler R, Gillis E, Lasman L, Safra M, Geula S, Soyris C, Nachshon A, Tai-Schmiedel J, Friedman N, Le-Trilling VTK, et al.: m(6)A modification controls the innate immune response to infection by targeting type I interferons. *Nat Immunol* 2019, 20:173-182.

233. Zhang Y, Wang X, Zhang X, Wang J, Ma Y, Zhang L, Cao X: RNA-binding protein YTHDF3 suppresses interferon-dependent antiviral responses by promoting FOXO3 translation. *Proc Natl Acad Sci U S A* 2019, 116:976-981.

234. Bonham KS, Orzalli MH, Hayashi K, Wolf AI, Glanemann C, Weninger W, Iwasaki A, Knipe DM, Kagan JC: A promiscuous lipid-binding protein diversifies the subcellular sites of toll-like receptor signal transduction. *Cell* 2014, 156:705-716.

235. Banchereau J, Briere F, Caux C, Davoust J, Lebecque S, Liu YJ, Pulendran B, Palucka K: Immunobiology of dendritic cells. *Annu Rev Immunol* 2000, 18:767-811.

236. Hong C, Luckey MA, Park JH: Intrathymic IL-7: the where, when, and why of IL-7 signaling during T cell development. *Semin Immunol* 2012, 24:151-158.

237. Moreno-Altamirano MMB, Kolstoe SE, Sánchez-García FJ: Virus Control of Cell Metabolism for Replication and Evasion of Host Immune Responses. *Front Cell Infect Microbiol* 2019, 9:95.

238. Lichinchi G, Gao S, Saletore Y, Gonzalez GM, Bansal V, Wang Y, Mason CE, Rana TM: Dynamics of the human and viral m(6)A RNA methylomes during HIV-1 infection of T cells. *Nat Microbiol* 2016, 1:16011.

239. Lichinchi G, Zhao BS, Wu Y, Lu Z, Qin Y, He C, Rana TM: Dynamics of Human and Viral RNA Methylation during Zika Virus Infection. *Cell Host Microbe* 2016, 20:666-673.

240. Tan B, Liu H, Zhang S, da Silva SR, Zhang L, Meng J, Cui X, Yuan H, Sorel O, Zhang SW, et al.: Viral and cellular N(6)-methyladenosine and N(6),2'-O-dimethyladenosine epitranscriptomes in the KSHV life cycle. *Nat Microbiol* 2018, 3:108-120.

241. McIntyre ABR, Gokhale NS, Cerchietti L, Jaffrey SR, Horner SM, Mason CE: Limits in the detection of m(6)A changes using MeRIP/m(6)A-seq. *Sci Rep* 2020, 10:6590.

242. Blázquez AB, Escribano-Romero E, Merino-Ramos T, Saiz JC, Martín-Acebes MA: Stress responses in flavivirus-infected cells: activation of unfolded protein response and autophagy. *Front Microbiol* 2014, 5:266.

243. Hao H, Hao S, Chen H, Chen Z, Zhang Y, Wang J, Wang H, Zhang B, Qiu J, Deng F, et al.: N6-methyladenosine modification and METTL3 modulate enterovirus 71 replication. *Nucleic Acids Res* 2019, 47:362-374.

244. McFadden MJ, McIntyre ABR, Mourelatos H, Abell NS, Gokhale NS, Ipas H, Xhemalçe B, Mason CE, Horner SM: Post-Transcriptional Regulation of Antiviral Gene Expression by N6-Methyladenosine. *bioRxiv* 2020:2020.2008.2005.238337.

245. Schoggins JW, Rice CM: Interferon-stimulated genes and their antiviral effector functions. *Curr Opin Virol* 2011, 1:519-525.

246. Gonzalez-Navajas JM, Lee J, David M, Raz E: Immunomodulatory functions of type I interferons. *Nat Rev Immunol* 2012, 12:125-135.

247. Teijaro JR: Type I interferons in viral control and immune regulation. *Curr Opin Virol* 2016, 16:31-40.

248. Banchereau J, Pascual V: Type I interferon in systemic lupus erythematosus and other autoimmune diseases. *Immunity* 2006, 25:383-392.

249. Huang M, Qian F, Hu Y, Ang C, Li Z, Wen Z: Chromatin-remodelling factor BRG1 selectively activates a subset of interferon-alpha-inducible genes. *Nat Cell Biol* 2002, 4:774-781.

250. Forster SC, Tate MD, Hertzog PJ: MicroRNA as Type I Interferon-Regulated Transcripts and Modulators of the Innate Immune Response. *Front Immunol* 2015, 6:334.

251. West KO, Scott HM, Torres-Odio S, West AP, Patrick KL, Watson RO: The Splicing Factor hnRNP M Is a Critical Regulator of Innate Immune Gene Expression in Macrophages. *Cell Rep* 2019, 29:1594-1609.e1595.

252. Perwitasari O, Cho H, Diamond MS, Gale M, Jr.: Inhibitor of κB kinase epsilon (IKK(epsilon)), STAT1, and IFIT2 proteins define novel innate immune effector pathway against West Nile virus infection. *J Biol Chem* 2011, 286:44412-44423.

253. Seifert LL, Si C, Saha D, Sadic M, de Vries M, Ballentine S, Briley A, Wang G, Valero-Jimenez AM, Mohamed A, et al.: The ETS transcription factor ELF1 regulates a broadly antiviral program distinct from the type I interferon response. *PLoS Pathog* 2019, 15:e1007634.

254. Froggatt HM, Harding AT, Heaton NS: ETV7 represses a subset of interferon-stimulated genes that restrict influenza viruses. *bioRxiv* 2019:851543.

255. Liu J, Harada BT, He C: Regulation of Gene Expression by N(6)-methyladenosine in Cancer. *Trends Cell Biol* 2019, 29:487-499.

256. Zaccara S, Jaffrey SR: A Unified Model for the Function of YTHDF Proteins in Regulating m(6)A-Modified mRNA. *Cell* 2020, 181:1582-1595.e1518.

257. Gokhale NS, McIntyre ABR, Mattocks MD, Holley CL, Lazear HM, Mason CE, Horner SM: Altered m(6)A Modification of Specific Cellular Transcripts Affects Flaviviridae Infection. *Mol Cell* 2019.

258. Kariko K, Buckstein M, Ni H, Weissman D: Suppression of RNA recognition by Toll-like receptors: the impact of nucleoside modification and the evolutionary origin of RNA. *Immunity* 2005, 23:165-175.

259. Zhang C, Fu J, Zhou Y: A Review in Research Progress Concerning m6A Methylation and Immunoregulation. *Front Immunol* 2019, 10:922.

260. Shaw AE, Hughes J, Gu Q, Behdenna A, Singer JB, Dennis T, Orton RJ, Varela M, Gifford RJ, Wilson SJ, et al.: Fundamental properties of the mammalian innate immune system revealed by multispecies comparison of type I interferon responses. *PLoS Biol* 2017, 15:e2004086.

261. Lesbirel S, Wilson SA: The m(6)Amethylase complex and mRNA export. *Biochim Biophys Acta Gene Regul Mech* 2019, 1862:319-328.

262. Cui X, Zhang L, Meng J, Rao MK, Chen Y, Huang Y: MeTDiff: A Novel Differential RNA Methylation Analysis for MeRIP-Seq Data. *IEEE/ACM Trans Comput Biol Bioinform* 2018, 15:526-534.

263. Miller DM, Zhang Y, Rahill BM, Waldman WJ, Sedmak DD: Human cytomegalovirus inhibits IFN-alpha-stimulated antiviral and immunoregulatory responses by blocking multiple levels of IFN-alpha signal transduction. *J Immunol* 1999, 162:6107-6113.

264. Lin S, Choe J, Du P, Triboulet R, Gregory RI: The m(6)A Methyltransferase METTL3 Promotes Translation in Human Cancer Cells. *Mol Cell* 2016, 62:335-345.

265. Coots RA, Liu XM, Mao Y, Dong L, Zhou J, Wan J, Zhang X, Qian SB: m(6)A Facilitates eIF4F-Independent mRNA Translation. *Mol Cell* 2017, 68:504-514.e507.

266. Mao Y, Dong L, Liu XM, Guo J, Ma H, Shen B, Qian SB: m(6)A in mRNA coding regions promotes translation via the RNA helicase-containing YTHDC2. *Nat Commun* 2019, 10:5332.

267. Xu C, Liu K, Ahmed H, Loppnau P, Schapira M, Min J: Structural Basis for the Discriminative Recognition of N6-Methyladenosine RNA by the Human YT521-B Homology Domain Family of Proteins. *J Biol Chem* 2015, 290:24902-24913.

268. Love MI, Huber W, Anders S: Moderated estimation of fold change and dispersion for RNA-seq data with DESeq2. *Genome Biol* 2014, 15:550.

269. Ogino T, Banerjee AK: An unconventional pathway of mRNA cap formation by vesiculoviruses. *Virus Res* 2011, 162:100-109.

270. Boulias K, Toczydlowska-Socha D, Hawley BR, Liberman N, Takashima K, Zaccara S, Guez T, Vasseur JJ, Debart F, Aravind L, et al.: Identification of the m(6)Am Methyltransferase PCIF1 Reveals the Location and Functions of m(6)Am in the Transcriptome. *Mol Cell* 2019, 75:631-643.e638.

271. Sendinc E, Valle-Garcia D, Dhall A, Chen H, Henriques T, Navarrete-Perea J, Sheng W, Gygi SP, Adelman K, Shi Y: PCIF1 Catalyzes m6Am mRNA Methylation to Regulate Gene Expression. *Mol Cell* 2019, 75:620-630.e629.

272. Muller U, Steinhoff U, Reis LF, Hemmi S, Pavlovic J, Zinkernagel RM, Aguet M: Functional role of type I and type II interferons in antiviral defense. *Science* 1994, 264:1918-1921.

273. Li A, Chen YS, Ping XL, Yang X, Xiao W, Yang Y, Sun HY, Zhu Q, Baidya P, Wang X, et al.: Cytoplasmic m(6)A reader YTHDF3 promotes mRNA translation. *Cell Res* 2017, 27:444-447.

274. Whelan SP, Barr JN, Wertz GW: Identification of a minimal size requirement for termination of vesicular stomatitis virus mRNA: implications for the mechanism of transcription. *J Virol* 2000, 74:8268-8276.

275. Kennedy EM, Bogerd HP, Kornepati AV, Kang D, Ghoshal D, Marshall JB, Poling BC, Tsai K, Gokhale NS, Horner SM, et al.: Posttranscriptional m(6)A Editing of HIV-1 mRNAs Enhances Viral Gene Expression. *Cell Host Microbe* 2016, 19:675-685.

276. Sumpter R, Jr., Loo YM, Foy E, Li K, Yoneyama M, Fujita T, Lemon SM, Gale M, Jr.: Regulating intracellular antiviral defense and permissiveness to hepatitis C virus RNA replication through a cellular RNA helicase, RIG-I. *J Virol* 2005, 79:2689-2699.

277. Xie M, Xuan B, Shan J, Pan D, Sun Y, Shan Z, Zhang J, Yu D, Li B, Qian Z: Human cytomegalovirus exploits interferon-induced transmembrane proteins to facilitate morphogenesis of the virion assembly compartment. *J Virol* 2015, 89:3049-3061.

278. Shi G, Ozog S, Torbett BE, Compton AA: mTOR inhibitors lower an intrinsic barrier to virus infection mediated by IFITM3. *Proc Natl Acad Sci U S A* 2018, 115:E10069-e10078.

279. Bolger AM, Lohse M, Usadel B: Trimmomatic: a flexible trimmer for Illumina sequence data. *Bioinformatics* 2014, 30:2114-2120.

280. Dobin A, Davis CA, Schlesinger F, Drenkow J, Zaleski C, Jha S, Batut P, Chaisson M, Gingeras TR: STAR: ultrafast universal RNA-seq aligner. *Bioinformatics* 2013, 29:15-21.

281. Liao Y, Smyth GK, Shi W: featureCounts: an efficient general purpose program for assigning sequence reads to genomic features. *Bioinformatics* 2014, 30:923-930.

282. Heinz S, Benner C, Spann N, Bertolino E, Lin YC, Laslo P, Cheng JX, Murre C, Singh H, Glass CK: Simple combinations of lineage-determining transcription factors prime cis-regulatory elements required for macrophage and B cell identities. *Mol Cell* 2010, 38:576-589.

283. Martin M: Cutadapt removes adapter sequences from high-throughput sequencing reads. *EMBnet Journal* 2011, 17:10-12.

284. Ramírez F, Ryan DP, Grüning B, Bhardwaj V, Kilpert F, Richter AS, Heyne S, Dündar F, Manke T: deepTools2: a next generation web server for deep-sequencing data analysis. *Nucleic Acids Res* 2016, 44:W160-165.

285. Metsalu T, Vilo J: ClustVis: a web tool for visualizing clustering of multivariate data using Principal Component Analysis and heatmap. *Nucleic Acids Res* 2015, 43:W566-570.

286. Abell NS, Mercado M, Caneque T, Rodriguez R, Xhemalce B: Click Quantitative Mass Spectrometry Identifies PIWIL3 as a Mechanistic Target of RNA Interference Activator Enoxacin in Cancer Cells. *J Am Chem Soc* 2017, 139:1400-1403.

287. Cox J, Mann M: MaxQuant enables high peptide identification rates, individualized p.p.b.-range mass accuracies and proteome-wide protein quantification. *Nat Biotechnol* 2008, 26:1367-1372.

288. Cox J, Neuhauser N, Michalski A, Scheltema RA, Olsen JV, Mann M: Andromeda: a peptide search engine integrated into the MaxQuant environment. *J Proteome Res* 2011, 10:1794-1805.

289. Bates D, Mächler M, Bolker B, Walker S: Fitting Linear Mixed-Effects Models Using lme4. *Journal of Statistical Software* 2015, 67:48.

290. Frayling TM, Timpson NJ, Weedon MN, Zeggini E, Freathy RM, Lindgren CM, Perry JR, Elliott KS, Lango H, Rayner NW, et al.: A common variant in the FTO gene is associated with body mass index and predisposes to childhood and adult obesity. *Science* 2007, 316:889-894.

291. Dina C, Meyre D, Gallina S, Durand E, Körner A, Jacobson P, Carlsson LM, Kiess W, Vatin V, Lecoeur C, et al.: Variation in FTO contributes to childhood obesity and severe adult obesity. *Nat Genet* 2007, 39:724-726.

292. Speliotes EK, Willer CJ, Berndt SI, Monda KL, Thorleifsson G, Jackson AU, Lango Allen H, Lindgren CM, Luan J, Mägi R, et al.: Association analyses of 249,796 individuals reveal 18 new loci associated with body mass index. *Nat Genet* 2010, 42:937-948.

293. Olza J, Ruperez AI, Gil-Campos M, Leis R, Fernandez-Orth D, Tojo R, Cañete R, Gil A, Aguilera CM: Influence of FTO variants on obesity, inflammation and cardiovascular disease risk biomarkers in Spanish children: a case-control multicentre study. *BMC Med Genet* 2013, 14:123.

294. Boissel S, Reish O, Proulx K, Kawagoe-Takaki H, Sedgwick B, Yeo GS, Meyre D, Golzio C, Molinari F, Kadhom N, et al.: Loss-of-function mutation in the dioxygenase-encoding FTO gene causes severe growth retardation and multiple malformations. *Am J Hum Genet* 2009, 85:106-111.

295. Gerken T, Girard CA, Tung YC, Webby CJ, Saudek V, Hewitson KS, Yeo GS, McDonough MA, Cunliffe S, McNeill LA, et al.: The obesity-associated FTO gene encodes a 2-oxoglutarate-dependent nucleic acid demethylase. *Science* 2007, 318:1469-1472.

296. Mauer J, Luo X, Blanjoie A, Jiao X, Grozhik AV, Patil DP, Linder B, Pickering BF, Vasseur JJ, Chen Q, et al.: Reversible methylation of m(6)A(m) in the 5' cap controls mRNA stability. *Nature* 2017, 541:371-375.

297. Li L, Zang L, Zhang F, Chen J, Shen H, Shu L, Liang F, Feng C, Chen D, Tao H, et al.: Fat mass and obesity-associated (FTO) protein regulates adult neurogenesis. *Hum Mol Genet* 2017, 26:2398-2411.

298. Hess ME, Hess S, Meyer KD, Verhagen LA, Koch L, Brönneke HS, Dietrich MO, Jordan SD, Saletore Y, Elemento O, et al.: The fat mass and obesity associated gene (Fto) regulates activity of the dopaminergic midbrain circuitry. *Nat Neurosci* 2013, 16:1042-1048.

299. Karra E, O'Daly OG, Choudhury AI, Yousseif A, Millership S, Neary MT, Scott WR, Chandarana K, Manning S, Hess ME, et al.: A link between FTO, ghrelin, and impaired brain food-cue responsivity. *J Clin Invest* 2013, 123:3539-3551.

300. Li Z, Weng H, Su R, Weng X, Zuo Z, Li C, Huang H, Nachtergaele S, Dong L, Hu C, et al.: FTO Plays an Oncogenic Role in Acute Myeloid Leukemia as a N(6)-Methyladenosine RNA Demethylase. *Cancer Cell* 2017, 31:127-141.

301. Yang S, Wei J, Cui YH, Park G, Shah P, Deng Y, Aplin AE, Lu Z, Hwang S, He C, et al.: m(6)A mRNA demethylase FTO regulates melanoma tumorigenicity and response to anti-PD-1 blockade. *Nat Commun* 2019, 10:2782.

302. Wei J, Liu F, Lu Z, Fei Q, Ai Y, He PC, Shi H, Cui X, Su R, Klungland A, et al.: Differential m(6)A, m(6)A(m), and m(1)A Demethylation Mediated by FTO in the Cell Nucleus and Cytoplasm. *Mol Cell* 2018, 71:973-985.e975.

303. Liu SJ, Tang HL, He Q, Lu P, Fu T, Xu XL, Su T, Gao MM, Duan S, Luo Y, et al.: FTO is a transcriptional repressor to auto-regulate its own gene and potentially associated with homeostasis of body weight. *J Mol Cell Biol* 2019, 11:118-132.

304. Spector DL, Lamond AI: Nuclear speckles. *Cold Spring Harb Perspect Biol* 2011, 3.

305. Ritchie ME, Phipson B, Wu D, Hu Y, Law CW, Shi W, Smyth GK: limma powers differential expression analyses for RNA-sequencing and microarray studies. *Nucleic Acids Res* 2015, 43:e47.

306. Dölken L, Ruzsics Z, Rädle B, Friedel CC, Zimmer R, Mages J, Hoffmann R, Dickinson P, Forster T, Ghazal P, et al.: High-resolution gene expression profiling for simultaneous kinetic parameter analysis of RNA synthesis and decay. *Rna* 2008, 14:1959-1972.

307. Choe J, Lin S, Zhang W, Liu Q, Wang L, Ramirez-Moya J, Du P, Kim W, Tang S, Sliz P, et al.: mRNA circularization by METTL3-eIF3h enhances translation and promotes oncogenesis. *Nature* 2018, 561:556-560.

308. Gal-Ben-Ari S, Barrera I, Ehrlich M, Rosenblum K: PKR: A Kinase to Remember. *Front Mol Neurosci* 2018, 11:480.

309. Jackson RJ, Hellen CU, Pestova TV: The mechanism of eukaryotic translation initiation and principles of its regulation. *Nat Rev Mol Cell Biol* 2010, 11:113-127.

310. Kim Y, Lee JH, Park JE, Cho J, Yi H, Kim VN: PKR is activated by cellular dsRNAs during mitosis and acts as a mitotic regulator. *Genes Dev* 2014, 28:1310-1322.

311. Fu Y, Zhuang X: m(6)A-binding YTHDF proteins promote stress granule formation. *Nat Chem Biol* 2020, 16:955-963.

312. Xu J, Chen Q, Tian K, Liang R, Chen T, Gong A, Mathy NW, Yu T, Chen X: m6A methyltransferase METTL3 maintains colon cancer tumorigenicity by suppressing SOCS2 to promote cell proliferation. *Oncol Rep* 2020, 44:973-986.

313. Liu J, Dou X, Chen C, Chen C, Liu C, Xu MM, Zhao S, Shen B, Gao Y, Han D, et al.: N (6)-methyladenosine of chromosome-associated regulatory RNA regulates chromatin state and transcription. *Science* 2020, 367:580-586.

314. Fan HQ, He W, Xu KF, Wang ZX, Xu XY, Chen H: FTO Inhibits Insulin Secretion and Promotes NF-κB Activation through Positively Regulating ROS Production in Pancreatic β cells. *PLoS One* 2015, 10:e0127705.

315. Zhang Q, Riddle RC, Yang Q, Rosen CR, Guttridge DC, Dirckx N, Faugere MC, Farber CR, Clemens TL: The RNA demethylase FTO is required for maintenance of bone mass and functions to protect osteoblasts from genotoxic damage. *Proc Natl Acad Sci U S A* 2019, 116:17980-17989.

316. Zheng YG, Wu J, Chen Z, Goodman M: Chemical regulation of epigenetic modifications: opportunities for new cancer therapy. *Med Res Rev* 2008, 28:645-687.

Biography

Michael J. McFadden graduated with a Bachelor of Science degree in Genomics and Molecular Genetics from Michigan State University in May 2014. At Michigan State, Michael worked with Dr. Zhiyong Xi, studying the tripartite interaction between mosquitoes, the endosymbiotic bacterium *Wolbachia*, and vector-borne pathogens. From this work, Michael co-authored multiple publications and received Michigan State's Gerhardt Award for outstanding microbiology research.

Michael began his PhD in August 2015 at Duke University in the Department of Molecular Genetics and Microbiology and joined Dr. Stacy Horner's laboratory, where his dissertation research focused on characterizing regulators of the type I IFN response. Michael has also studied viruses within the Flaviviridae family and antiviral innate immunity, resulting in numerous co-author publications and a first-author publication titled "A fluorescent reporter-based system for imaging Zika virus infection in real-time" in *Viruses* in 2018. He has also published two review articles titled "Protect this house: cytosolic sensing of viruses" in *Current Opinion in Virology* in 2017, and "N6-methyadenosine regulates host responses to viral infection" in *Trends in Biochemical Sciences*. Michael has received several awards during his graduate studies, including the Chancellor's Scholarship from Duke in 2015 and an NIH Viral Oncology Training Grant appointment in 2016. He received poster awards at the Duke-UNC Viral Oncology Symposium and the North Carolina RNA Society Symposium in 2019. He was also a Preparing Future Faculty Fellow and received a Certificate in College Teaching from Duke University. He completed his PhD in the Department of Molecular Genetics and Microbiology in December 2020.